POLITECNICO DI MILANO

Dipartimento di Ingegneria Biomedica

Scuola di Ingegneria Industriale e dell'Informazione

Biofluid Dynamic Analysis of Abdominal Aortic Aneurysm Treated with Chimney Graft Technique

Relatore: Prof. Alberto Cesare Luigi Redaelli

Correlatore: Prof. Roger Tran-Son-Tay

Tesi di laurea magistrale di

Rosamaria Tricarico matr. 786624

Anno accademico 2013/2014

To my family who has always been there to support me and encourage me

ACKNOWLEDGMENTS

I would like to express my appreciation to my committee chair, Professor Tran-Son-Tay for his availability in every situation despite the distance, and for the amazing opportunity he gave me of working in his Laboratory with his team.

I would like to thank my committee members, Professor M. Sarntinoranont and Dr. Berceli for the opportunity they gave me to share and discuss with them about such important topics.

Particular regard to Dr. Berceli who has represented the bearing of my study research and a real compass during this year abroad; he has been able to make me feel part of his team since the first day of collaboration. He showed me the importance of working connection through the love for research, and he continually and convincingly conveyed a spirit of adventure to research beside true passion for his job. Without his guidance and persistent help this thesis would not have been possible.

I sincerely thank you to Dr. H. Yong who directly assisted me in the everyday work in the Laboratory. He introduced me to the computational analysis and he shared with me his precious experience in the field, he has been an important point of reference for my research. Thank to my Lab-mate Tony who welcomed me at my arrival and shared with me the Lab-life during this year.

I thank the University of Florida and Malcom Randall VA Medical Center in Gainesville for the opportunity of collaboration and the allowed to process and analyze data of their patients.

A sincere thank you to Professor Baselli, and my Italian advisors Professor Redaelli who let me live this amazing experience which gave me the opportunity to improve my skills in my field of research.

A big thank to Politecnico of Milan and Atlantis CRISP Dual Degree Program that offer such a powerful chance of learning not only in science but even in life.

I would like to thank my family who gave me the force to engage my year of study abroad with serenity; they are and always will be the point of reference of my life, great examples of hard work, source of admiration, comparison, comfort. My uncles and aunts, cousins (especially those on the other part of the globe), second degree cousins, thanks to exist and to be present in my life.

A huge thank to my friends the nearer and the farer ones, they shared with me every single experience and emotion, both difficulties and moments of happiness. My old friends, friends of life, people who I always will love, and I will always bring with me in my heart. And new friends. I have met awesome people in Gainesville; and among them I found my family abroad, shoulders to cry on, and hands to give five for achieved goals.

A particular thank to my Italian and French colleagues of the Atlantis CRISP Dual Degree Program, who shared with me this awesome experience of life and studying, from our first day together during the summer school experience until the last day in Gainesville; because although everything we have been able to support and help each other, with a smile on our faces always and together. Thanks Sarah, Enrico, Pierre, Manelle who I shared University of Florida experiences with, Guillaume and Ilyes in Houston, and Alex in Milan, with who I spent the three weeks in Strasbourg.

Thank to Leda, Eustachio, Dominga, Aldo, Donatella, Noemi, Giorgio, Benedetta, and Roberta, who gave me everything I needed in every moment I needed despite the distance.

Thank to Pablo, Jack, Patty, Anja, Jonathan, Rini, and Aniruddh who have been able to discover who I really am and helped me to discover more about myself; they have been present every day in my experience abroad and I feel lucky to have met them, and have had their opinions and support since the beginning.

I would recommend and suggest a similar experience to every student, the awesome international environment has been an amazing present for life and it represented a place where to learn all together. This is just the right way to experience and grow up, to learn and understand that life is in our hands and we can and should do everything to change it in the way we want, to reach our goals and happiness.

I learnt a lot and I grew as human being, woman, friend, student, and I am really grateful to all of you, without you I would not have been able to accomplish this big goal.

TABLE OF CONTENTS

page

APPENDIX

LIST OF TABLES

LIST OF FIGURES

LIST OF ABBREVIATIONS

AA/ AAA/ JAA	Aortic aneurysm/ Abdominal aortic aneurysm/ Juxtarenal aortic aneurysm
CAD	Coronary artery disease
CCA	Left common carotid artery
CG	Chimney graft
CHF	Chronic heart failure
COPD	Chronic obstructive pulmonary disease
CT	Computed tomography
EVAR/ChEVAR	Endovascular aortic repair/ Chimney endovascular aortic repair
FBE	Fenestrated branched endograft
ILT	Intraluminal thrombus
LSA	Left subclavian artery
MRI	Magnetic resonance imaging
OAR	Open aneurysm repair
SMA/ IMA	Superior/ Inferior mesenteric artery
TEE	Trans-esophageal echocardiography

Abstract of Thesis Presented to the Graduate School
of the University of Florida in Partial Fulfillment of the
Requirements for the Degree of Master of Science

BIOFLUID DYNAMIC ANALYSIS OF ABDOMINAL AORTIC ANEURYSM TREATED WITH CHIMNEY GRAFT TECHNIQUE

By

Rosamaria Tricarico

August 2014

Advisor: Redaelli Cesare Alberto Luigi

Major: Biomedical Engineering

The chimney technique to extend landing zones for endovascular aortic repair (ChEVAR) has been increasingly used to treat the branched portions of the aorta. Although successful in the short-tem, long-term durability has been questioned due to concerns about device interactions and interferences in branch vessel anatomy implicit to ChEVAR. This study was performed to determine local anatomic and hemodynamic changes that result from ChEVAR and to define the critical parameters that correlate to stent graft thrombosis.

Patients undergoing ChEVAR were evaluated with CT imaging pre and post-operatively, and images were used to reconstruct the vessel 3D-geometry. Computational fluid dynamic (CFD) simulations were used to evaluate changes in cross-sectional areas, pressure, and wall shear stress in the superior mesenteric (SMA) and renal arteries.

Due to the inherent configuration of each visceral artery, it was found that ChEVAR had varying effects on the 3D conformation of the vessels, and consequently on the hemodynamics. In the SMA, which has a natural caudal orientation, the conformational change was modest, and there were minimal changes in the local flow dynamics. However, dramatic changes in the 3D configuration of the naturally perpendicular renal arteries were observed, with the stents forcing

the vessels into a caudal orientation. These changes resulted in significant perturbations in flow dynamics, with up to a 300% elevation increase in both the local wall shear stress and pressure gradient. Despite striking anatomic and hemodynamic changes from pre-op, only 3 of 13 branch grafts occluded within the follow-up period. An analysis of those factors associated with graft thrombosis demonstrates that a change in the maximum shear stress greater than 35 Pa (350 dynes/cm2) was correlated with branch graft occlusion. The spatial distribution of wall shear, both pre-operatively and following stent graft placement, for the three patients who demonstrated branch graft occlusion demonstrate a markedly elevated shear stress in the interval preceding graft failure. Pressure gradients greater than 2000 Pa (15 mmHg) or minimum lumen areas less than 20 mm^2 were not associated with graft thrombosis.

The placement of intravascular stents in aortic branch vessels often leads to an unavoidable change in vessel conformation, causing significant modifications in the local flow patterns. In particular, the perpendicular orientation of the renal arteries was forced into a caudal angle by the stents inducing dramatic hemodynamic changes. The natural caudal orientation of the SMA was minimally affected, and demonstrated fewer alterations in these flow patterns.

While changes in cross-sectional area, local pressure gradient, and wall shear stress are commonplace, marked elevations in wall shear appear to be predictive of impending branch graft failure. These findings suggest a potential role for CFD analysis in the follow-up evaluation of complex aortic endograft repairs.

ESTRATTO IN ITALIANO

INTRODUZIONE e BACKGROUND

L'aneurisma aortico (AA) e' un complesso disturbo vascolare che consiste nella dilatazione dell'aorta (circa 3 cm nel tratto toracico se 2 cm nel tratto addominale). Ha patogenesi multifattoriale con fattori di rischio legati a componenti genetiche e ambientali, che risultano in un indebolimento locale della parete aortica. E' un distrurbo silente, che negli ultimi stadi puo' presentare sintomi causati dall'imminente rottura dell'aneurisma; l'emorragia interna causata da rottura, se non trattata in tempo, puo' condurre a shock e decesso del paziente.

In generale, gli aneurismi aortici addominali (AAA) colpiscono tra il 6-9% della popolazione modiale industializzata sopra i 65 anni di eta'.[5,6] Il 3-9% degli di essi non viene diagnosticato fino alla rottura, ed il tasso di mortalita' in seguito a rottura dell' aneurisma raggiunge il 90%.

Il riparo dell'AA ha due principali obiettivi: la prevenzione da rottura e il mantenimento della perfusione periferica. Esistono approcci chirurgici differenti per il riparo aortico, le due principali macro- famiglie sono l'open repair e le piu' recenti tecniche endovascolari. Fra gli approcci endovascolari piu' utilizzati vi sono la Fenestrated branched endovascular (FBE) e la Chimney graft techniques (CG), che nella maggior parte dei casi vedono il coinvolgimento della arteria mesenterica superiore e delle arterie renali (sporadicamente anche il tronco celiaco).

Inizialmente, la chimney endovascular aortic repair (ChEVAR) e' stata utilizzata allo scopo di ripristinare il flusso sanguigno in ramificazioni aortiche incidentalmente o intenzionalmente coperte dallo stent aortico durante la TEVAR per pazienti affetti da juxtarenal AAA. La CG consiste nell'utilizzo di uno stent aortico ed n chimney stents dedicati alle

ramificazioni aortiche, che vengono inseriti nel lume dell'arteria, in pressione fra la parete aortica e lo stent.

La ChEVAR per l'estensione delle landing zones nelle riparazioni endovascolari aortiche e' stata utilizzata sempre piu' frequentemente nell'ultimo decennio, in quanto ha mostrato potenziale nel trattamento di situazioni aneurismatiche con anatomia critica in cui sono coinvolte le arterie renali e mesenteriche, nel trattamento di casi d'urgenza (casi in cui la FBE viene esclusa per lunghe tempistiche di manifattura degli stents), ed ha dunque il vantaggio dei minori costi di manifattura. Sebbene siano stati ottenuti buoni risultati nel breve termine, il lungo termine ha mostrato risultati chirurgici discutibili a causa di riadattamenti anatomici dei vasi dotati di stent che hanno portato al fallimento degli stessi nel post- intervento.[16]

Questo studio ha lo scopo di determinare i cambiamenti anatomici ed emodinamici che risultano dalla ChEVAR e di definire i parametri critici correlati ai casi di trombosi che si verificano all'interno di vasi dotati di stent graft. Nello specifico, e' stato ipotizzato che le analisi di sezioni trasversali, sforzi di taglio e differenze di pressione possono fornire buoni indici per il riconoscimento del fallimento degli stent graft e rappresentare strumenti di trigger per la prevenzione e cura del caso paziente- specifico.

METODI

Sono stati analizzati cinque pazienti, da un gruppo di 49 operati nel North Florida/South Georgia Veterans Health Affair of Gainesville (Florida), affetti da anerusma aortico addominale trattato con tecnica chirurgica Chimney Graft. Due donne e tre uomini fra i 65 ed gli 83 anni che presentano casi ipertensione, ed altre comorbidita' (CAD, CHF, COP) come e' solito nei pazienti sottoposti a ChEVAR.

Durante gli interventi chirurgici sono stati utilizzati stent graft della Zenith® (Cook Medical®, Bloomington, Indiana, IN) per il lume aortico ed iCAST™ pallone- espandibile in PTFE (Atrium Medical Corporation, Hudson, NH) per la tecnica chimney adottata sulle ramificazioni aortiche.

I pazienti sono stati monitorati nel tempo (0 – 45 mesi) con Computed Tomography Angiography (CTA) e alcuni mesi post- intervento alcuni stents hanno presentato occlusioni causate da trombi e coauguli sanguigni. Inoltre, per alcuni interventi si e' ritenuta necessaria l'occlusione intenzionale di una delle due arterie renali grazie all'utilizzo di coils in platino con fibre sintetiche che ne agevolano l'embolizzazione (COOK® Medical Nester®), decisione chirurgica determinata dallo scarso flusso sanguigno nel rene interessato (funzionamento non fisiologico) o criticita' della situazione anatomica.

Le geometrie 3D sono state ricavate dalla segmentazione delle immagini CT sulla piattaforma commerciale per 3D e 4D data analysis, Amira®, e sono state utilizzate per la costruzione di modelli aortici paziente- specifici.

Le geometrie sono state levigate in superficie con il software Geomagic Studio® e successivamente estese in lunghezza grazie a Vascular Modeling Toolkit (VMTk, collezione di librerie per la ricostruzione 3D, l'analisi geometrica e analisi di superfici per image- based modeling di vasi sanguigni). L'estensione del vaso deriva dalla necessita' di avere profili di velocita' sviluppati sui boundary layers delle geometrie in particolare nei tratti di interesse, e per evitare reverse flow all'uscita dalle arterie.

ANSYS® ICEM CFD™ Meshing Software (R14.5) e' stato utilizzato per la creazione della mesh. Sono state generate mesh global Delunay con tre boundary layers allo scopo di

ottenere 1.5-2 milioni di elementi che hanno dimostrato garantire buoni risultati in termini di convergenza delle simulazioni in tempi adeguati.

Infine, sono state eseguite simulazioni computazionali fluidodinamiche (CFD) in Ansys FLUENT allo scopo di valutare i cambiamenti temporali successivi all'intervento sulle arterie di interesse. Sono state impostate le caratteristiche fluidodinamiche del sangue ipotizzato fluido incomprimibile, omogeneo, Newtoniano con viscosita' $\mu = 0.0035$ Kg/m/s e densita' $\rho = 1050$ Kg/m^3 nella geometria del tronco aortico addominale idealizzata a parete rigida.

Sono state risolte le equazioni di Navier-Stokes sfruttando il metodo dei volumi finiti tramite simulazioni fluidodinamiche a tempo transiente usando Upwind di second'ordine per la quantita' di moto e la pressione, lo schema SIMPLE (Semi Implicit for Pressure Limited Equation) come algoritmo di pressure-velocity coupling e valori di scaled residuals di 10^{-5}.

Sono state impostate condizioni al contorno stazionarie e di no-slip alla parete, ed una curva di velocita' paziente- specifica sull'inlet aortico (con 2122.39 ml/min di flusso sanguigno in ingresso a livello addominale post- tronco celiaco), pressione nulla sull'inlet, percentuali di outflow sugli outlet delle arterie (18.5% per le arterie renali, 19% per la sma, nel caso standard) e dimensioni di time step di 0.002 sec. Su ciascuna geometira sono state, inoltre, eseguite simulazioni nei due casi: ± 25% del flusso sanguigno standard considerato, allo scopo di analizzare anche cambiamenti legati e differenti flussi sanguigni correlati a peso ed altezza del singolo paziente.

In seguito, sono state calcolate le centerlines in VMTk sulle geometrie delle ramificazioni aortiche prive di estensioni e sono stati elaborati i risultati in MatLab al fine di ottenere dati inerenti alle sezioni trasversali e alle centerlines leggibili dal software di visualizzazione e analisi dati Tecplot 360 (Tecplot Inc, Bellevue, Washington).

Infine, sono stati elaborati i dati in Excel allo scopo di estrarre curve di pressione intravasale, sforzi di taglio alla parete (wss) e sezione trasversale (csa) sulle arterie mesenteriche superiori (sma) e sulle arterie renali dei cinque pazienti nell'istante di picco della curva di velocita' (0.22/0.9 sec = 110^{o} time step).

RISULTATI

Tre pazienti su cinque hanno presentato occlusione (fallimento) di uno stent graft: il Paziente1 (1 mese post- intervento) sull'arteria renale sinistra, il Paziente 2 (7 mesi post-intervento) sulla arteria mesenterica superiore, il Paziente 3 (13 mesi post- intervento) sull'arteria renale sinistra. Durante l'intervento dei Pazienti 2 e 5 si e' ricorsi all'occlusione intenzionale rispettivamente sulle arterie destra e sinistra. Infine il Paziente 4 ha avuto impianto dello stent graft solo sull'arteria renale sinistra, la destra e la sma mostravano funzionamento fisiologico, senza duqnue necessitare supporto ed espansione del lume di questi vasi.

Sono state analizzate curve di pressione totale, pressione statica, sforzi di taglio e sezioni trasversali lungo l'estensione dei tre vasi d'interesse per ciascun paziente nel caso standard.

Sono stati rilevati casi di differenze di pressione statica negativa tra l'inlet del vaso e il suo outlet, la spiegazione di questo fenomeno viene trovata nella legge di Bernoulli, secondo cui il flusso in questi segmenti di arteria sarebbe guidato dalla pressione dinamica (inerzia).

In generale, le geometrie dei cinque pazienti hanno presentato ingenti cambiamenti morfologici che hanno causato variazioni in termini emodinamici dal pre- al post- intervento. Le arterie renali hanno un orientamento in natura perpendicolare alla direzione aortica nel pre-intervento, che subiscono un brusco cambiamento nel post- intervento assumendo conformazione caudale causata dallo stent. Al contrario, la sma ha un orientamento caudale in natura che, in

genere subisce minori variazioni confromazionali nel post- intervento, generando moderati cambiamenti emodinamici.

I risultati di maggior rilievo sono stati ottenuti in termini di sforzi di taglio. Il valore di picco di wss sulla arteria mesenterica superiore e' nel range di 2-40 Pa per i cinque pazienti; i valori di picco degli sforzi di taglio su vasi privi di stent (pertanto con fluidodinamica fisiologica) sono di circa 2.5 Pa.

Sulla arteria renale destra, il picco di wss e' nel range di 13- 127 Pa. I Pazienti 1 e 3 hanno mostrato valori molto elevati (96- 127 Pa), una possibile spiegazione e' stata individuata nella geometria delle arterie: entrambe presentano gravi stenosi dovute a kinking dello stent e/o compressione da parte di un'altra arteria.

Infine, i valori di picco degli sforzi di taglio alla parete sull'arteria renale sinistra sono nel range di 10-190 Pa; in particolare il Paziente 2 e 4 hanno mostrato valori fra i 175-190 Pa causati da stenosi e kinking del vaso.

Concludendo, sulle arterie dotate di stent nel post- intervento si osservano interessanti cambiamenti in termini di sforzi di taglio alle pareti che secondo uno studio di Malek et al. (1999) [12] sono valori piu' che sufficienti a determinare rischio di occlusioni (wss>7 Pa).

DISCUSSIONI

Nei cinque pazienti analizzati, i cambiamenti morfologici sulla sma, che ha una conformazione per natura caudale, sono risultati modesti ed hanno mostrato ridotti cambiamenti nelle dinamiche del flusso locale. Al contrario, importanti differenze morfo- emodinamiche sono emerse fra le configurazioni 3D pre- e post- intervento sulle arterie renali, che hanno direzione in natura pressoche' perpendicolare a quella aortica, ma che viene forzata ad una configurazione

caudale nel post-intervento. Questi cambiamenti sono tradotti in significative perturbazioni nella fluidodinamica con valori di wss e differenze di pressione fino a tre volte superiori.

Da notare, d'altra parte, che nonostante gli evidenti cambiamenti anatomici ed emodinamici dalle situazioni pre- intervento alle post- intervento, solo 3 stent graft su 13 sono falliti a causa di trombi nel periodo di follow-up.

Successive valutazioni sull'analisi dei fattori associati alla trombosi hanno dimostrato che in caso di occlusione dello stent, le variazioni del valore di massimo wall shear stress sono risultati superiori a 35 Pa (350 Dynes/cm^2). Inoltre, la distribuzione spaziale di sforzi di taglio, in entrambi i casi pre- e post- operativi per i tre pazienti che hanno presentato occlusioni ha mostrato elevati valori di wss nelle configurazioni precendenti all'occlusione. Al contrario, valori di differenze di pressione superiori a 2000 Pa (15 mmHg) o valori di lume delle arterie inferiori a 20 mm^2 sono risultati non direttamente associabili a casi di trombosi.

CONCLUSIONI

Il posizionamento di stents intravascolari nelle ramificazioni aortiche a livello addominale spesso conduce ad inevitabili cambi nella conformazione del vaso, causando significativi cambiamenti a livello della fluidodinamica locale. Tra i cambiamenti in termini di sezioni trasversali, differenze di pressione locali e sforzi di taglio, i marcati cambiamenti negli sforzi di taglio sembrano essere un valido indice di allarme per stent in procinto di fallimento. In generale, questi risultati suggeriscono un potenziale ruolo delle analisi di simulazioni CFD per valutazioni di follow-up di casi di riparazioni aortiche con endograft.

CHAPTER 1
INTRODUCTION

1.1 Overview and Rational

Biomechanics is the scientific field that applies the laws of mechanics and physics to living organisms, in order to gain a greater understanding of life performance through modeling, simulation and measurement. The general role of biomechanics is to understand the mechanical cause-effect relationships that determine the dynamics of living organisms.

Biofluid dynamics is a branch of biomechanics and it may be defined as the study of fluid flow, fluid-structure interaction, heat and mass transfer in living systems, and in particular, mammalian organisms and implanted medical devices.

The circulatory system is one of the major areas of research in the biofluid dynamic field, but understanding human body biofluid dynamics is not easy; in vivo experiments are not easy to perform, and non-invasive experiments are useful but not always give the desired result. Thus, both theoretical and computational biofluid dynamics play a major role in the understanding of human body biofluid dynamics.

Computational fluid dynamics (CFD) uses numerical methods to solve the fundamental non-linear differential equations that describe fluid flow (the Navier-Stokes and allied equations) for predefined geometries and boundary conditions.

CFD simulations have many advantages (Figure 1-1); first of all, they provide a non-intrusive, virtual modeling technique with powerful visualization capabilities. Engineers in any field can evaluate the performance of a wide range of system configurations on the computer - saving the time, expense, and disruption required to make actual changes onsite.

EXPERIMENTS	SIMULATIONS
Quantitative **description** of flow phenomena using measurements	Quantitative **prediction** of flow phenomena using CFD software
• for one quantity at a time	• for all desired quantities
• at a limited number of points and time instants	• with high resolution in space and time
• for a laboratory-scale model	• for the actual flow domain
• for a limited range of problems and operating conditions	• for virtually any problem and realistic operating conditions
Error sources: measurement errors, flow disturbances by the probes	Error sources: modeling, discretization, iteration, implementation

Figure 1-1. Comparison between experimental analysis and CFD simulations. Advantages and disadvantages.

Computational Fluid Dynamics gives chance to a cheaper, faster, parallel and more multi-purpose analysis than experimental studies since physical modifications are not necessary, it is able to analyze any kind of problem in any realistic condition, predicting many parameters at a time, with high space- time resolution, for the actual flow domain; moreover, it is becoming more and more reliable, thanks to great improvements of schemes and methods upon which CFD is based.

Nowadays, Computational fluid dynamic analysis has been successfully applied in multiple fields – from over a broad range of disciplines that include environmental, aerospace, mechanical, electrical, chemical, and biomedical engineering. [1,2]

In particular, CFD is also used to study respiratory and circulatory systems and diseases (congenital heart disease, heart failure, ventricle function, aortic disease, and carotid and intra-cranial cerebrovascular diseases), nasal ducts, auditory system, etc.

The scientific world has recognized numerical diagnostics as a big valid help into medical decision-making; CD-adapco[a] and ASME[b] subcommittees are involved in getting CFD and Finite element analyses (FEA) qualified to help speed up the U.S. Food & Drug Administration (FDA) approval process. When accepted, this ruling could be groundbreaking for the legal, medical and engineering realms.

One important step toward this goal is the recent FDA recognition of simulation as "essential to medical device evaluation". This opinion has just been written up by Cheryl Liu, a senior product experience technical specialist at Dassault Systems' SIMULIA life sciences division[c].[1]

In this study, Computational fluid dynamic simulations have been performed on patient-based geometries of abdominal aortic aneurysm treated with chimney graft technique. This technique has shown great potential since it allows the treatment of urgent cases at a lower manufacture costs, but may have higher failure risk than the most common fenestrated technique.

The objective of this project is to evaluate hemodynamic situations on patient- based abdominal aortic conformations, particularly focusing on the morphological and fluid dynamical changes in renal arteries and superior mesenteric artery. Up to now, most of the CFD studies focused on the hemodynamics on the aneurysm sac, usually ignoring the smaller side arteries. Our challenge is to manually create 3D geometries from CT scan segmentations of the abdominal

[a] CD-adapco is a multinational computer software company that authors and distributes applications used for computational fluid dynamics (CFD) products.

[b] ASME (founded in 1880 by a small group of leading industrialists) is a not-for-profit membership organization that enables collaboration, knowledge sharing, and skills development across all engineering disciplines, toward a goal of helping the global engineering community develop solutions to benefit lives and livelihoods.

[c] Dassault Systemes' SIMULIA (founded by A. M. Dessault, 1981) is a French software company that specializes in the production of 3D design software, 3D digital mock-up and product lifecycle management solutions.

aortic tract (from some centimeters proximal to the superior mesenteric artery until few centimeters distal to the renal arteries), and study the differences between the pre- and post-surgery situations for each patient. Finally, 3-D flow simulations inside actual blood vessel geometries will be performed. The results is to provide a better understanding of the possible hemodynamic modifications that this technique can bring, relationship between anatomical changes and hemodynamics, and their roles in distal perfusion and stent thrombosis, thanks to simulations obtained from the 3D meshed geometries.

1.2 Specific Aims

1.2.1 Aim 1

Selection of the 5 study cases, geometries and clinical conditions for our project. The procedures for both pre and post surgeries comprehends five steps: CT segmentation, geometry smoothing and extension, geometry meshing, mesh simulation and hemodynamic data elaboration. Critical parameters of evaluation be regular geometry, number of CTs (at least two post- operative), and no fenestrated technique.

Determine two control cases versus more complex cases where the patients had chimney graft technique performed on all their SMA and renal arteries and showed after surgery stent failure (spontaneous lumen occlusions). Therefore, control cases must have no complications or failures of any chimney stent in the period of time monitored after surgery.

1.2.2 Aim 2

Creation of five patient- specific studies, focusing on each medical record, clinical indications and pre and post- surgery CT scans. Analysis of each patient's pre and post operation CTs (two to five). Morphology and hemodynamic parameters such as pressures on the wall and centerilines, and wall shear stresses for every patient have been collected for each PreOp and PostOp situations, and evaluated during the monitored period of time (before the surgery to 6

months- 2 years). The specific purpose is to observe clinical modifications during the time among the pre- and post- operative conditions for each patient.

1.2.3 Aim 3

Perform 3-D flow analysis for all cases. The goal of this aim is to investigate if there is a correlation between hydrodynamic parameters, vessel anatomy, and clinical outcome.

Comparison among the five patients' situations will been performed from a morphological and hemodynamic point of view. The final purpose is to try to generalize what was initially a patient-specific evaluation by trying to observe which parameters are constant and which ones change in our analysis, evaluating their plausible causes and possible improvements

CHAPTER 2
BACKGROUND

2.1 Abdominal Aortic Aneurysm: Clinical Problem and Statistics

The Aortic aneurysm (AA) is a complex degenerative vascular disorder which consists of a dilation of the aorta to greater than 1.5 times normal size (around 3 cm in the thoracic tract, 2 cm in the abdomen). Its pathogenesis is multifactorial with genetic and environmental risk factors[a], and the end result is an underlying weakness in the wall of the aorta at that specific area.

It is a silent disease, often without symptoms, but it may occasionally cause physical pain in the later stages[b], which is a sign of impending rupture. In case of free rupture, massive internal hemorrhage results, and, unless treated immediately, shock and death can occur within minutes to hours. [3–5]

Many types of Aortic Aneurysms exist; according to the universal classification system, they took their name from the area in which they occur (Figure 2-1):

- Arch
- Thoracic (ascending, descending)
- Thoraco-Abdominal (TAAA, from I to IV)
- Abdominal (AAA): suprarenal (the aneurysm includes the origin of renals or above without involvement of the superior mesenteric artery); juxta- or para- renal (the aneurysm originates just after the renals); infra- renal (with a segment of undilated aorta)

The prevalence of AAA located in the infra-renal section of the aorta is at least three times higher than that of thoracic aortic aneurysms and dissections.

[a] Risk factors: tobacco use, hypertension, diabetes mellitus, hyperlipidemia, chronic obstructive pulmonary disease (COPD), cardiac disease, carotid occlusive disease (COD), renal insufficiency, and presence of other aneurysms.[3]

[b] Stages defined by symptoms and clinical presentation: asymptomatic (*Stage I*); intact but symptomatic (*Stage II)*; contained rupture (*Stage III)*; free rupture (*Stage IV*). [3]

Overall, Abdominal Aortic Aneurysms affect 6-9% of the industrialized world aged over 65. In fact, it has an age-at-onset approximately around 75 years and is predominantly a disease of Caucasian males with 6:1 male: female ratio. [5,6]

3-9% of AAs go undetected until rupture (rupture is three times more likely in women), and the mortality from ruptured aneurysms is 90%. In the United States, aortic aneurysm rupture causes more than 15,000 deaths per year. In particular, the Abdominal Aortic Aneurysm represents the 18th most common cause of death in the world population, the 15th if we consider only those aged over 65.[4,5,7,8]

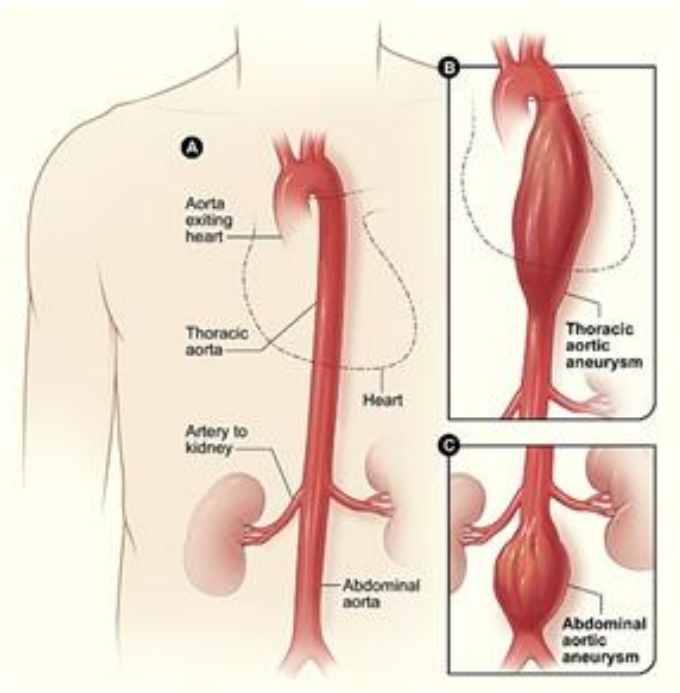

Figure 2-1. Sample of physiological aorta and pathological aorta. A) Sample of normal aorta; examples of B) thoracic and C) abdominal aortic aneurysm.

2.2 Aneurysm Formation and Growth: Histology and Biomechanics

Currently, the maximum diameter is the criterion to be used used to determine the severity of an AAA. Unfortunately, this criterion is only a general rule and not a reliable indicator since autopsy studies have reported both small aneurysm ruptures and very large aneurysms without

rupturing.[5,9] The maximum diameter criterion is based on the law of Laplace that states that wall tension increases with vessel radius:

$$T \propto P \cdot R \tag{2-1}$$

where T represents the tension of a cylindrical vessel, P the internal pressure, R the radius (establishing a linear relationship between diameter and wall stress). However, aneurysms are complex structures, not regular cylinders, and more than one radius of curvature is involved, therefore the law fails to predict realistic wall stresses.

From a biomechanical point of view, rupture events occur when acting wall stresses exceed the tensile strength of the degenerated aortic abdominal wall. From a more general and extensive perspective, the stress state in a body is determined by several factors such as geometry, material properties, load and boundary conditions. Thus, in order to fully understand the clinical problem and be able to analyze it, it is fundamental to capture the mechanical response of the aortic tissue and its changes during aneurysmal formation. In fact, even though the causes of the AA are still unclear, the process of the aneurysm formation has been analyzed for decades and is fully understood.[5]

Soft biological tissues have a unique and very complex structure that can be regarded as either active or passive. The active components arise from the activation of the smooth muscle cells while the passive response is governed primarily by the elastin and collagen fibers. The distribution and the arrangement of the collagen fibers, in particular, have a significant influence on the mechanical properties because they attribute anisotropic properties to the tissue according to the aortic segment (thoracic or abdominal). As well as being anisotropic, the material response of soft biological tissue is also highly non-linear.[10]

During Aortic Aneurysm formation, this complex structure and its mechanical properties change because of remodeling of its components and become slowly weaker. AAA formation and growth are correlated with high peripheral resistance and pro-inflammatory hemodynamics including low and oscillatory wall shear stress (WSS) and extended clearance time of blood particles, induced by stagnation and recirculation of blood flow in the dilated abdominal aorta. Low and disturbed WSS (<4 dyne/cm2 or 0.4 Pa, Figure 2-2) is hypothesized to induce athero-prone gene expression via mechanoreceptors on endothelial cells, and alter the function of atherosclerosis-associated molecules.[11,12]

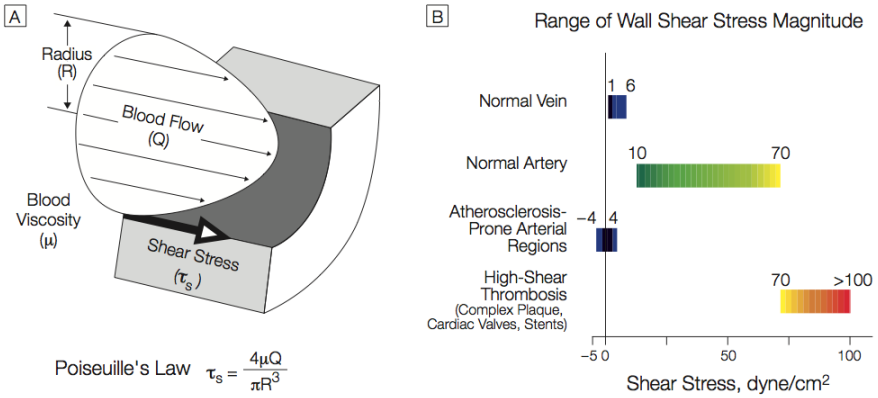

Figure 2-2. Hemodynamic Wall Shear Stress. A) Cross Sectional Schematic diagram of a blood vessel, illustrating hemodynamic shear stress. B) Tabular diagram illustrating the range of wall shear stress magnitudes encountered in vein, arteries, and low shear stress and high shear stress pathologic states. [12]

From a histological point of view, the AA consists of migration of macrophages and T and B lymphocytes with unclear reasons; they excrete enzymes (proteases and elastases), causing chronic inflammation with destruction of the extracellular matrix, remodeling of the wall layers and reduction in number of the smooth muscle cells. In particular, degradation of the major connective tissue components has been observed (elastin, collagen, fibronectin, laminin, and proteoglycans); the elastin degradation brings to dilation of the artery, subsequently collagen degradation causes the wall rupture. The aortic wall weakens and dilates and finally it can break as a result of the high pressure of intraluminal blood flow. [13]

AAAs are characterized by signs of local chronic inflammation of the aortic wall, decreasing in the number of smooth muscle cells in the aortic media layer, and fragmentation of the extracellular matrix of the aorta at the site of the aneurysm. Researches are trying to demonstrate that the chronic inflammation observed in AAAs is a consequence of a unregulated autoimmune response against autologous components of the aortic wall that persists inappropriately.[1]

In AAA cases, the aortic and smaller arteries' lumens usually show calcifications, and approximately 75% of AAAs have an intraluminal thrombus (ILT) in the aorta (clearly observed in CT scans), yet its role remain unclear. Some authors have suggested that rupture is associated with growth of thrombus in the aneurysm; some suggested that blood entering thrombus may have a role in rupture. On the other hand, other investigators have reported that intraluminal thrombus exerted protective influences against aneurysm rupture, since some studies have reported that ILT significantly lowered aneurysm wall stress. It was proposed that mural thrombus acted as a fibrous network adherent to the aneurysm wall and since this network also had to stretch with the aneurysm, the dilation of the aneurysm under pressure was reduced in the presence of thrombus. Although the thrombus transmitted most of the luminal pressure to the aneurysm wall, the reduction in dilation (strain) was thought to be important in reducing the overall wall stress. Nonetheless, it may be a barrier to the diffusion of oxygen and nutrients from the blood stream to the inner (avascular) portion of the wall, and it sequesters leukocytes and platelets that produce proteases and growth factors as well as control local levels of plasmin, which in turn activate matrix metalloproteinases (MMPs)[c]. Hence, thrombus likely plays key chemo-mechanical roles in evolving AAAs and it must be understood and modeled.[7,14]

[c] The MMPs are zinc-dependent endopeptidases; they play an important role in tissue remodeling associated with various physiological or pathological processes such as morphogenesis, angiogenesis, tissue repair, metastasis, etc.

Moreover, atherosclerosis has been associated with aortic aneurysm for long time, but each of these diseases affects different layers of the aortic wall. Atherosclerosis mainly affects the intima, causing occlusive disease, while aortic aneurysm is a disease of the media and adventitia.

Atheroma occurs in atherosclerosis (Figure 2-3); an atheroma is an accumulation of degenerative material in the tunica intima. The material mostly consists of macrophage cells, or debris, containing lipids (cholesterol and fatty acids), calcium and a variable amount of fibrous connective tissue. These materials accumulate in the artery wall, which may narrow the artery lumen and restrict blood flow. Moreover, calcification forms among vascular smooth muscle cells of the surrounding muscular layer, specifically in the muscle cells adjacent to atheromas and on the surface of atheroma plaques and tissue.

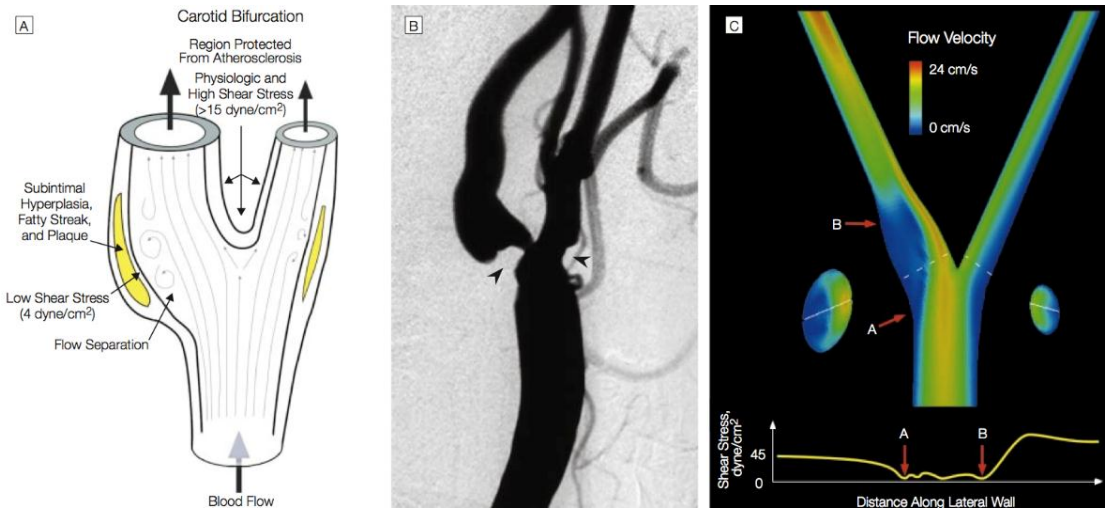

Figure 2-3. Localization of atherosclerosis lesions its process. A) Schematic illustration of atherosclerosis nature and its tendency to involve the outer walls of vascular bifurcations. B) Left lateral carotid angiogram of embolic stroke in the left temporal lobe. Focal narrowing at the outer walls of both the internal and external carotid artery (arrowhead). C) Velocity map of the carotid bifurcation at the end-systole using CFD modelling illustrates the lower velocities seen at the lateral edges (blue). The computed wall shear stress shows the focal low shear stress magnitude at the outer wall which corresponds exactly to the atherosclerosis prone areas of the carotid bifurcation (B zone). D) Sequence of atherosclerosis process formation.[12]

[c]Recent data suggests active role of MMPs in the pathogenesis of Aortic Aneurysm. Excess MMPs degrade the structural proteins of the aortic wall.

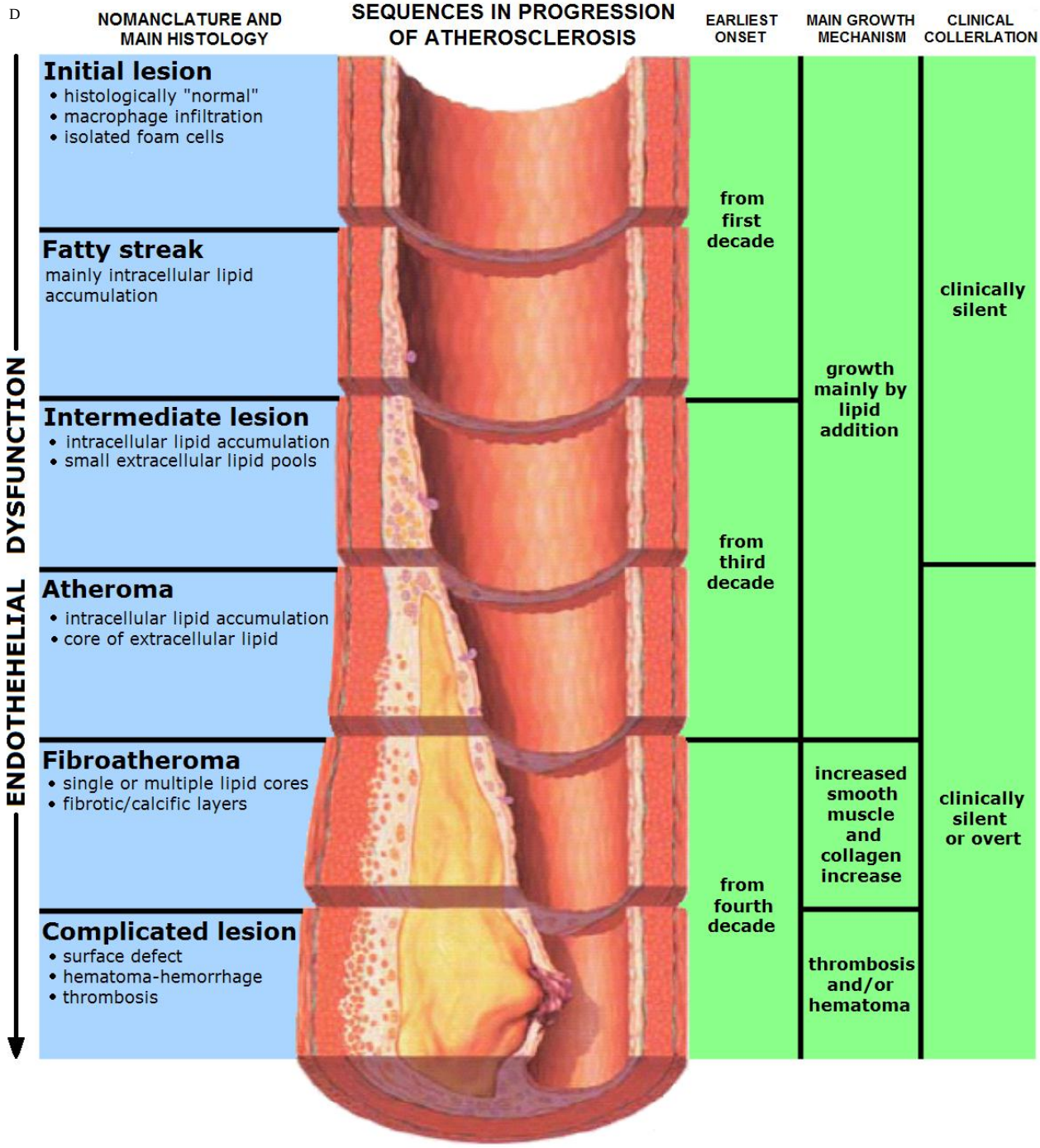

Figure 2-3. Continued

2.3 Aortic Aneurysm Diagnostic and Repair Techniques

Basic diagnostic techniques such as electrocardiography and chest radiography can yield misleading results; the misevaluation of morphological aspects can lead to immediate or late failure of the procedure (Figure 2-4, A).

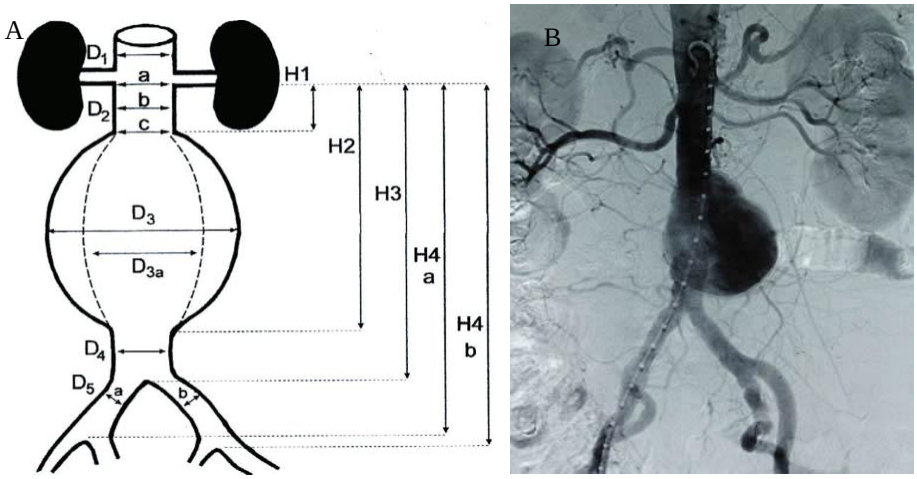

Figure 2-4. Abdominal aortic aneurysm diagnostic and measurements. A) Preoperative measurement[5]. B) Aortogram showing an abdominal aortic aneurysm.

Current techniques for AA diagnosis are computed tomography (CT), trans-esophageal echocardiography (TEE), magnetic resonance imaging (MRI), and aortography (Figure 2-4, B). These four techniques provide variable information as to the site of origin, extent of aneurysm, etc.

Aortography is considered by many to be the best diagnostic tool for its accuracy in defining the anatomy of the AA. Magnetic resonance angiography and CT are also extremely useful because they allow the evaluation of surrounding structures, such as the trachea and left main bronchus, as well as the status of main branch arteries. [15]

The two primary goals of aortic aneurysm repair are prevention of aneurysm rupture and maintenance of peripheral perfusion. There are different techniques for the Aneurysm repair, the main two are the open repair and the endovascular repair.

The first open surgical case was in Paris (France) 1951, when Dubost reported successful replacement of the infrarenal aorta with a human arterial graft; unfortunately, up to now it has still the best long-term results, with 3-7% of 30-days mortality (percentage that increases significantly for patients with comorbidities).

Open repair technique (open aneurysm repair, OAR) consists of the aneurysm resection and replacement of the diseased aorta segment with an appropriately sized synthetic prosthetic graft made of expanded poly-tetrafluoroethylene (ePTFE[d]) or poly-ethylene terephthalate (PET[e]). If the aortic root is involved, composite root replacement with a mechanical valve conduit may be performed and a re-implantation of the coronary arteries into the graft is required. Others biological alternatives, such as xenografts and human allografts exist, but they have problems of availability and risk of vasculopathy or rejection.

In general, open repair procedures present high mortality and morbidity levels, and the optimal timing of the surgery is difficult to predict; moreover, they cannot be used in cases of patients with comorbidities (compromised clinical situation). [16]

On the other hand, there are minimally invasive approaches, the Endovascular Aortic Repairs (first EVAR in Argentina, 1991, when Dr. Parodi described the first successful transfemoral intraluminal graft implantation). EVARs present a 30-days mortality of 1-2% and show positive aspects such as the minimally invasive procedure (applicable for patients with comorbidities), low rate of peri and post-operative mortality and morbidity, significantly reduced intraoperative blood loss, shorter hospital stay, and faster recovery. Contras of EVARs are the

[d] ePTFE well known as Gore-Tex®, W.L. Gore, USA 1969

[e] PET is a thermoplastic polyester, commercial name Dacron® (or Terylene®, UK) J. R. Whinfield, UK 1941

significantly higher re-intervention rate and higher cost of primary procedure if compared with the open surgery procedure (Figure 2-5).

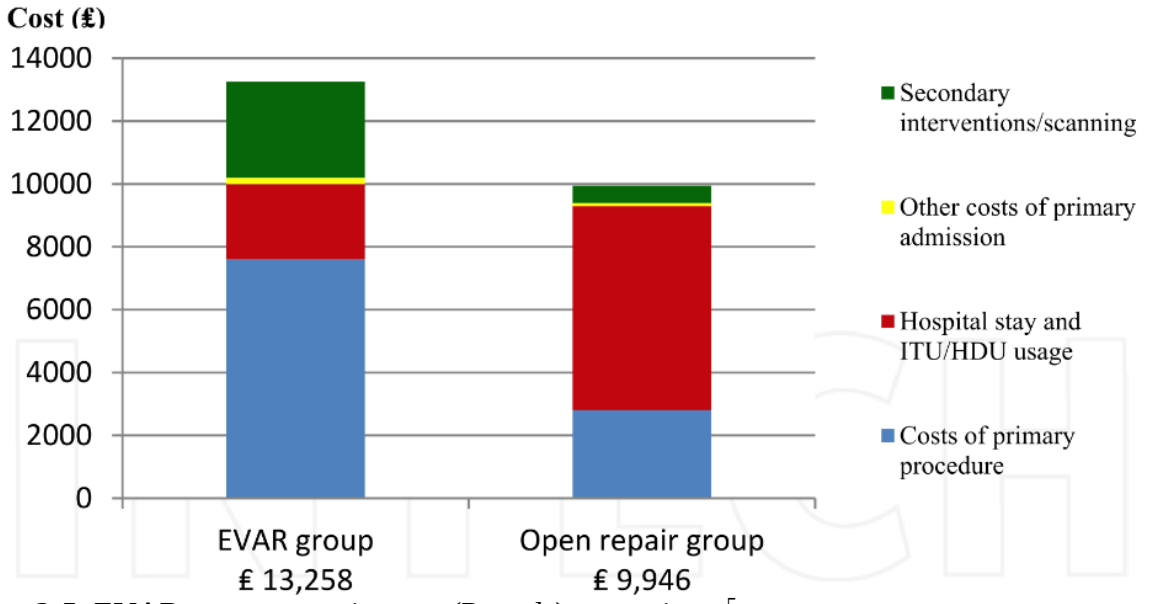

Figure 2-5. EVAR vs open repair costs (Pounds) per patient. [5]

Although current surgical treatments give interesting results, there is a need to develop non-surgical approaches to manage small aneurysms. Thus, a targeted drug development will require detailed information about the pathogenesis of aneurysms, which at the present time is still limited regardless of major discoveries involving the role of immune system and genetic factors in the development of aneurysms.[4]

2.4 EVARs: Fenestrated Branched vs Chimney Graft Techniques

Nowadays there are two principal EVAR techniques, the fenestrated side-branched endograft (FBE) and the snorkel/ chimney graft technique (ChEVAR).

Figure 2-6 shows the descending aorta branches, and the location of arteries usually involved in abdominal aortic surgery.

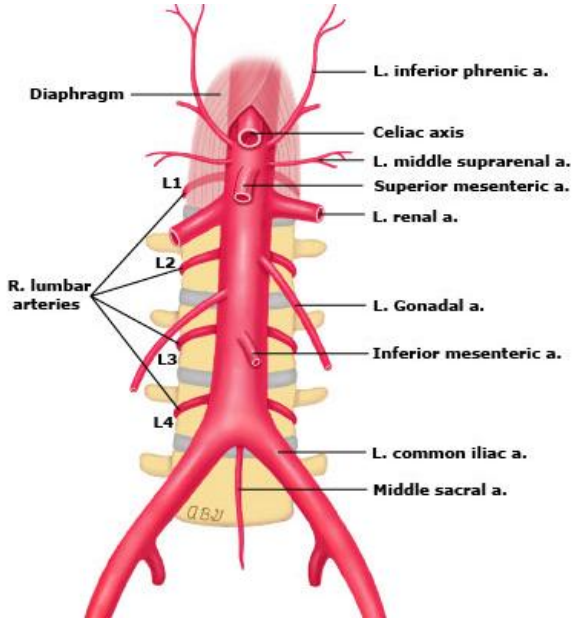

Figure 2-6. Descending aorta branches (R. = right; L. = left; a. = artery

In the Fenestrated technique, surgeons use one main graft for the aorta and one or more stent(s) for renal arteries, superior mesenteric artery (SMA), inferior mesenteric artery (IMA), and/or celiac trunk, etc. These secondary stents are stitched to the main graft in order to re-create the situation by an anatomical and physiological point of view.

FBE technique represents a solution for patients with aneurysms that do not have an adequate proximal or distal sealing zone[f]; it showed good long-term results, but it cannot be used in emergency settings as it requires meticulous preoperative planning and time for manufacture (4-6 weeks) with consequent high costs.

The ChEVAR was initially used to restore blood flow in aortic branches accidentally or intentionally covered during TEVAR in the aortic arch for patients with juxtarenal AAAs, and in urgent cases when off-the-shelf devices need to be employed.

[f] The sealing zone is defined as the proximal (so called 'neck')/distal attachment site needed to obtain an adequate fixation of the endoprosthesis.[17]

The chimney graft (CG) consists of using one main graft for the aorta and one or more chimney stent(s) for renal arteries, SMA, IMA, and/or celiac trunk, etc. In this case these secondary stents are fitted in the aortic vessel near the main graft. This technique can be used in urgent cases, when a diseased segment is unsuitable due to vessel tortuosity, and in general as option for aortic aneurysms involving critical side branches, such as renal and superior mesenteric arteries; on the other hand, though, it presents no long-term results and a relative high number of clinical failures (stented arteries occlusions). [16]

EVAR is a widely used technique for the treatment of infrarenal aortic aneurysms; however, management of juxtarenal aortic aneurysms remains controversial. In particular, Figure 2-6 shows an example of evaluation pathway to follow in order to choose the appropriate surgical technique in case of JAA.

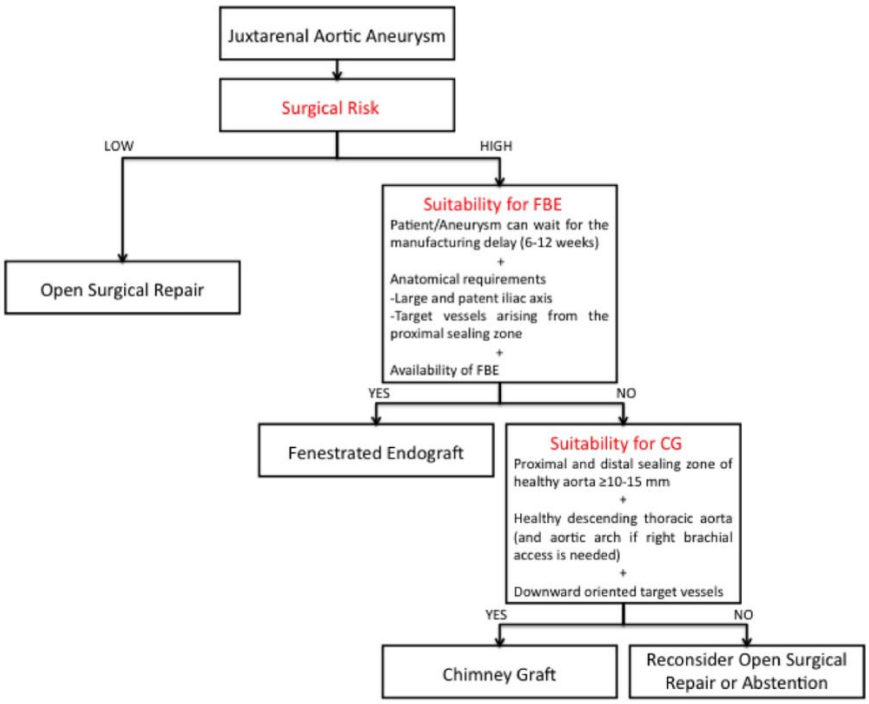

Figure 2-6. Example of treatment algorithm of juxtarenal aortic aneurysms with diameter ≥ 55 mm. [18]

By now, it has been demonstrated that FBE is a valid alternative to open surgery, with promising early and long term results; however, the strict anatomic requirements, high costs, and long manufacturing delays limit its applicability. On the other hand, because of the lack of long-term results and the high and still unclear risk of stent failures, Chimney Grafts have been advocated as a possible endovascular alternative for aortic aneurysms with contraindications to FBE. [18]

Up to now, nobody has had CG results for JAA patients amenable to FBE to conclude that CGs are inferior to FBE. Coscas et al. (Paris, 2011)[18] demonstrated that aneurysm exclusion can be achieved with cheaper and immediately available technique, the CG; therefore, comparative studies should be undertaken to ensure the superiority of one technique over the other.

Further technical improvements might render FBE technology applicable to patients with challenging anatomy who undergo CG in the current era, and the development of off-the-shelf FBE devices for emergent cases could restrain the use of CG in the future. Coscas' research group confirmed that, until such devices are available, CG represents a feasible option for patients with emergent needed treatments or critical anatomical situations, with the advantage of being immediately available and may be cheaper than FBE. [18]

2.5 ChEVAR: Technique and Stent Types

The Chimney Graft is a stent placed parallel to the aortic stent-graft to preserve flow to a vital aortic branch; the CG technique can be used as a planned operation but also as a rescue procedure to salvage a side branch unintentionally covered during EVAR.

ChEVAR has been used in the renal arteries, SMA, left subclavian artery (LSA), left common carotid artery (CCA), and innominate artery. The renal arteries and SMA are cannulated in an antegrade fashion. The guidewire is passed into the aorta and snared from a brachial approach; the CG is inserted in an antegrade direction from the arm.[16]

The grafts are classified in different manners. Nowadays the most used are the bifurcated (Aortic bi-iliac, anatomical classification); they can be modular (most of them) or unibody (Powerlink, Figure 2-7).[5]

a) Anaconda *b) Talent* *c) Zenith* *d) Powerlink*

Figure 2-7. Most common endoprosthesis types and brands. [5]

The characteristics of an ideal stent graft are[5]:

- Low overall cost;
- Stent-graft size ranging;
- Long durability (metallic ultrastructure and graft material);
- Good biocompatibility and sealing capacity;
- Delivery device flexibility, lowest delivery device size;
- Radial force stability;
- Customization.

In general, no stent has ideal mechanical properties for a CG. Both balloon-expandable and self-expanding stents are used at the surgeon's discretion. The choice is dictated by a preference for either flexibility or radial strength. Covered stents are mainly used in an attempt to reduce the risk of leakage. Undoubtedly, dedicated stents combining flexibility and strength may increase the applicability of the CG technique.[19]

Complications of EVAR are varied and include stent mechanism breakage, distal graft migration, groin hematoma, graft limb thrombosis, peripheral embolization, and, most commonly, perigraft leak, otherwise known as endoleak. They are defined as blood flow outside the lumen of the endograft and within the intact aneurysm sac. An endoleak may perfuse the aneurysm sac

leading to aneurysm expansion and may be rupture. It represents the inability to obtain or maintain secure seal between the aortic wall and the graft. The incidence of endoleaks is in range of 14%. They are classified in four types (Table 2-1).[5,20]

Table 2-1. Classification of endoleaks. Both types I and III are significant risk factors for late aneurysm rupture and should be treated. Types II are considered benign and type IV usually resolves spontaneously during the post procedure period. [5]

Type Endoleak	Endoleak Description
I	Attachment site leaks • Proximal end of endograft • Distal end of endograft • Iliac occlude (plug)
II	Branch leaks (collateral back bleeding) • Simple (one) • Complex (two or more branches)
III	Graft defect (modular dissociation) • Minor < 2 mm • Major ≥ 2 mm
IV	Graft material porosity

Ohrlander et al. (2008)[16] analyzed an early CG- associated endoleak and observed that there is a limit to the size a CG can be and still provide a seal: the larger the CG, the larger the gutters along the device (Figure 2-8).

Experimental investigations are currently underway to assess the optimal properties of the aortic stent-graft and CG needed for proximal seal and side branch patency.

Figure 2-8. Transverse section of a thoracic GC; the arrows indicate gutters along the CG.[16]

2.6 ChEVAR and CFD Analyses: State of the Art

Most of the available scientific articles that use CFD simulations are more specifically focused on the Abdominal Aortic Aneurysm disease, used different devices, and possible causes of failure; they study hemodynamic parameters (such as velocity, pressure, wall shear stress) on the actual aortic aneurysm wall, usually on the tract just before iliac bifurcation to some centimeters after of infra- renal aneurysm; some of them evaluated fluid dynamic differences between a free and a stented aneurysm and comparing those results with analytical or experimental studies.

Morris et al. (Limerick (IRL), 2004) [21] compared a numerical solution (CFD simulations) to a an analytical one, and obtained a mathematical model to predict the in vivo pulsatile drag forces acting on bifurcated stent grafts used in endovascular treatment of AAA. The objective of this study was to quantify the range of typical pulsatile drag forces acting on bifurcated stent grafts, since the authors believe that these forces are one of the main reasons for the reported stent graft migrations over a long time period. EVAR offers considerable promise as a minimally invasive clinical treatment; however, the success of the surgical procedure is greatly dependent on overcoming device design, fixation, durability and deployment, which are not mutually exclusive.

Li and Kleinstreuer (North Carolina, 2006) analyzed biomechanical factors affecting stent graft migration, focusing on a representative AAA model with bifurcating stent graft thanks to fluid–structure interaction (FSI) solver.

In a first paper[22] the authors showed that securely placed graft shields the diseased AAA wall from the pulsatile blood pressure and hence keeps the maximum wall stress 20 times below the wall stress value in the non-stented AAA. From their numerical results, the sac pressure is reduced significantly but remains non-zero and transient, caused by the complex fluid–structure interactions between luminal blood flow, endovascular graft wall, stagnant sac blood, and

aneurysm wall. The time-varying drag force on the graft exerted by physiological blood flow is unavoidable, and they concluded that the risk of graft migration is very high for patients with severe hypertension.

In 2006, Li and Kleinstreuer published a second article[23], confirming that solution for AAA/ stent graft deformation, sac pressure and wall stresses, as well as the downward forces acting on the stent graft. Simulation results indicated that implanting a bifurcating stent can significantly reduce sac pressure, mechanical stress, pulsatile wall motion, and maximum diameter change in AAAs; hence, it may restore normal blood flow and prevent AAA rupture effectively. Their results showed that drag force magnitude depends on multi-factors including blood flow conditions, as well as stent and aneurysm geometries. Specifically, AAA neck angle, iliac bifurcation angle, neck aorta-to-iliac diameter ratio, stent graft size, and blood waveform play important roles in generating a fluid flow force potentially leading to stent migration. The maximum wall stress on the aneurysm sac decreases from 0.59 to 0.03 MPa; whereas the maximum wall stress on the bifurcating stent reaches 1.76 MPa near the junction. Clearly, a proper stent placement can significantly reduce sac pressure and AAA wall stress. Indeed, other studies in Anaheim (CA), based on computational finite element models, reported that the majority of stress is absorbed by the SG after repair reducing AAA wall stresses by 90%.

Finally, in 2007[24], Li and Kleinstreuer numerically analyzed representative asymmetric aneurysms in the abdominal aorta using FSI solver, and focusing on parameter such as the transient 3D blood flow and pressure distributions as well as aneurysm wall stresses. Geometric AAA variations studied included the degree of asymmetry, neck angle and bifurcation angle, and then their impacts on the hemodynamics and biomechanics. The simulation results indicated that the assumption of symmetric AAA geometry may strongly underestimate AAA-wall stress. The

neck angle influences the blood flow field substantially. A large neck angle, resulting in strong wall curvatures near the proximal neck, can produce no-physiological blood flow patterns and elevated wall stresses. The iliac bifurcation angle affects blood flow patterns insignificantly but plays an important role in wall-stress concentrations on the aortic sac.

Segalova et al. (Stanford, 2011) [25] evaluated design of AAA endografts in a patient-specific model using CFD. There are several FDA-approved endografts currently available in the U.S. market and one of the key features of each endograft's geometry is the location at which its body bifurcates into two limbs, which then extend into the iliac arteries. Some devices place the bifurcation point closer to the renal arteries, while other devices maintain a single lumen until splitting at the aortic bifurcation. Their purpose has been to evaluate the hemodynamic consequences on these different devices. They used CTA data from four patients with AAAs to build patient-specific models using 3D segmentation. For each patient, they constructed a model from the patient's preoperative CTA data. They included in the aortic segmentation the following nine arteries in each model: hepatic, splenic, superior mesenteric, left renal, right renal, left external iliac, right external iliac, left internal iliac, and right internal iliac. In addition, geometries characterizing three distinct endograft designs were created, differing by where each device bifurcated into two limbs. CFD was used to simulate blood flow, utilizing patient-specific boundary conditions. Pressures, flows, and displacement forces on the endograft surface were calculated. The curvature and surface area of each device were quantified for all patients. The results indicate that all curvature, device surface area, and patient blood pressure influence the magnitude of displacement force acting on the device. Endograft design may influence the displacement force experienced by an implanted endograft, with the proximal bifurcation design showing a small advantage for minimizing the displacement force on endografts.

Other few studies focused on the segmentation of the entire abdominal tract (above the celiac artery until the iliac bifurcation) evaluating the hemodynamic parameters on it.

Humphrey and Taylor (Texas- Stanford, 2008) overviewed the main characteristics of the intracranial and abdominal aortic aneurysms, the two most common types of aneurysm. They finally claimed that focus has been mainly on pulsatile flows through rigid, idealized axisymmetric models, with blood modeled as an incompressible Newtonian fluid and outlet boundary conditions prescribed to be constant pressure. Moreover, most of the studies do not include major branches immediately proximal to AAAs (celiac, superior mesenteric, and renal arteries). These branches significantly influence conditions in the infrarenal aorta in normal subjects and likely influence conditions in AAAs. They concluded that more realistic analyses need to be performed thanks to more accurate anatomical and physiological models and inclusion of wall properties. In particular, non-linear wall properties, and hemodynamics, which in turn dictate the evolving cell mechanobiology that is responsible for matrix turnover and the possible rupture of aneurysms. They stated there is a need to couple FSI models over a cardiac cycle with long-term growth and remodeling (G&R) models of the evolving wall, and they call them fluid-solid-growth (FSG) models. Simulations of G&R of the vasculature will require, as input, the mechanical forces (or tractions) that the fluid exerts on the wall.[7]

Suh et al. (Stanford, 2011) studied hemodynamic changes quantified in AAA with increasing exercise intensity using image-based CFD. They started with the hypothesis according to which the progression of AAA may be slowed by altering the hemodynamics in the abdominal aorta through exercise[9]. Ten subject-specific models were constructed from magnetic resonance angiography data and physiologic boundary conditions were derived from measurements made during dynamic exercise. They measured the abdominal aortic blood flow at rest and during

exercise, and quantified mean wall shear stress (WSS), oscillatory shear index, and particle residence time. They observed that an increase in the level of activity correlated with an increase of mean WSS and a decrease of OSI at three locations in the abdominal aorta, and these changes were most significant below the renal arteries. As the level of activity increased, particle residence time in the aneurysm was significantly decreased. Most of the reduction of particle residence time occurred from rest to the mild exercise level, suggesting that mild exercise could be a solution for reducing flow stasis in AAAs.[11]

A really interesting and recent study on the hemodynamic of renal artery stenosis has been performed from the the Department of Diagnostic Radiology in collaboration with Shanghai Medical College of Fudan University. Zhang et al. (Shanghai, 2013) evaluate the feasibility of CFD simulations in analysis of renal artery stenosis based on unenhanced MR angiography (MRA). Renal artery stenosis (RAS) is the cause of hypertension on renal vessels in approximately 1–5 % of hypertensive patients. Thirty hypertensive patients with unilateral renal artery stenosis and ten controls cases; peak systolic velocity for steady-state simulations has been detected by Ultrasound (US). Stenosis grades and hemodynamic variables at the stenosis of main renal artery, including pressure difference (PD), velocity and mass flow rate (MFR), were analyzed. For normal renal arteries, the average PD, velocity and MFR were all in the reported normal physiological range. However, for stenotic arteries, the translesional PD and velocity of main renal arteries increased with the severity of stenotic degrees, while the MFR decreased (Figure 2-9). 50 % diameter stenosis was the threshold at which all three hemodynamic parameters experienced significant changes. They concluded that the combination of unenhanced MRA with CFD is a good attempt to utilize completely noninvasive methods for comprehensive evaluation of renal artery stenosis.

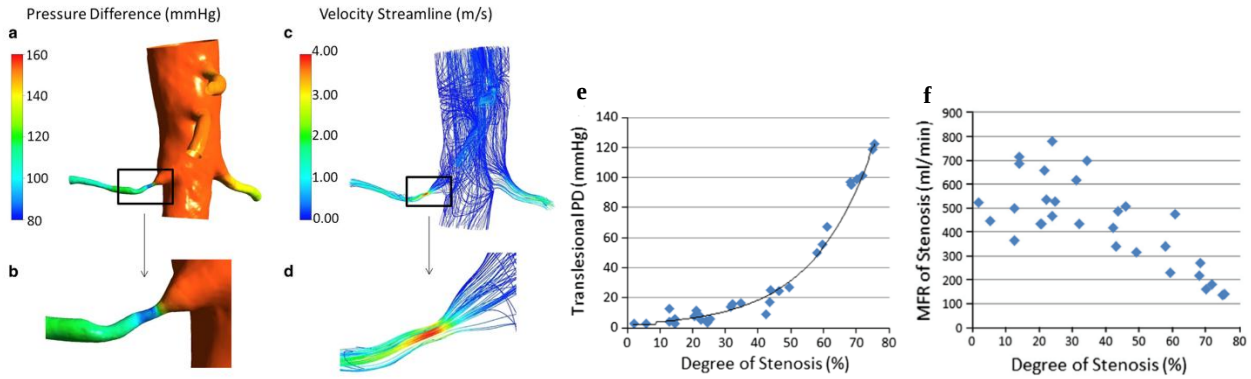

Figure 2-9. Detailed results of Pressure Difference (PD) and velocity of a hypertension case and a diameter stenotic degree of 59.4 % of the right main renal artery. a) PD of the whole domain. b) Translesional PD (mean 55.06 mmHg) of enlarged stenotic part of right main renal artery. c) Velocity streamline of the whole domain. d) Velocity detail (maximum 3.76 m/s) of enlarged stenotic part. e) Scatterplot showing um of the static pressure difference (PD) of different stenosis. f) Scatterplot of mass flow rate (MFR) of stenosis.

CHAPTER 3
METHODS

3.1 Patient Data and General Situation

Contrast-enhanced Computed Tomography Angiography (CTA) scans of five AAA patients who underwent ChEVAR were obtained from the North Florida/South Georgia Veterans Health Affair of Gainesville (Gainesville, FL).

All the patients present comorbidities, and some of them had other aortic repairs in the past, this is a pretty normal scenario for patients who undergo ChEVAR. In particular, the three male and two female patients between 65 and 83 years old present hypertension, none suffer diabetes, renal insufficiency or cerebrovascular accidents, two of them are smokers and some of them had other comorbidities, such as coronary artery disease (CAD), congestive/chronic heart failure (CHF), and chronic obstructive pulmonary disease (COPD) (Table 3-1).

Table 3-1. Patients' data and health background. Possible comorbidities: Smoking, Hypertension, Diabetes, Renal Insufficiency, CVA (cerebrovascular accident), COPD (chronic obstructive pulmonary disease), CAD (coronary artery disease), CHF (chronic heart failure). OAR = open aneurysm repair.

Patient #	Age [years]	Gender	Smoking	Hypertension	Diabetes/ Renal Insufficiency/ CVA	Total Comorbidities	Prior Aortic Repair	Prior Aortic Repair- year
1	66.6	M	1	1	0	2	1	OAR - 2005
2	76	M	0	1	0	1	1	Ancure[a] - 2000
3	83	M	1	1	0	3 (COPD)	0	--
4	75	F	0	1	0	4 (COPD, CAD, CHF)	0	--
5	65	F	0	1	0	3 (COPD, CAD)	1	EVAR - 2007

[a] Ancure endograft (Guidant Corporation, Indianapolis, IN, USA) received marketing approval from Food and Drug Administration (FDA) in 1999; now it is no longer on the market.

All five patients underwent surgeries in 2009; one suffered suprarenal AAA, one juxtarenal AAA and one other presented a post-open surgery situation. Zenith stent grafts have been used in the aortic lumen during the surgical operation and every patient needed between two and three iCAST stent grafts (in PTFE) for the Chimney technique (Figure 3-1, Table 3-2).

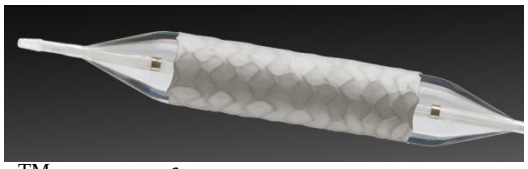

Figure 3-1. Perifferical ICAST™ stent graft in PTFE.

iCAST™ balloon-expandable stent graft is an Atrium Medical Corporation (Hudson, NH) device. It came on the market in 2006, one of the first cases scientifically described was a successful repair of splenic artery aneurysm.[26] The iCAST covered stent has a PTFE film lamination technology to maximize stent conformability to the vessel wall and a one-step balloon deployment technique.

Table 3-2. Pre-surgery description and surgery information.

Patient #	Procedure Date	Aneurysm Type	Stent Graft Type	# Aortic Devices	Proximal Covering Zone	Distal Extention	# Chimney stent	Chimney description [mm]: SMA L-Renal R-Renal
1	11/30/09	Post-surgical Thoraco-AAA	Zenith	1	Supra-SMA	Infrarenal Aortic	3	9x38 iCast; 7x38 iCast; 7x38 iCast
2	10/21/09	Suprarenal AAA	Zenith TX2	1	Supra-SMA	Infrarenal Aortic	2	8x59 iCast; 7x59 iCast; --
3	12/16/09	Suprarenal AAA	Zenith EVAR	1	Supra-SMA	Infrarenal Aortic	3	7x38 iCast; 5x59 iCast 6x59 iCast;
4	9/16/09	Juxtarenal AAA	Zenith EVAR	2	Supra-Renal	Infrarenal Aortic	1	-- -- 6x38 iCast
5	10/21/09	Infrarenal AAA	Zenith TX2	1	Supra-SMA	Infrarenal Aortic	2	8x59 iCast; -- 7x59 iCast;

Zenith ® stent graft is a Cook Medical product; Cook ® (1963, Bloomington, Indiana, IN) started his business in the healthcare field with production of wire guides, needles and catheters. Today, Cook Medical makes 16,000 products that serve 13 hospital lines, and they represent one of the top devices available on the market. Figure 3-2 shows the two model of devices used for the five patients.

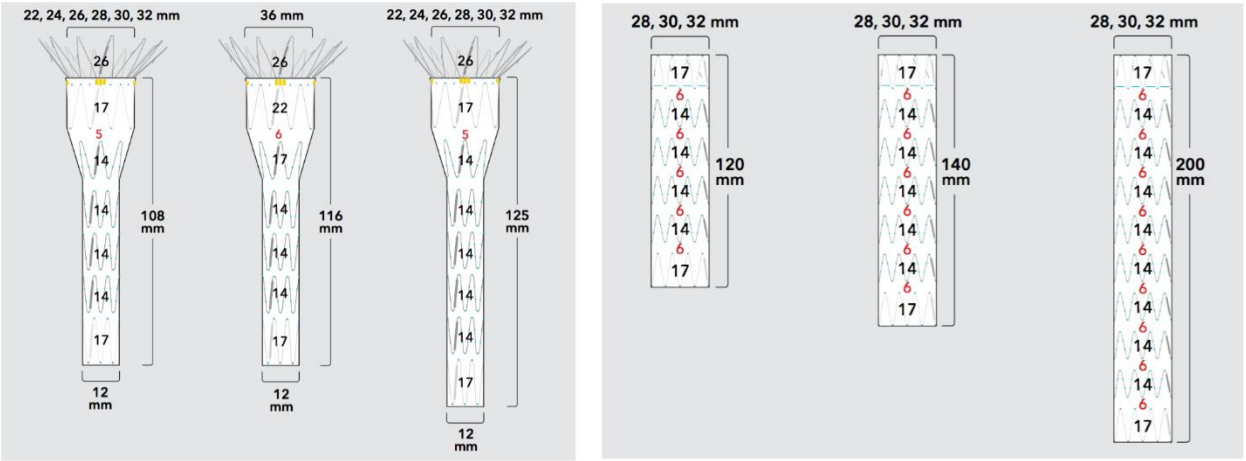

Figure 3-2. Aortic stents. A) Zenith EVAR (Zenith Renu AAA Ancillary) 3 out of 5 different sizes. B) Zenith TX2 3 out of 6 different sizes.

PreOp and PostOp situations were monitored by Computed Tomography Angiography (CTA) and some stent failures, due to thrombosis, were discovered within few months after surgery (Table 3-3). Moreover, in two cases surgeons decided to intentionally cover one renal artery; a decision that is made when the blood flow in this vessel is not already enough (the kidney is not working physiologically) and to put another chimney stent would worsen the situation due to its position for example. This technique envisages use of embolization coils in platinum with synthetic fibers (Figure 3-3).

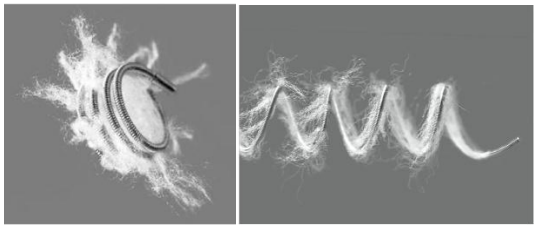

Figure 3-3. COOK® Medical Nester® embolization coil.

Table 3-3. Imaging modality and after surgery information.

Patient #	Imaging Modality	# CTA Postop	Stent with Thrombosis	Stent with Thrombosis Description	Time of Stent with Thrombosis [months]	Notes
1	CTA	4	1	L renal	0.5	
2	CTA	3	1	SMA (asymptomatic)	7.4	R-Renal intentionally covered;
3	CTA	2	1	L renal	11.5	
4	CTA	3	0	--	--	
5	CTA	5	0	--	--	L-Renal intentionally covered

One pre-operative CT (few days/ months before surgery) and more post-operative CTs (few days, around 1 month, 6-8 months, and 12-14 months after surgery for almost every patients, plus around 22 months, 34 months and 45 months after surgery only for one patient) have been considered for this study (Table 3-4).

Table 3-4. Computed Tomography scan dates. PreOp = few days/ months (d-m) before surgery; PostOp1 = few days (~d) after surgery; PostOp2 ≅1 month after surgery; PostOp3 = 6-8 months after surgery; PostOp4 = 12-14 months after surgery; PostOp5 ≅ 22 months after surgery; PostOp6 ≅ 34 months after surgery; PostOp7 ≅ 45 months after surgery.

Patient	PreOp (d-m)	OR Date	PostOp1 (~d)	PostOp2 (~1 m)	PostOp3 (6-8 m)	PostOp4 (12-14 m)	PostOp5 (~22 m)	PostOp6 (~34 m)	PostOp7 (~45 m)
1	11/27/09	11/30/09	12/02/09	12/11/09	7/9/10	2/18/11	--	--	--
2	7/10/09	10/21/09	10/22/09	11/23/09	5/28/10	--	--	--	--
3	11/16/09	12/16/09	--	1/22/10	--	11/30/10	--	--	--
4	8/7/09	9/16/09	9/22/09	10/16/09	3/5/10	--	--	--	--
5	10/19/09	10/21/09	--	11/20/09	5/28/10	--	8/5/11	8/17/12	9/10/13

Finally, data about technical success, intra- and post-operative complications, and deaths have been taken. Only one patient incurred in intraoperative thrombosis case, but all of them pursued technical success.

The technical success[b] is defined as the proper placement of the graft by using endovascular techniques, it must be maintained for 30 days after the procedure without death or

[b] Technical success consists of successful access to the arterial system using a remote site, successful deployment of the endoluminal graft with secure proximal and distal fixation of the attachment devices without persistent perigraft endoleakage, and patent endoluminal graft without significant twist, kinks, or obstruction >20% by intraoperative angiogram diameter measurements.[3]

need for standard aortic reconstruction. It differs from the clinical success for the absence of perigraft endoleak. Thus, clinical success can be claimed, even if the patient has a persistent endoleak that seals spontaneously within 6 months and does not develop aneurysmal expansion or rupture. Therefore, graft endoleaks that persist longer than 6 months or aneurysms that expand should be considered clinical failures.3

Two of the five patients had endoleaks after few days/ some months (Table 3-5).

Table 3-5. Technical success, IntraOp and PostOp complications. Y= yes; N=no; 1= no data, but apparently positive result; 0= no data, but apparently negative result.

# Patient	Technical Success	Intra Operative Complications	Endoleak	Time 1st Endoleak [months]
1	1	0	N	
2	Y	N	N	
3	1	0	N	
4	Y	N	Type 1	0.2 -1
			Type 2	5.6
5	Y	R brachial thrombosis (realized POD#1)	Type 1a	34.4

The last two patients of the 5 will be considered as controls since they did not present any complications or stent failure (the fifth patient had only an intentional occlusion of the left renal artery during the surgery, but it is not considered a complication); moreover, the fourth patient has two non-stented arteries which could represent pathological but still working vessel situations.

The purpose of this study is to determine local hemodynamic changes caused by unavoidable modifications in vessels conformation after ChEVAR. Computational fluid dynamic (CFD) simulations have been used to evaluate changes in superior mesenteric artery (SMA) and renal arteries cross-sectional areas, pressure, and wall shear stress.

The following paragraphs will analyze technical procedures and the hypothesis assumed for this study.

3.2 Step 1: Segmentation in Amira

The images have been processed utilizing the commercial software platform for 3D and 4D data analysis, Amira.

Amira® is a powerful, multifaceted software platform for visualizing, manipulating, and understanding biomedical data coming from different types of sources and imaging modalities.

The segmentation of the inner lumen of the abdominal aortic tract included SMA and renal arteries. The celiac artery has not been included in the segmentation process because it was not always possible for every patient, due to the lack of contrast in some CT scans.

Tissues within the window have different shades of gray (brightness) and visible contrast.

The intensity of different materials (shades of gray) values may reach -1000 in case of air and around 3000 in case of metals. I usually chose a set data window between -200 and 800, which gives a bright and clear view of the aortic situation; only the part where there is blood flow needs to be segmented. This introduces one first hypothesis, in the aortic lumen the wall of the segmented zones will be assumed aorta wall even if sometimes it is thrombus material between the wall and the actual lumen (Figure 3-4).

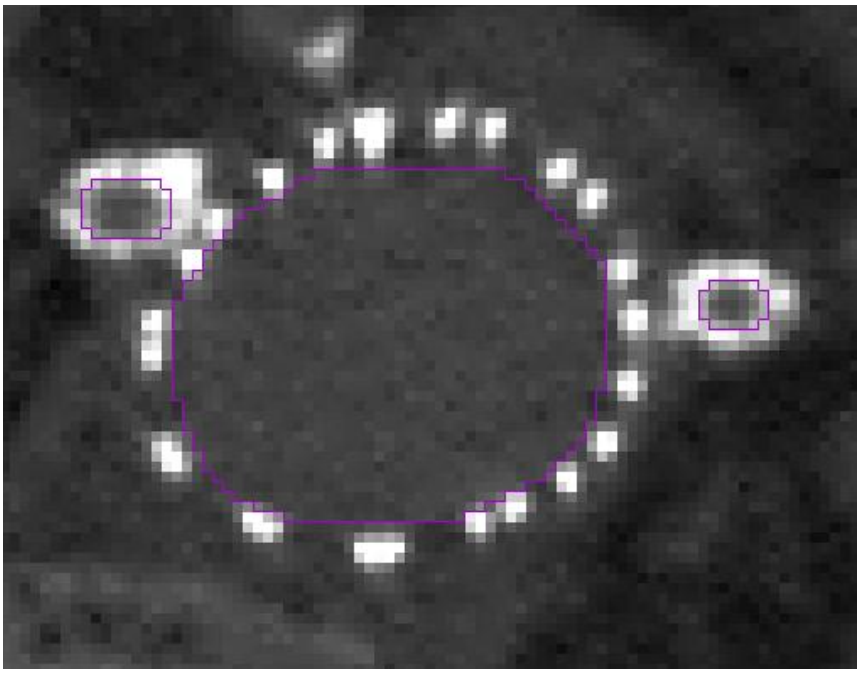

Figure 3-4. Example of CT segmentation in Amira. The purple line represents the segmented areas. It is possible to observe a brighter area, on the right renal artery, which is a small calcification on the vessel wall.

A similar hypothesis will be assumed for the segmentation of the chimney stents; their structure would give different response to the flow, but during the simulations they will be consider the same material as vessel wall. The main segmentation criterion has been the presence of fluid contrast, in case of insufficient quantity of contrast, the vessel segmentation has been stopped at the end of the stent. Other criteria have been the presence of artery bifurcations and vessel length.

The white areas represent either stents or calcifications (usual intensity of around 800-1500 for calcifications and 1500-3000 for stents), the areas with blood (greyscale, with intensity up to 300) can be recognized thanks to the contrast liquid used during the imaging procedure; sometimes thrombosis' areas are visible in the lumen and their color is darker than blood areas' color, because of lack of contrast. Thrombus can form within few days or months, therefore they can be observed between one CT and the next (few days/ 6 months); on the other hand, formation of calcifications needs longer periods.

The thickness of the arterial wall could not be detected from the CT scans so a uniform value of 1.8 mm was assumed for both the pre- and post- operative models; the thickness of the stents and stent grafts that is assumed to be around 0.2 mm for Zenith devices has been segmented around 0.8-1.6 mm. This is for one main reason, CT scans (with voxel dimensions either 0.74x0.74x1 or 0.84x0.84x1 or 0.93x0.93x1) have usually shown around two pixels layers as stent thickness, most likely due to artefacts; this means a thickness of stent around 1.6 mm instead of 0.2 mm (Figure 3-5).

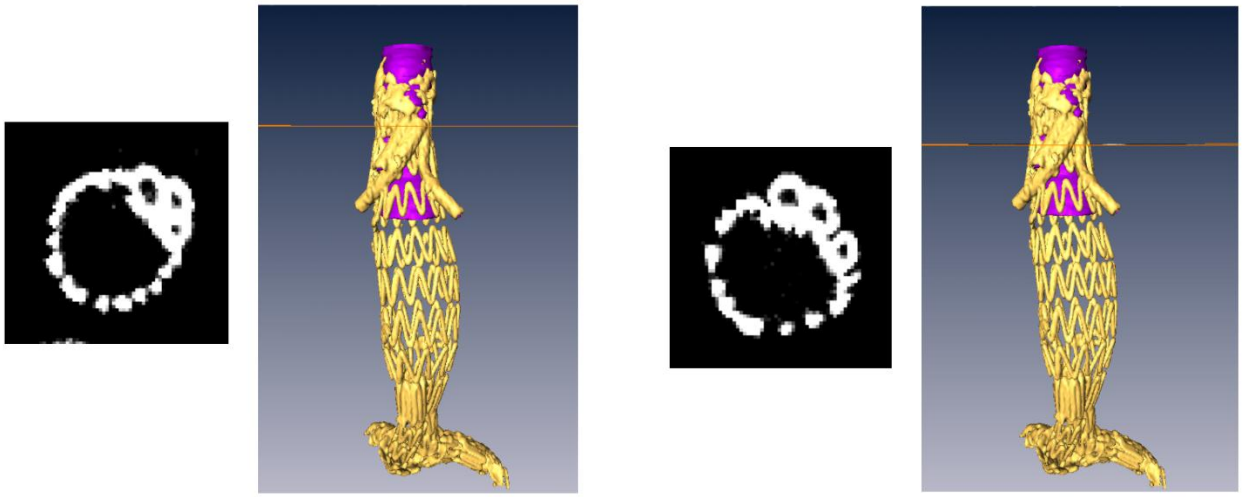

Figure 3-5. Examples of thickness of the stents due to artefacts, with 3D segmented geometries inside the stent.

In order to overcome this issue, a larger area than the one shown in CT scans needs to be included in the segmented lumen for the smaller vessels (leaving out of the lumen one layer of voxel, equal to 0.8 mm circa as stent thickness). This could not be the solution in areas close to the aorta lumen, where it would cause a 3D geometry with incorrect connections between the main lumen and the smaller vessel. That is why a double layer of voxels correspondent to stent thickness around 1.6 mm has been segmented in proximal lumen of the smaller arteries.

For patients who received Zenith EVAR stent graft implantation (Figure 3-2, A), some hypotheses have been assumed in the main lumen segmentation. The issue regards the upper part of the abdominal aorta segmentation (just before the SMA), where the stent graft begins; its metallic structure, 26 mm long, makes the blood flow pass through it, but it could cause hemodynamic perturbations. Nonetheless, the presence of this metallic structure and its consequences have been mostly ignored, in order to give priority to the creation of a better geometry and mesh.

The final 3D geometries, representing the lumen of aorta vessel and stent graft, come from 100 segmented slices (around 10 cm long) from around 3 cm before the SMA to around 3 cm

after the last renal artery; finally, smoothed surfaces were generated from them (Figure 3-6, saved as .stl format file).

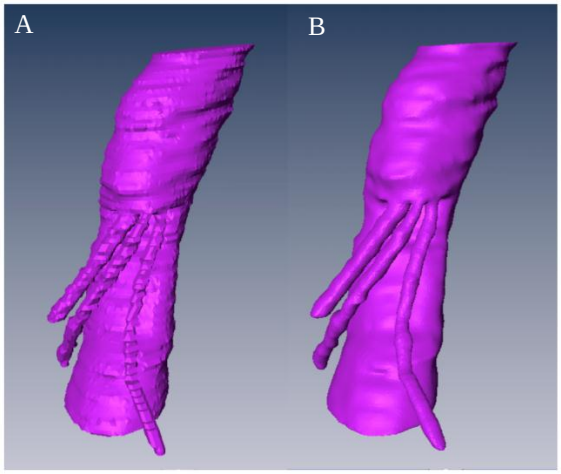

Figure 3-6. Examples of geometry in Amira pre- and post- smoothing. A) Segmented unsmoothed geometry. B) First geometry smoothing in Amira.

3.3 Step 2 and 3: Surface Smoothing in Geomagic and Geometry Extension in VMTk

The smoothed surfaces have been processed in Geomagic Studio, where the noise and spikes were reduced (Figure 3-7, A). Geomagic Studio® is the complete toolbox for transforming 3D scanned data into highly accurate surface, polygon and native CAD models.

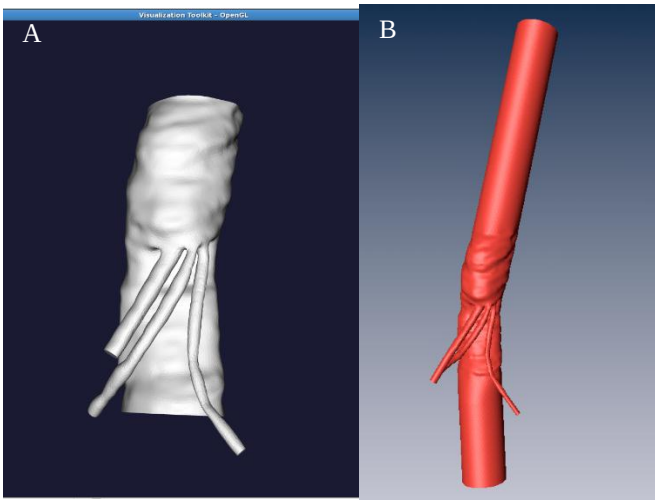

Figure 3-7. Example of pre- and post- extension geometry. A) Example of geometry after noise reduction and spike remotion. B) Example of geometry extension.

The ends of geometries have been cut to have a better shape and left open in order to be extended in the Vascular Modeling Toolkit (VMTk), as .stl files.

Vascular Modeling Toolkit is a collection of libraries and tools for 3D reconstruction, geometric analysis, mesh generation and surface data analysis for image-based modeling of blood vessels.

The extension at the inlet is needed in order to assure fully developed velocity profiles were formed at the boundary layer in the original geometry (tracts of interest), and at the end of the vessels in order to reduce the reverse flow at the outlets. Reverse flow is a phenomenon which happens for example when the outflow is near a recirculation zone; it means that is incorrectly entering fluid from the outside.

The geometries have been extended 5 times the vessel diameter size at the aortic output and 10 times for the inlet and all the smaller output (SMA and renal arteries, Figure 3-7, B).

The extended domains at the inlet and outlets were only for the purpose of the simulation and were not included in the analysis of flow characteristics (VMTk reads and creates .stl files).

3.4 Step 4: Meshing in Ansys ICEM CFD

The extended geometries have been meshed using ANSYS® ICEM CFD™ Meshing Software (R14.5). It is a commercial software used for CAD and mesh generation, it can create structured, unstructured, multi-block, and hybrid grids with different cell geometries.

In computational fluid dynamics, the mesh or grid is a discrete representation of the geometry as a finite number of nodes (grid points) and elements (control volume into which domain is broken up, otherwise named cells). In fact, the need of this concept is to convert a continue problem into a discrete one in order to be solved by a computational point of view. Essentially, it assigns cells over which the fluid dynamics problem is solved; several parts of the mesh are grouped into regions (zones) where boundary conditions may be applied in order to

solve the numerical problem. The mesh may be composed by many cell types, triangle and quadrilateral 2D prism, tetrahedrons, pentahedrons, hexahedrons, and pyramids (3D).

Moreover, mesh has a significant impact on the rate of CFD simulation convergence (or even lack of convergence), solution accuracy and CPU (process) time required.

Mesh quality is a really important goal to achieve. The mesh density should be high enough to capture all relevant flow features. The grid adjacent to the wall should be fine enough to resolve the boundary layer flow[c]. A poor quality grid will cause inaccurate solutions and/or slow convergence.

After creation of parts (aorta_outlet, aorta_wall, inlet, SMA, R_renal, L_renal) in the geometry, extraction of the feature curves at inlet and outlets, and creation of material point (body), global Delaunay mesh with three boundary layers (max element between 1.2-2 and minimum element size 0.1-0.7) has been generated, in order to get around 1-2 million elements for each extended geometry (Figure 3-9).

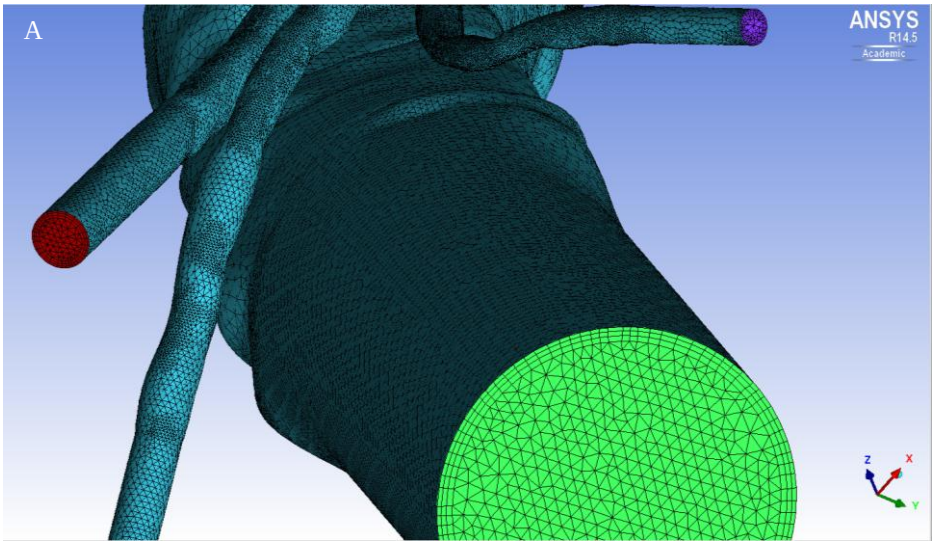

Figure 3-8. Example of meshed geometry. A) Aorta outlet; B), C), D) the smaller outlets, respectively SMA, right renal and left renal arteries.

[c] There are four main measures of quality: skewness, smoothness (change in size), minimum angle, and aspect ratio.

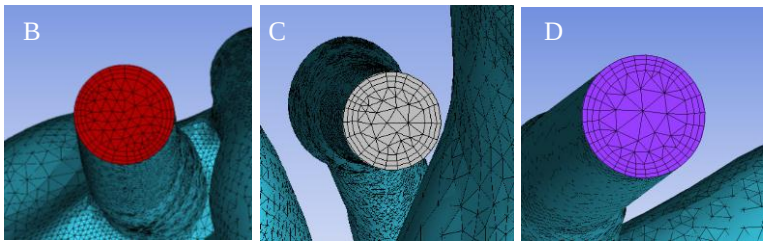

Figure 3-8. Continued.

1-2 million elements meshes resulted to be the best choice in terms of achieved convergence, hemodynamic results and simulation time. Mesh experiments have been performed; it resulted that meshes around 500 thousands elements do not reach convergence and show lower hemodynamic values (Figure 3-9, blue line); meshes around 5 million elements showed convergence but hemodynamic results are the same of 1-2 million element meshes (Figure 3-9, respectively green and red curves), and the simulations lasted more than 5 times longer.

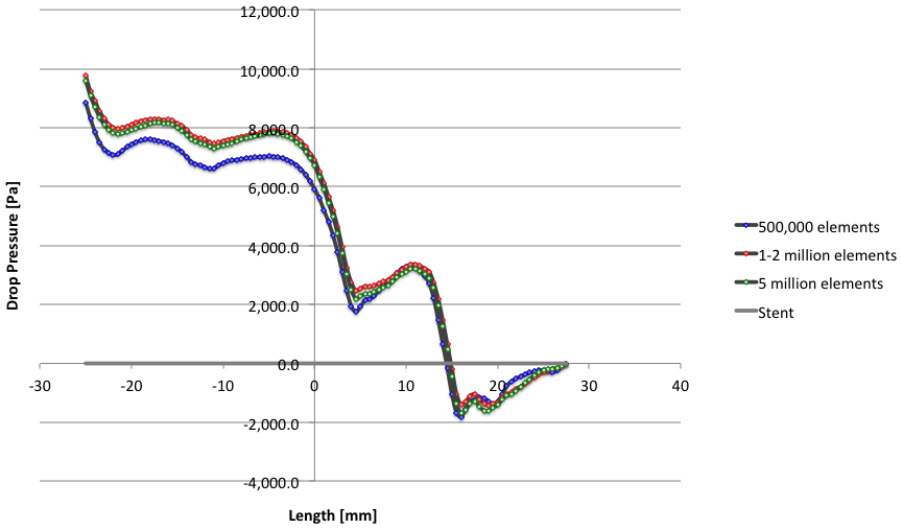

Figure 3-9. Mesh experiments. Difference of pressure on PostOp1's patient 3 computed on diverse number of elements' meshes.

The mesh methods (Octree, Delaunay algorithms) define where to locate the interior nodes; they are inserted incrementally into the boundary mesh, redefining the triangles or tetrahedral locally, so the new node is inserted to maintain the chosen criterion. In Delaunay mesh algorithm, nodes are introduced for instance in a regular lattice (rectangular, triangular, etc.), in

triangle centroid, triangle circumcenters, etc. In order to guarantee the mesh quality, Delaunay triangulations maximize the minimum angle of all the triangles ($\alpha > 30°$, as predefined value).

Every mesh has been globally smoothed, using quality (up to 0.2), minimum angle (up to 18^o) and aspect ratio criterions (up to 0.2; 20 smoothing iterations for all of them); it has been finally checked in order to correct errors (such as duplicate elements, uncovered surfaces, missing internal faces, volume orientation, surface orientation, and hanging elements) and possible problems (such as multiple edges, triangle boxes, single edges, non-manifold vertices, and unconnected vertices).

Ansys Fluent as output solver and Nastran as common structural solver have been finally set for each meshed geometries (.msh file format) in order to be loaded and read in Fluent.

3.5 Step 5: Simulations in Ansys Fluent

After checking of domain extents through 'mesh scale' and face area statistics check, the fluid parameters have been set. Incompressible, homogeneous, Newtonian (constant viscosity) fluid in a rigid geometry have been assumed for the fluid flow simulations, considering value of blood density ρ = 1050 Kg/m^3 and blood viscosity $\mu = 0.0035$ Kg/m/s.

Transient Navier-Stokes governing equations were solved by Ansys Fluent on the basis of the finite volume method. The Mass Balance (3-1) and simplified Navier-Stokes (3-2) equations for an incompressible, homogeneous, Newtonian liquid are, respectively:

$$\rho \nabla \cdot v_i = 0 \tag{3-1}$$

$$\rho \frac{\partial v_i}{\partial t} + \rho v_j \cdot \nabla v_i - \nabla \cdot \sigma_{ij} = 0 \tag{3-2}$$

where ρ is the density, v_i the velocity vector in the blood vessel (the index indicates the three directions on the axes x_1, x_2, x_3), σ_{ij} is the fluid stress tensor on the three directions (i = 1, 2 , 3), each of the ones will be derived in the three directions (j = 1, 2, 3). The first term represents

the inertial component, the second the convective component (centrifuge accelerations), and the third the 'forces' on surfaces.

The constitutive equation:

$$\sigma_{ij} = -\delta_{ij}\, p_i + \lambda\, \delta_{ij} V_{kk} + 2\mu V_{ij}, \tag{3-3}$$

where p_i is the pressure, δ_{ij} is defined as

$$\begin{cases} \delta_{ij} = 1 & if\ i \neq j \\ \delta_{ij} = 0 & otherwise, \end{cases}$$

the stress gradient, V_{kk} is

$$V_{kk} = V_{11} + V_{22} + V_{33}, \tag{3-4}$$

and the velocity gradient, V_{ij} is

$$V_{ij} \triangleq \frac{1}{2}\left(\frac{\partial v_i}{\partial x_j} + \frac{\partial v_j}{\partial x_i}\right) \tag{3-5}$$

is used to solve the system.

These equations were then discretized, using second order for pressure and second order Upwind for momentum as spatial discretization. These two methods compute an approximation of velocity and pressure values based on three points instead of two (first order), they guarantee stability and they are pretty quick computational methods. SIMPLE (Semi Implicit for Pressure Limited Equation) scheme as pressure-velocity coupling algorithm has been used.

The standard relaxation parameters of solution control have been used, 0.3 for pressure and 0.7 for momentum.

Scaled residuals of x-velocity, y-velocity, z-velocity, and continuity have been set to 10^{-5}; the concept of residuals comes from the computational analysis problem which does not give exact results (like in case of analytical solutions); there is always going to be an error that we can impose to be smaller than an arbitrary number. Solver residuals represent the absolute error in the solution of a particular variable. Saving residuals code in the 'execute commands' panel has been

set, in order to check residuals at the end of simulations and solutions convergence. A standard initialization has been imposed for every simulation.

Boundary conditions of a stress free outflow, stationary and no-slip conditions at the walls, and uniform inlet velocity profile have been implemented to obtain the solution.

First, steady state simulations have been executed to have a first rapid result and double check of the mesh quality; a symbolic constant velocity of 0.1 m/s has been set each time. Then transient simulations were launched with hypothesis of pulsatile blood flow.

The applied flow rate waveform is shown in Figure 3-10 which depicts the blood flow through the infra-renal abdominal aorta of a general patient under resting conditions (re-elaborations of Taylor's curves[27]).

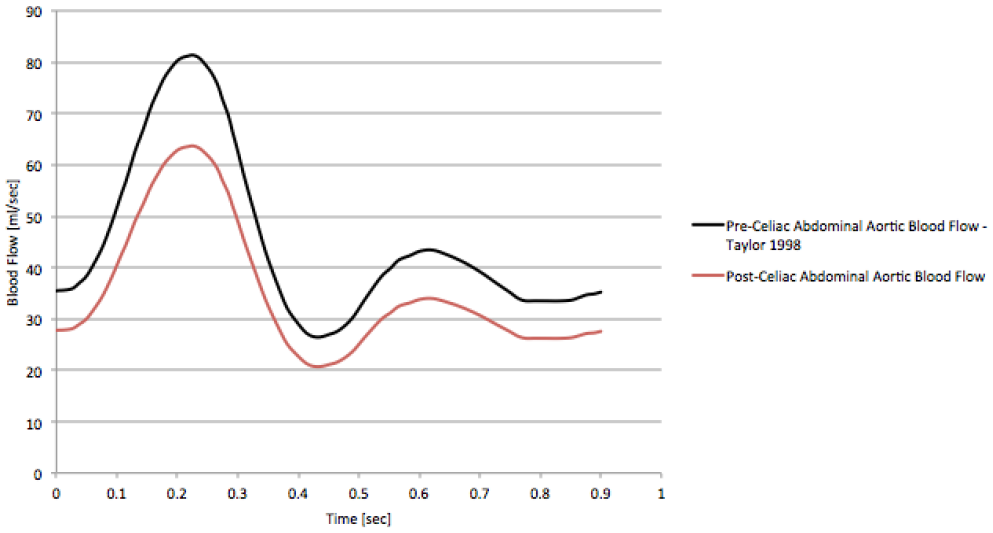

Figure 3-10. Flow rate wave at the abdominal aorta inlet.

Since the celiac artery has not been segmented, the waveform of blood flow after the celiac artery has been used at the inlet of the abdominal aorta for the 3D model simulations (Figure 3-10, red curve). This has been computed considering a blood flow of 2711.3 ml/min as pre-celiac flow rate in the aorta, and subtracting 21.72% of this flow rate (equal to 588.9 ml/min, blood flow in the celiac artery); 2122.4 ml/min has been obtained as blood flow going into the

renal arteries, superior mesenteric artery and infrarenal aortic segment (through the bifurcation into the legs). These numbers have been computed thanks to elaboration of data extracted from image files (blood flow curves in the abdominal tract[27]) by using Matlab code. The velocity inlet data set has been computed from this curve for each patient by using the values of inlet areas and the well-known formulas, which relates the flow rate (Q) and the velocity (v) through the area (A):

$$Q = v \cdot A \tag{3-3}$$

Simulations with +/- 25% of the values of blood flow at the aorta inlet have been computed (Figure 3-11), in order to have a wider panorama of situations, since this value is strongly variable among subjects, and to understand how the hemodynamic parameters change depending from the flow rate variability. Moreover, hypothesis of zero pressure has been set at the aorta inlet.

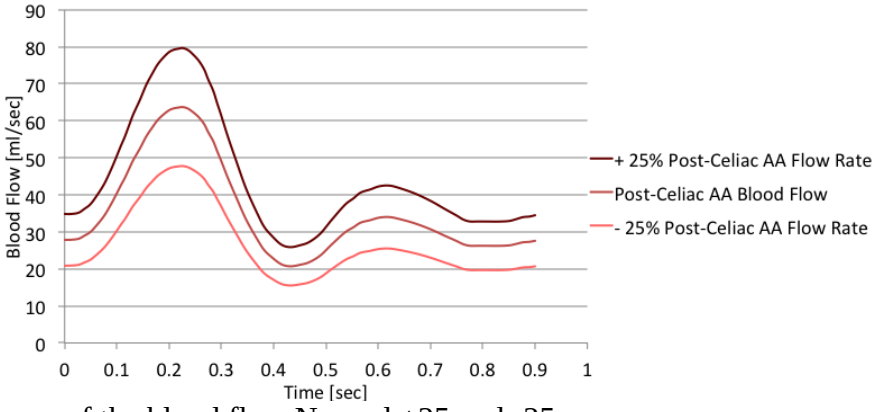

Figure 3-11. Curve of the blood flow Normal +25 and -25.

In a normal situation, the outflow boundary conditions have been fixed as follow: 18.5% for each renal artery, 19% for the superior mesenteric artery (SMA) and 44% for the main aorta outlet in case of no occlusions; these approximations come from the curve of Taylor[27]. Table 3-6 shows a complete scenario of the boundary condition percentages in cases of SMA or renal artery occlusions.

Table 3-6. Outflow boundary conditions, in four possible cases (normal flow, SMA occlusion, renal occlusion, SMA and renal occlusion). The case of SMA occlusion and no occluded renal artery never happened for any of the five subjects.

	NO RENAL ARTERY OCCLUSION			WITH RENAL ARTERY OCCLUSION		
	Blood	Blood Flow Percentages [%]		Blood	Blood Flow Percentages [%]	
Outlets	Flow [ml/min]	Regular flow	SMA occlusion	Flow [ml/min]	Renal occlusion	Renal and SMA occlusions
SMA	403/0	19	0	424/0	20	0
Left Renal	394	18.5	23	0/555	0/26	0/32.5
Right Renal	394	18.5	23	555/0	26/0	32.5/0
Main Aorta	931	44	54	1153	54	67.5

In particular, a decreasing of flow rate (Figure 3-12, green curve) at the inlet has been hypothesized in case of SMA occlusion, since the tissue sprinkled by the SMA (duodenum, transverse colon, and pancreas) would receive blood from other vessels (celiac artery and its branches) located in the upper abdominal aortic tract.

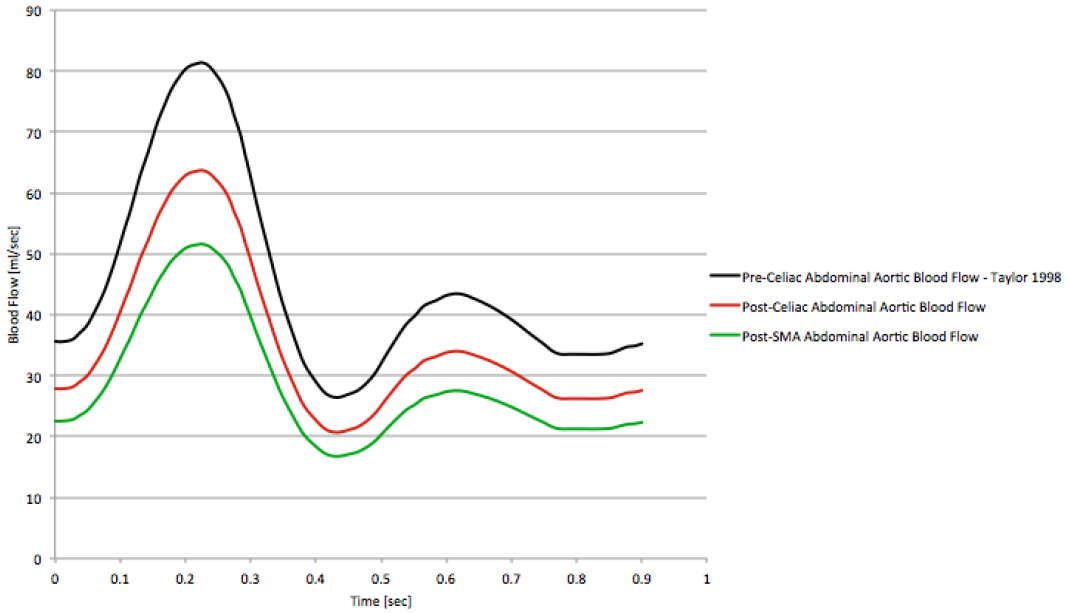

Figure 3-12. Curve of blood flow [ml/sec] at a pre-celiac level (black), post-celiac level (red), and post-SMA level of the abdominal aortic tract (green).

Transient simulations of 550 time steps for a time step dimension of 0.002 sec have been imposed. These values come from 0.9 sec of a pulse duration, divided by 0.002 (reasonable dimension of time step); 100 time steps have been added (450+100) in order to be able to discard

the first 100 steps that may give less precise results, because of their proximity to the beginning of the simulation. The results have been saved every 10 time steps.

Files .cas and .dat have been obtain and have been elaborated in Tecplot.

3.6 Step 6: Centerlines Computation in VMTk and Data Elaboration in Tecplot

Centerlines have been computed in VMTk from the .stl file of geometry without extension, and the .dat file processed in Matlab with two codes, in order to obtain the .dat files of cross_sectional_areas, centerlines and centerlines_normal useful for Tecplot to compute the values of wall shear stresses and pressure on the wall. The cutoff value has been chosen between 7 and 30 for every geometry.

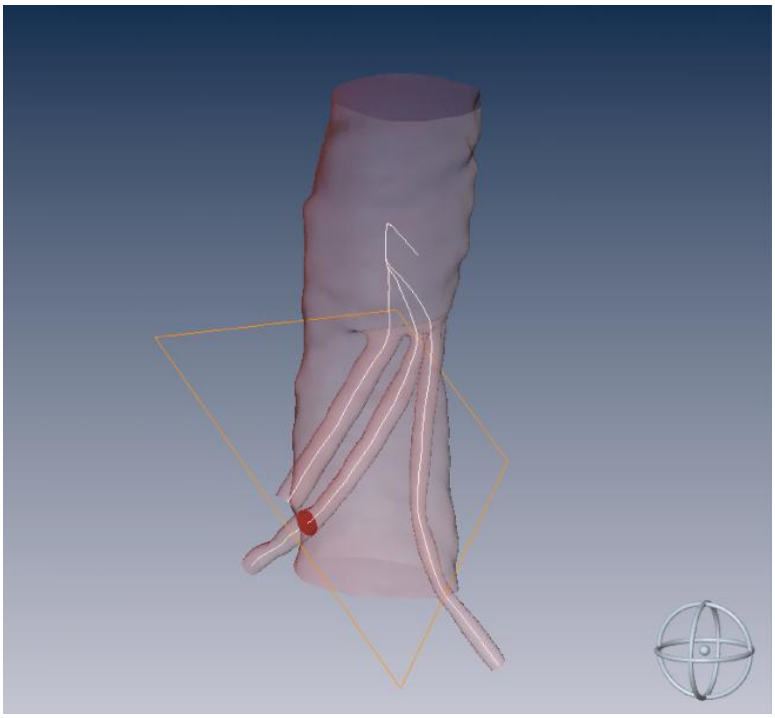

Figure 3-13. Centerlines in Amira.

Centerlines (Figure 3-13) are powerful descriptors of the shape of vessels; they are determined as weighted shortest paths traced between two extreme points[28]. In order to ensure that the final lines are central, the paths cannot lie anywhere in space, but are bound to run on the

place where the centers of maximal inscribed spheres[d] are defined (Voronoi diagram of the vessel model). The algorithm implemented in VMTk for centerlines computation starts from surface models, and has the advantage that it is quite stable to perturbations on the surface.

Tecplot 360 is a visualization software tool (Tecplot Inc, Bellevue, Washington) that is able to analyze complex data, arrange multiple layouts, and show CFD and CAE post-processing data.

Values at the peak of the flow rate curve have been analyzed since it could represent the worst case in term of wall shear stress (WSS) and difference of pressures. It corresponds at 0.22 sec = 110^{o} time step, according to the formula:

$$\frac{Time\ [sec]}{Time\ step\ size\ [sec]} = \#\ time\ steps$$

Fluent files .cas and .dat at 110 time step have been loaded using a 'Laplacian averaging to nodes'. Centerlines and Centerlines_normal files .dat have been loaded per each geometry (for the three flow rates hypothesized rate); macro (.mrc) file codes have been used to compute the cross sections in Tecplot.

It has been proved (Figure 3-14) that the mean value of pressures on the circumference of each cross sectional area is in the same range of the pressures on the centerlines, therefore it is reasonable to assume that the pressure on the whole cross sectional areas is in the same range; thus, the values of difference of static pressure have been evaluated on the circumferences of the CSA, but the values of total pressure has been computed on the centerlines since the dynamic pressure on the wall is zero.

[d] A sphere inscribed in an object is said to be maximal when there's no other inscribed sphere that contains it.

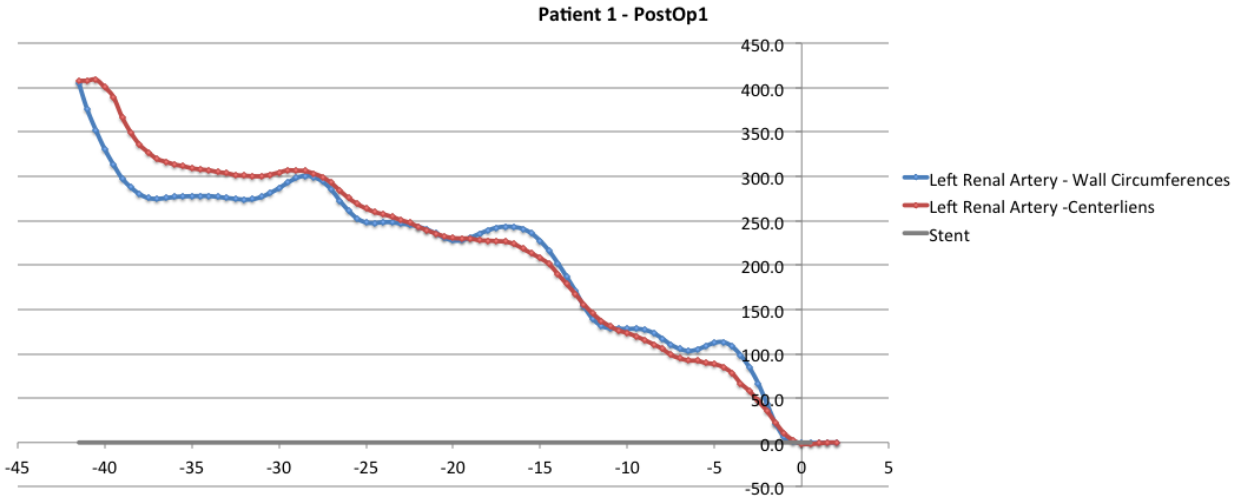

Figure 3-14. Comparison of values of difference of static pressure on the wall of the vessel and on the centerlines.

Tecplot computes pressures in Pascal; instead, values of wall shear stress are computed in Dyne/cm^2, thus they needed conversion to Pascal.

Files (.txt) containing values of wall shear stresses and pressures at 0.22 sec (#110 time step) have been obtained from Tecplot; they have been finally elaborated in Excel in order to obtain curves of WSS, total pressure, difference of static pressure, and intra- lumen areas along the SMA, right renal and left renal arteries' length.

CHAPTER 4
RESULTS

4.1 Segmented, Smoothed and Extended 3D Geometries

Smoothed and extended geometries have been obtained from each CT scan for every patient.

A clear panorama of before- and after- surgery situations of the vessels of interest for each patient's CT is shown in Table 4-1.

Table 4-1. Vessels with Chimney stent grafts, occlusions, and failures. Working/free vessel (√), occluded vessel (⊗), intentionally occluded vessel (coil = §), working stented vessel ($\surd_{stent}$), stenotic stented vessel ($\surd_{ss}$), occluded stent ($\otimes_{stent}$).

Patient #	Vessels	PreOp (d-m)	PostOp1 (~d)	PostOp2 (~1 m)	PostOp3 (6-8 m)	PostOp4 (~13 m)	PostOp5 (~22 m)	PostOp6 (~34 m)	PostOp7 (~45 m)
1	SMA	√	$\surd_{stent}$	$\surd_{stent}$	$\surd_{stent}$	$\surd_{stent}$			
	Rr	√	$\surd_{stent}$	$\surd_{stent}$	$\surd_{ss}$	$\surd_{ss}$	--	--	--
	Lr	√	$\surd_{stent}$	$\otimes_{stent}$	$\otimes_{stent}$	$\otimes_{stent}$			
2	SMA	√	$\surd_{stent}$	$\surd_{ss}$	$\otimes_{stent}$				
	Rr	√	§	§	§	--	--	--	--
	Lr	√	$\surd_{stent}$	$\surd_{stent}$	$\surd_{stent}$				
3	SMA	√		$\surd_{stent}$		$\surd_{stent}$			
	Rr	√	--	$\surd_{ss}$	--	$\surd_{ss}$	--	--	--
	Lr	√		$\surd_{stent}$		$\otimes_{stent}$			
4	SMA	√	√	√	√				
	Rr	√	√	√	√	--	--	--	--
	Lr	√	$\surd_{stent}$	$\surd_{stent}$	$\surd_{stent}$				
5	SMA	√		$\surd_{stent}$	$\surd_{ss}$		$\surd_{stent}$	$\surd_{stent}$	$\surd_{stent}$
	Rr	√	--	$\surd_{stent}$	$\surd_{stent}$	--	$\surd_{stent}$	$\surd_{stent}$	$\surd_{stent}$
	Lr	√		§	§		§	§	§

Patient 1 had bilateral crossing renal and SMA chimney stents; he did not have endoleaks issues after surgery. The left chimney failed after 1 month (PostOp2); interestingly, this stent was less stenotic than the right, but it occluded pretty soon after surgery. Stenosis developed in right renal chimney at renal origin on PostOp3, because of compression (>50%) between the arotic stent graft and the left renal artery, but it stabilized on PostOp4.

The second patient had implantation of two chimney stents on the SMA and left renal artery, the right renal was intentionally occluded. No endoelaks on the stents have been shown; SMA had abrupt angulation, but no frank kink/stenosis on the first after surgery CT (PostOp1),

severe kink/stenosis on the second CT (PostOp2), and finally the chimney failed because of thrombosis (PostOp3).

The third patient had three chimney stents that cross each other; the right renal stent was compressed by SMA stent (>50%, PostOp2) and the left renal chimney occluded as shown on the second CT (PostOp4). This patient did not have endoleaks either.

The chimney stent on the left renal artery of the fourth patient was affected by type Ia endoleak; the other two non-stented vessels did not present any issue.

Finally, the fifth patient needed an intentional occlusion of the left renal artery and two chimney grafts on the SMA and right renal artery. The first CT (PostOp2) showed a pretty good post- surgical situation; the second (PostOp3) presented a compression on the SMA and a developed endoleak around stent. Aneurysmal degeneration and no further stent compression have been observed on the third CT (PostOp5), but there is still endoleak around SMA chimney; in the PostOp6 endoleak continued worsening involving both SMA and R renal chimneys, and enlarging paravisceral aneurysm is observed. The last CT (PostOp7) showed continued progression of paravisceral AAA, enlarging endoleaks, but no stent compression. None of the five patients showed any vessel occlusion before the surgery.

Since it has been assumed a constant flow rate for all cases, it is interesting to evaluate the variability of the area inlets along the time (among CTs) for each patients; this is an important parameter since the velocity inlet is determined by it. What we are observing is actually the inlet area of extended aorta geometry, it varies between 500 and 1,600 mm^2; the first patient had biggest inlet areas in the last after- surgery configuration, while the third patient showed the smallest inlet areas in the first CT after surgery (PostOp2).

The actual values of areas at the inlet of each geometry and the comparison between inlet area (radius) in PreOp situations and average of the PostOp conformations are presented in Table 4-2 and Table 4-3 respectively.

Table 4-2. Inlet area of the extended aorta geometries for each patient during the time of interest.

	AREAS [mm^2]							
Patient	PreOp (d-m)	PostOp1 (~d)	PostOp2 (~1 m)	PostOp3 (6-8 m)	PostOp4 (12-14 m)	PostOp5 (~22 m)	PostOp6 (~34 m)	PostOp7 (~45 m)
1	897.600	1,226.421	1,272.563	1,377.441	1,579.549	--	--	--
2	723.751	723.109	650.012	738.905	--	--	--	--
3	691.706	--	567.252	--	632.585	--	--	--
4	1,1012.659	1,078.769	1,064.363	1,038.299	--	--	--	--
5	490.472	--	524.030	568.294	--	538.839	544.165	555.351

Table 4-3. Inlet area of the extended aorta geometries for each patient in PreOp and PostOps (Average ± Standard Deviation) situations and radius of the ideal circumference with those values of area lumen.

	AREAS [mm^2]		RADIUS [mm]	
Patient	PreOp (d-m)	PostOps	PreOp (d-m)	PostOps
1	897.600	1363.994 ± 156.983	16.903	20.837 ± 7.069
2	723.751	704.009 ± 47.425	15.178	14.970 ± 3.885
3	691.706	599.919 ± 46.197	14.838	13.819 ± 3.835
4	1,1012.659	1060.477 ± 20.513	17.954	18.373 ± 2.555
5	490.472	546.136 ± 16.746	12.495	13.185 ± 2.309

The first and the fourth patients showed the largest areas at the inlet. The firth patient showed the smallest inlet areas. In particular, the first patient has a pretty small PreOp inlet area as compared to the PostOp situations, where the area keeps growing and becomes 1.76 times larger than the inlet area of the PreOp conformation 14 months later, as observed in the last CT. The inlet areas for all the other patients remain pretty constant during that time period.

4.2 Meshed Geometries

Every geometry has been meshed while trying to maintain thewith a number of elements around 1-2 million in order to provide good simulations without computing excessive computation. Although the number of slices segmented and the extension ratio are the same for every geometry, The variability of the number of elements in the mesh among CTs and patients (Table 4-4) is usually caused by the geometry conformation, which is pretty different from one

patient to another, from PreOp geometry to a PostOp geometry, and usually among PostOp CTs too.

Table 4-4. Number of element of the mesh for every 3D geometry, for every patient.

	NUMBER OF MESH ELEMENT							
Patient	PreOp (d-m)	PostOp1 (~d)	PostOp2 (~1 m)	PostOp3 (6-8 m)	PostOp4 (12-14 m)	PostOp5 (~22 m)	PostOp6 (~34 m)	PostOp7 (~45 m)
1	1,109,784	1,055,253	940,402	1,159,815	1,001,573	--	--	--
2	1,876,631	1,016,382	998,077	1,046,368	--	--	--	--
3	995,972	--	1,251,157	--	1,134,936	--	--	--
4	1,493,564	1,383,286	1,126,170	1,650,496	--	--	--	--
5	2,014,167	--	1,753,462	1,091,228	--	1,158,134	1,073,138	1,189,205

The range of number of elements for all the geometries is 1,250,873 ± 309,538. The second and fifth patients have higher number of element on some of their geometries; the result of this could be a better simulation, even if the variation of element number is most likely not so relevant.

4.3 Convergence of Fluent Simulations

The concept of convergence is a pretty subjective one. It depends from how close to zero we want our error to go. By imposing 10^{-5} as scaled residuals, almost every simulation obtained convergence without fluctuations; the PreOp and PostOp2 of the third patient, the PreOp and PostOp2 of the fourth patient, and the PreOp of the fifth patient have continuity residual that do not converge. In the worst case, this could mean that the mass flow could be not well balanced. But analyzing the net flow rate for these 5 cases of no continuity- residual convergence, it resulted very small (between $3.8\ 10^{-14}$ % and $1.9\ 10^{-13}$ % of the total flow rate), thus it does not represent an issue for the simulation analysis. It has been possible to observe that PreOp geometries have shown more convergence problems, possibly due to their complicated conformations.

4.4 Data Elaboration: Total Pressure, Difference of Static Pressure, Wall Shear Stress and Cross Sectional Area

The hemodynamic situation along the SMA and renal arteries during the time (CTs) for each patient will be shown in the following paragraphs. The analyzed parameters are total pressure on centerlines, gradient of total pressure, difference of static pressure (ΔP) on the vessels wall, wall shear stress (WSS), and cross sectional area (CSA). Graphs of gradient of total pressures and difference of static pressure are shown in the Appendixes.

Curves of WSS and total pressure along the length of the three vessels have been created in three different situations: 2122.39 ml/min of blood flow at the inlet (the 'normal case', the computation of this value from Taylor curve has been explained in paragraph 0, page 62), + 25% and - 25% of the normal flow rate. The following results refer to the normal flow rate case. Examples of $\pm$ 25% of the normal flow rate results are shown in Appendix C (Patient 3).

In the simulations the intraluminal pressure at the inlet has been set equal to zero, then a transformation of the total pressure data has been performed in order to assume the intraluminal pressure at the inlet equal to 100 mmHg (13,332.24 Pa). The difference of static pressure has been computed by subtracting the value of static pressure at the point of interest by the value of static pressure at the end of the vessel that is why same vessels lengths would be needed for data evaluation. But segmentation of the vessel till its end has not been always possible, because of lack of contrast or sometimes bifurcations, and different length of the same vessel have been obtained for different CT. Since the length of the segmented vessel is important in difference of pressure evaluation, the length of the PreOp artery has been considered until the point in which the longest PostOp vessel length has been segmented, in order to be able to properly evaluate and compare values of pressure.

Values of total pressure along the vessel would expect to be higher on the proximal zones of the vessel compared to distal ones; in case they are lower phenomenon of recirculation may be the explanation of this result. On the other hand, positive difference of static pressure is expected for flow, but sometimes the static pressure at the proximal part of the vessel is lower than the distal one, which means that the blood flow is driven by inertia.

Each graph will show the length of the stent (grey line on the x-axes), and the parameter of interest along the vessel length for every single CT. Values located on the negative part of the x-axes represent the length of the chimney grafts inside the aorta lumen (they are in contact with the aorta graft in the chimney configuration), the actual vessel wall starts from the zero to the positive part on the x-axes. This system will let a proper comparison among the different CT situations.

Results of the different inlet velocity imposed (normal flow -Taylor's curve-, +25%, -25%) will be also presented.

4.4.1 Patient 1

The hemodynamical results for the abdominal aortic configuration of the pre- operatively CT are really different from the last PostOp, in which the stented left renal artery does not appear because it was occluded after PostOp1 (Figure 4-1 and Figure 4-2).

The renal arteries, which have perpendicular orientation in the PreOp CT, show a crossing and caudal conformation after surgery (PostOp1); the left renal artery presents a stenosis already in PreOp conformation where it curves. In fact, around 1 month after surgery the left renal artery occluded (PostOp2), but it is the right renal that showed a worse stenosis, which stabilized till PostOp4.

From these images it is possible to notice that both static pressure drop and WSS vary a lot along the two renal and less on the mesenteric arteries.

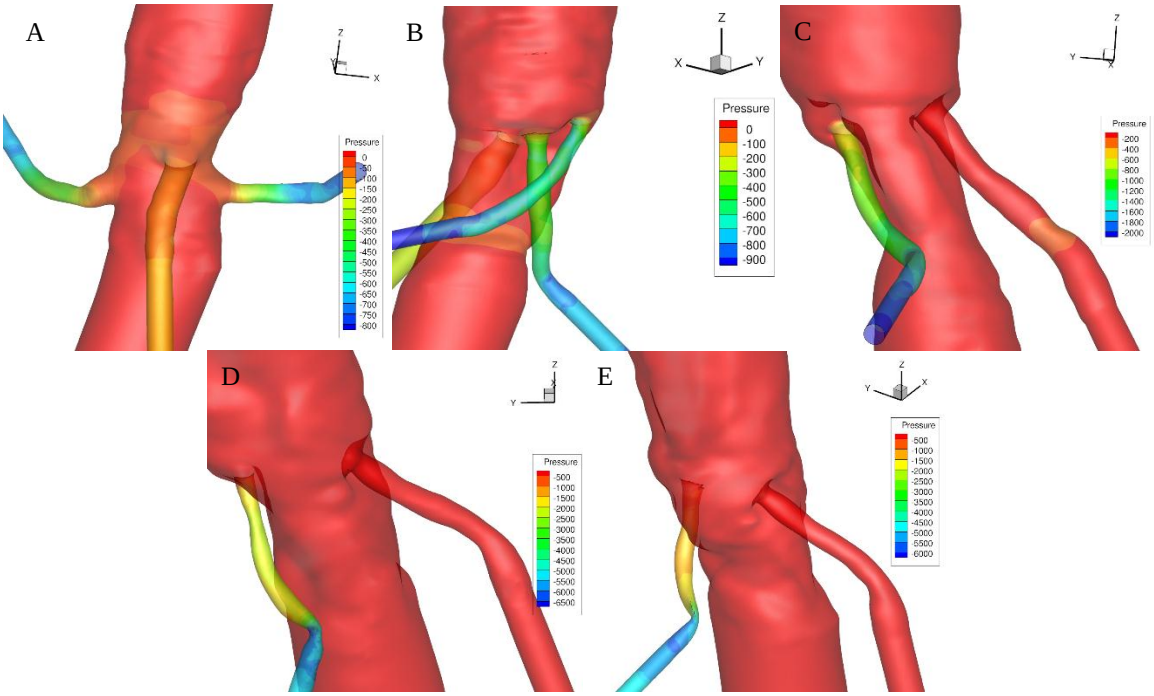

Figure 4-1. Static pressure on the wall on the abdominal tract of Patient 1. A) PreOp; B) PostOp1; C) PostOp2; D) PostOp3; E) PostOp4.

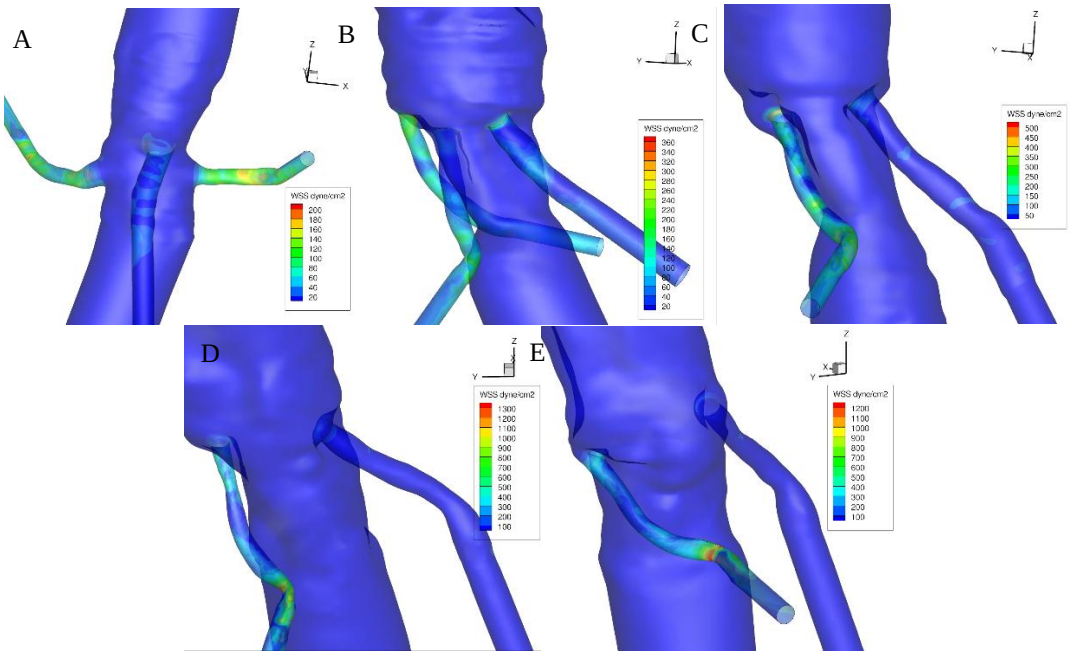

Figure 4-2. Wall shear stress of the abdominal tract of Patient 1. A) PreOp; B) PostOp1; C) PostOp2; D) PostOp3; E) PostOp4.

4.4.1.1 Superior Mesenteric Artery

The superior mesenteric stent is about 3 cm long, only the last 2 cm go into the proper vessel, the first centimeter stay in the aortic lumen (neck).

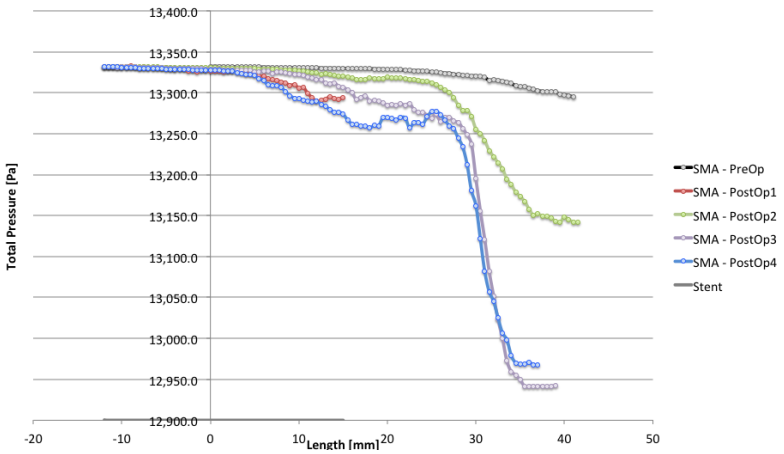

Figure 4-3. Graph of total pressure along the superior mesenteric artery of the Patient 1.

The values total pressure drop (Figure 4-3) along the vessel in the PreOp configuration is around 40 Pa. For after- surgery CTs, total pressure drops increase from PostOp1 (~40 Pa) to PostOp3 (around 400 Pa) and finally decrease again in the PostOp4 reaching 350 Pa. In particular, the total pressure within the SMA's stent located in the aortic lumen is almost constant; as soon as the stent goes into the actual vessel the value of total pressure decrease and after 3 centimeters it strongly decreases especially in the last two configurations. This represents the point where the vessel suddenly turns and decreases its cross sectional areas (CSAs).

The highest difference of static pressure on the SMA wall is on the PreOp configuration around 100 Pa. For after- surgery CTs, in general, higher static pressure differences increase from PostOp1 (60 Pa) to PostOp3 (around 140 Pa) and finally decrease again in the PostOp4 reaching 100 Pa. Negative static pressure drops are obtained in all the after- surgery situation in the zones where the stent is in the vessel or directly on the vessel wall. In the PostOp1 and PostOp2 configurations, we can observe a difference of static pressure of few mm before the end of the vessel (1- 2 cm), this represents the point where the vessel suddenly turns and decreases its cross sectional areas (CSAs) causing a brutal increase in pressure drop.

The wall shear stresses on the SMA (Figure 4-4) during the PreOp were in a range of 1- 3 Pa, the WSS range of the PostOp situations reaches 18 Pa in the last two CTs. In general, even if the WSS do not change significantly (order of magnitude 10^1), higher values are observed at the beginning of the stent, at the beginning of the proper vessel, and finally at the end of the stent.

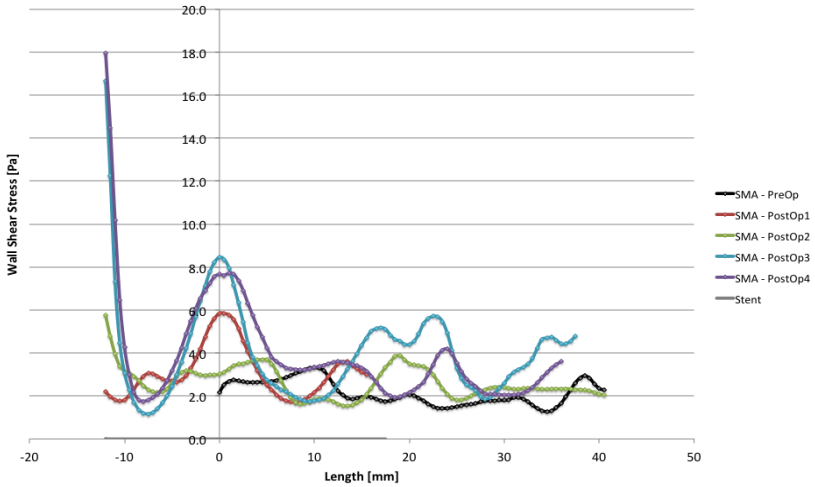

Figure 4-4. Graph of WSS along the superior mesenteric artery of the Patient 1.

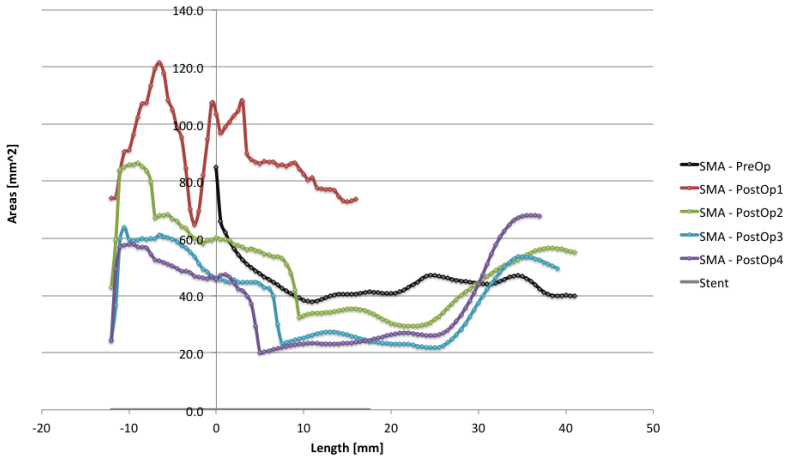

Figure 4-5. Graph of cross sectional area along the superior mesenteric artery of the Patient 1.

The highest value of CSA (Figure 4-5) reached in the PreOp situation is around 85 mm^2 (with maximum values ranging between 40-85 mm^2) at the beginning of the vessel where the physiological conformation of the artery shows the typical funnel-shape.

From the first CT after- surgery to the last one, the morphological situation changes a lot. Few days after surgery, the lumen of the artery appears larger (65- 120 mm^2) because of the

presence of the stent, but already 1 month later it becomes smaller (30- 85 mm^2), and finally it stabilizes in a range of 20- 60 mm^2 as seen in the last two CTs (after 7 and 13 months). It is interesting to observe what seems to be a kink/ compression of the vessel (between 1 and 2.5 cm downstream from the beginning of the vessels) on the last three CTs.

4.4.1.2 Right Renal Artery

The right renal stent is about 5 cm long and 3/5 of it are inside the inner aortic lumen.

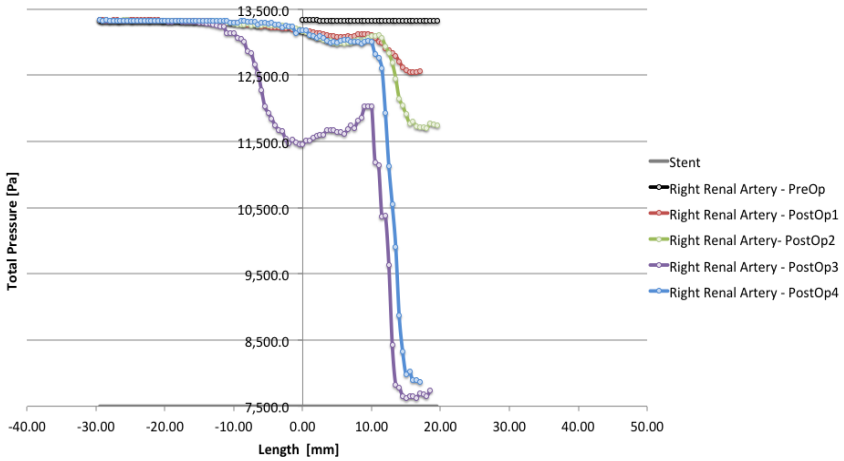

Figure 4-6. Graph of total pressure along the right renal artery of Patient 1.

The total pressure (Figure 4-6) in the PreOp configuration is almost constant along the artery. The total pressure is pretty constant along the stent in the intra- aortic lumen except for the PostOp3 where it present already a drop of about 2000 Pa; in the first three PostOps the values are pretty similar in the first 1.5 cm of the actual vessel and then it drops down drastically with a difference of pressure of about 5000 Pa in the PostOp4.

The difference of static pressure in the PreOp configuration is around 300 Pa. It presents reasonable values in the first two PostOp (lower than 1000 Pa), but they are really high (around 4500 Pa) in the last two CTs. Only the first two CTs after surgery present negative values of ΔP, and they are at the end of the stent.

This could be a case of hypertension on right renal artery.

The range of the wall shear stresses (Figure 4-7) on the right renal artery on the PreOp is 2-12 Pa, for the PostOp situations, and almost reaches 100 Pa in the last two configurations.

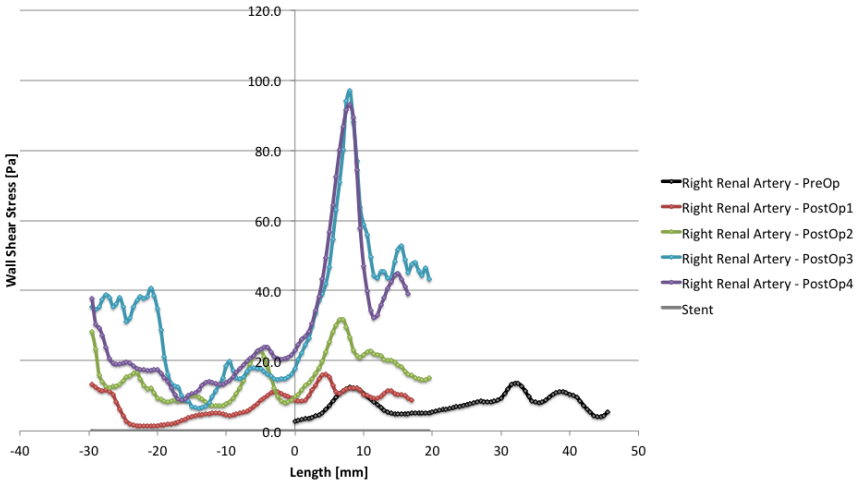

Figure 4-7. Graph of WSS along the right renal artery of Paient 1.

There is a visible change of the WSS from the first to the last PostOp; in general, high values are observed at the beginning of the stent, and less than 1 cm after the beginning of the proper vessel. It is interesting to see that in this zone there are already relatively high shear stresses at the wall in the PreOp, and that they increase from 12 to 95 Pa from the PreOp to the Last two PostOp conformations.

The range of areas on the right renal artery (Figure 4-8) before the surgery is 15- 60 mm^2, with the peak at the beginning of the vessel for the funnel-shape conformation.

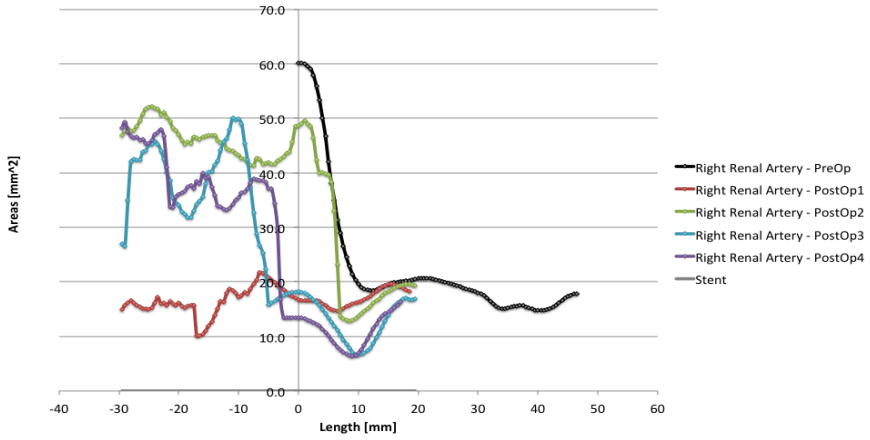

Figure 4-8. Graph of cross sectional area along the right renal artery of Patient 1.

In PostOp1 the areas decrease to 10- 20 mm^2. In the other after- surgery situations the range increases again; the highest values of CSA are observed at the beginning of the stent (30-50 mm^2) and the smallest ones are at the end where the stent graft is already in the vessel. In particular, there is a visible stenosis 1 cm after the beginning of the vessel.

4.4.1.3 Left Renal Artery

The left renal artery stent is about 4.5 cm long and it comes out into the vessel for only for few millimeters. The vessel occluded after the first CT (PostOp1).

Figure 4-9 shows the curve of total pressure in the PreOp and PostOp1 configurations since the vessel occluded in less than a month.

The difference of total pressure along the left renal artery in the PreOp configuration is around 500 Pa; fairly high values are observed in PostOp1 along the stent length, around 2,300 Pa.

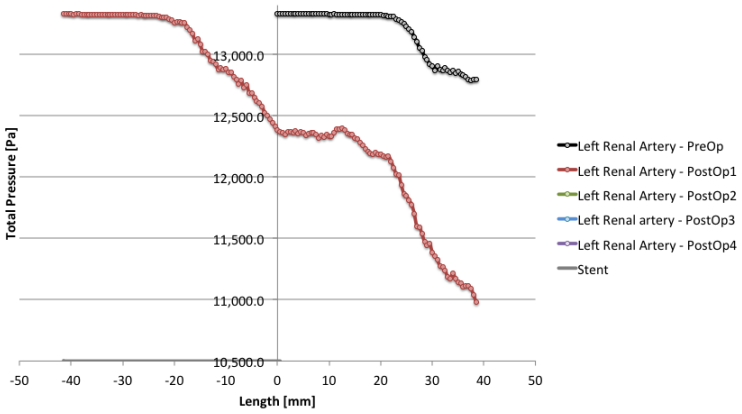

Figure 4-9. Graph of total pressure along the left renal artery of Patient 1.

The difference of static pressure along the left renal artery in the PreOp configuration is around 700 Pa (70 Pa if we consider it only on the overlap tract). Fairly high values are observed in PostOp1 along the stent length, with a peak of 400 Pa at the beginning of the stent (Graph in Appendix A).

The range of wall shear stress on the left renal artery (Figure 4-10) is between 5 and 15 Pa in the PreOp, and 10 and 45 Pa for the PostOp situations.

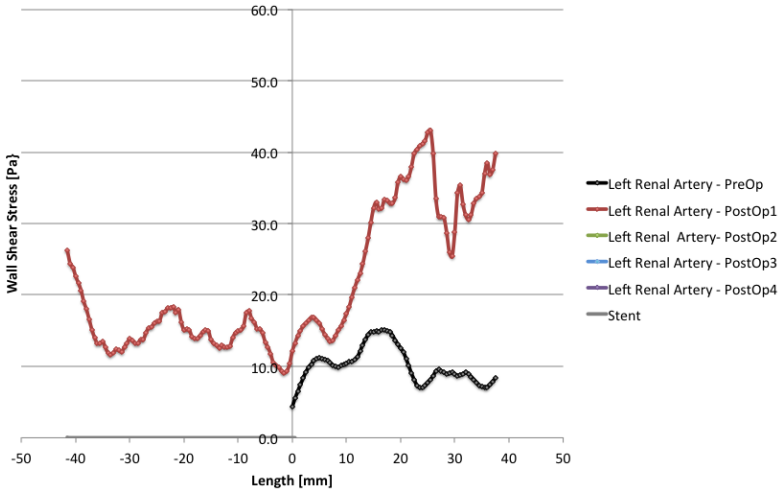

Figure 4-10. Graph of WSS along the left renal artery of Patient 1.

As usual the highest value in the after surgery conformation is at the beginning of the stent (most likely because of the compression in the aortic lumen); unfortunately it has been impossible to segment the actual vessel in order to compare these values with the PreOp, for the reasons explained in paragraph 3.2.

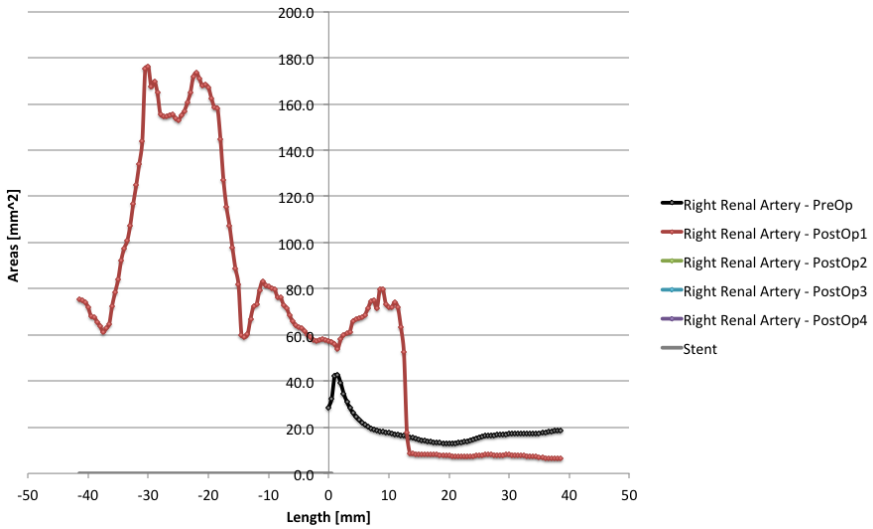

Figure 4-11. Graph of cross sectional area on the left renal artery of Patient 1.

The CSAs on the left renal artery are in a range of 13- 42.5 mm^2 in the PreOp configuration (Figure 4-11), showing higher values at the beginning and smaller values around

17.5 mm^2 in the last part of the vessel. CSA values vary a lot in the PostOp1 configuration, reaching more than 170 Pa mm^2 at the beginning of the stent.

4.4.2 Patient 2

Patient 2's wall static pressure distributions and wall shear stress of PreOp, PostOp1, PostOp2 and PostOp3 geometries are shown in Figure 4-12 and Figure 4-13 respectively.

The abdominal aortic configuration of Patient 2 shows radically changes from the first post- surgery CT to the last CT (around 7 months later), where the blood flows only into the left renal artery, since the right renal has been intentionally occluded during the surgery and the stented SMA occluded after PostOp2.

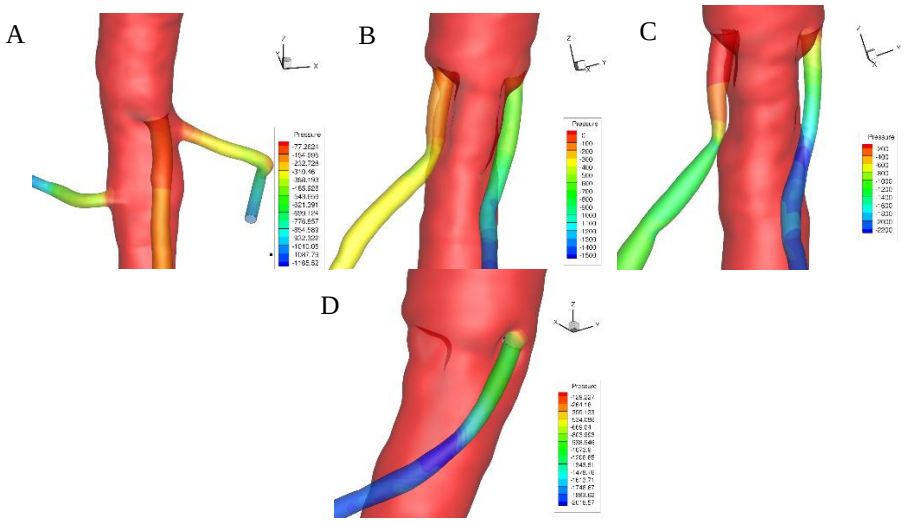

Figure 4-12. Static pressure on the wall on the abdominal tract of Patient 2. A) PreOp; B) PostOp1; C) PostOp2; D) PostOp3.

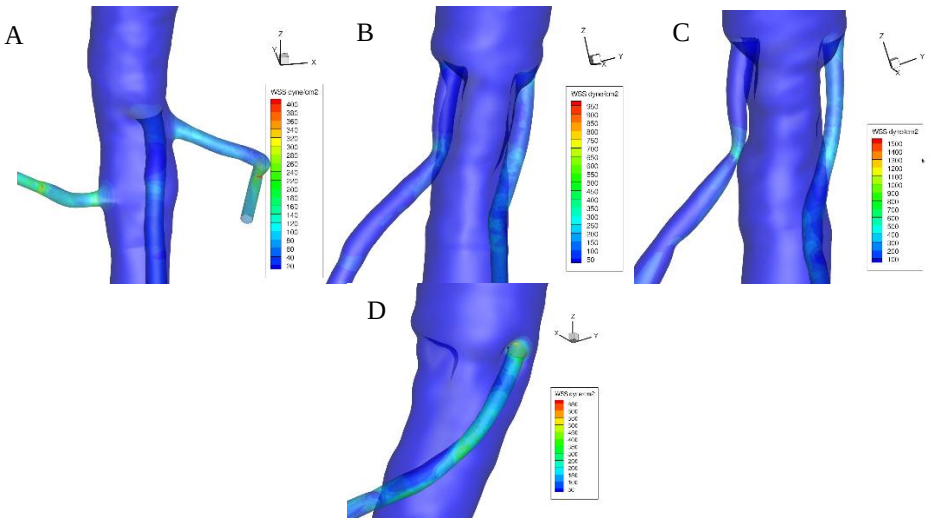

Figure 4-13. Wall shear stress on the abdominal tract of Patient 2. A) PreOp; B) PostOp1; C) PostOp2; D) PostOp3.

The renal arteries, that have perpendicular orientation in the PreOp CT, show a caudal conformation after surgery (PostOp1). From these images it is already noticeable that both the parameters of static pressure and WSS vary a lot along the two renal arteries and less along the mesenteric artery.

Graphs of total pressure, difference of static pressure, WSS, and cross sectional area of right and left renal arteries of Patient 2 are shown in the Appendix B.

4.4.2.1 Superior Mesenteric Artery

The superior mesenteric stent is about 5 cm long; the last 3 cm go into the proper vessel, and the first two cm are in contact with the main stent graft in the aortic lumen (neck).

The difference of total pressure on the vessel wall in the PreOp configuration is around 40 Pa. It is almost negligible in the aortic lumen in PostOps configurations, but it become higher after 1 cm of the actual vessel length. It increase from PostOp1 (around 350 Pa) to PostOp2 (750 Pa), after7 months the vessel occludes. Negative values of difference of total pressure are shown between 1- 4 cm of the actual vessel in PostOp1 and PostOp2 (Figure 4-14).

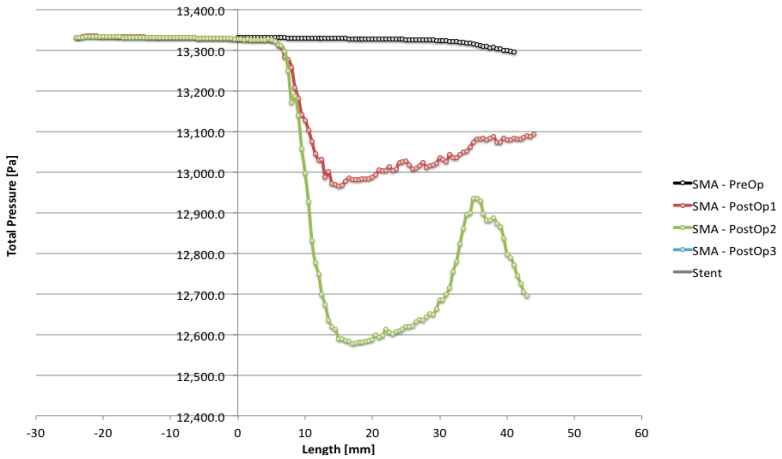

Figure 4-14. Graph of total pressure along the superior mesenteric artery of Patient 2.

The wall shear stresses on the SMA during the PreOp are in a range of 1-6 Pa (Figure 4-15).

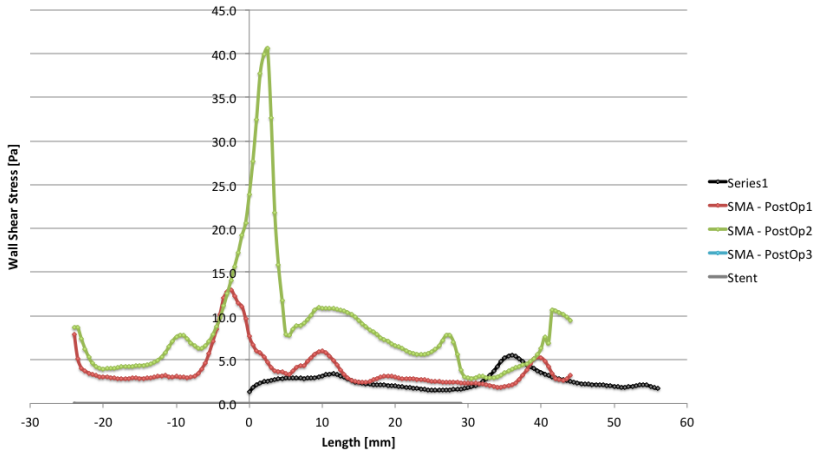

Figure 4-15. Graph of WSS along the superior mesenteric artery of Patient 2.

The WSS in the PostOp situations reaches a maximum value of 40 Pa in the last CTs. The peaks of WSS correspond to the transition from the aortic lumen into the actual vessel.

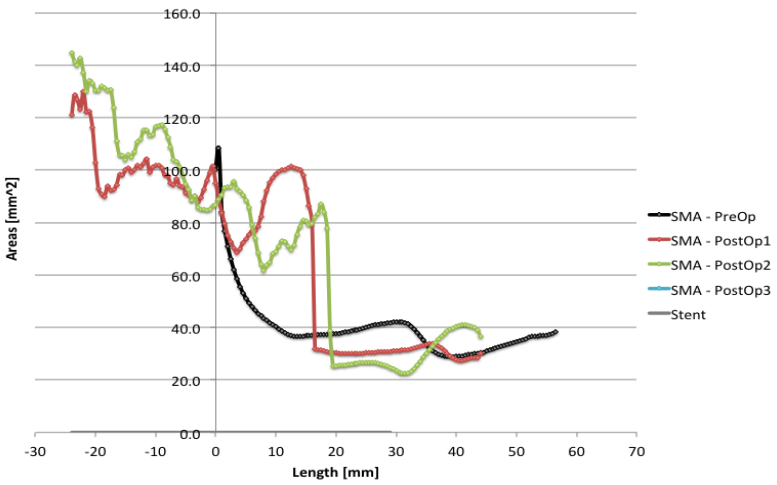

Figure 4-16. Graph Cross Sectional Areas on the superior mesenteric artery of the Patient 2.

The highest CSA (Figure 4-16) value reached in the PreOp situation is around 110 mm^2 (with a range between 30-110 mm^2) for the typical funnel-shape at the beginning of the vessel.

Few days after surgery, the lumen of the stent is around 70- 130 mm^2 in the intra- aortic lumen and it decreases to 30 mm^2, 1 centimeter before the end of the stent in the artery; the situation remains almost stable one month later (a stenosis is clearly visible in the geometry's pictures in PostOp1 and PostOp2).

4.4.2.2 Left Renal Artery

The stent in the left renal artery is about 5 cm long and it comes out into the vessel for only for few millimeters. The vessel occluded after the first CT (PostOp1).

PreOp shows CSA around 20- 30 mm^2 along the almost all the artery length, except for the peak of cross sectional areas (around 68 mm^2) located at the beginning of the vessel for the typical funnel-shape. Few days after surgery, the area of the inner lumen of the stent is around 40-60 mm^2, with a compression at the end of the stent that fits with the vessel dimension. The situation 1 month and around 6 months after- surgery is pretty similar, but on PostOp2 the areas' range is larger and the highest value at the beginning of the stent reaches 100 mm^2.

4.4.3 Patient 3

Patient 3's static pressure and wall shear stress distributions on the wall of PreOp, PostOp2 and PostOp4 geometries are shown respectively in Figure 4-17 and Figure 4-18

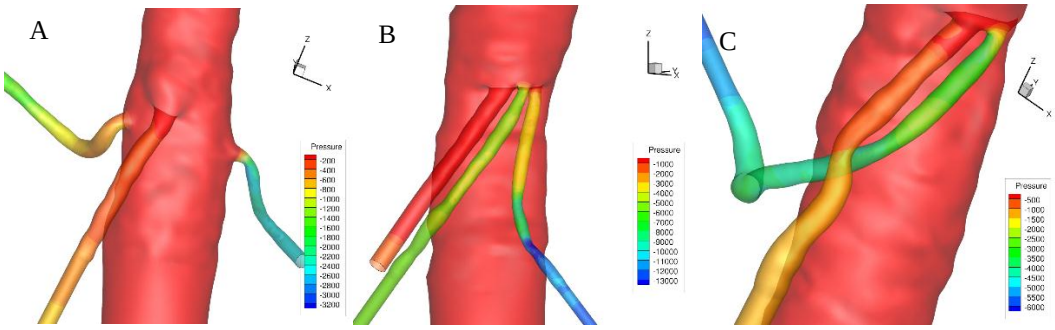

Figure 4-17. Static pressure on the wall on the abdominal tract of Patient 3. A) PreOp; B) PostOp2; C) PostOp4.

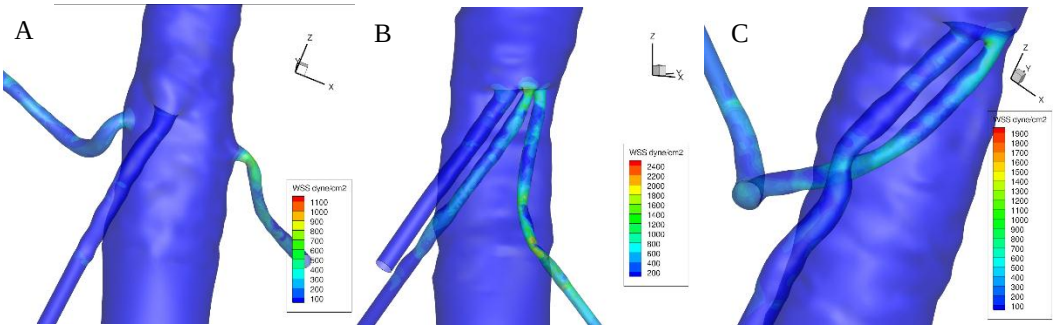

Figure 4-18. Wall shear stress on the abdominal tract of Patient 3. A) PreOp; B) PostOp2; C) PostOp4.

The abdominal aortic configuration varies consistently during the time; the renal arteries, that have perpendicular orientation in the PreOp CT, are forced into caudal conformation after surgery. The left renal artery occluded after PostOp1, but the right renal artery showed a critical compression between the SMA and the main lumen, since the first after surgery CT. From these images it is already possible to notice that both the parameters vary a lot along the two renal arteries and less on the mesenteric artery.

4.4.3.1 Superior Mesenteric Artery

The superior mesenteric stent is about 3 cm long, less than one centimeter goes into the proper vessel, the rest is in the aorta (neck).

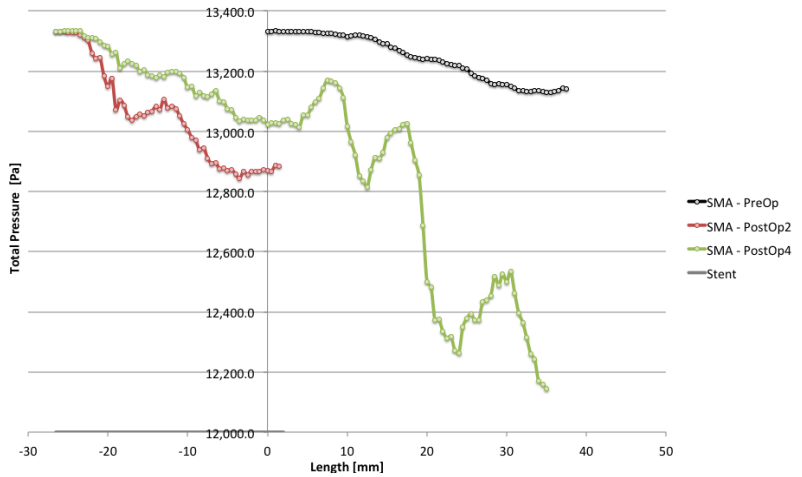

Figure 4-19. Graph of total pressure along the superior mesenteric artery of Patient 3.

In the PreOp configuration (Figure 4-19), the difference of total pressure is around 200 Pa; for after- surgery CTs a difference of total pressure of around 450 for PostOp2 and 1200 Pa in PostOp4 are observed at the beginning of the stent (intra- aortic lumen).

On the other hand, the difference of static pressure on the vessel wall in the PreOp configuration of the SMA is around 350 Pa; values around 500 Pa are observed in PostOp4 at the beginning of the vessel.

For after- surgery CTs, the peak of difference of static pressure is around 800 Pa in PostOp4 at the beginning of the segmented vessel. Negative values of this parameter are shown in both PostOp2 and PostOp4. In this case it is necessary to remember that the length of the segmented vessel is very different from PostOp2 and PostOp4; discarding PostOp4's data after millimeter 2 of the vessel length, the peak value would be around 700 Pa (still higher than 300 Pa) and lightly negative values would be observed in the same zone of PostOp2.

The wall shear stresses on the SMA (Figure 4-20) during the PreOp are in a range of 3- 9 Pa; in the PostOp situations, they reaches 20- 25 Pa in the PostOp2 inside the aortic lumen, where it remains almost stable. The highest values of WSS in PostOp4 is 30 Pa located soon after the beginning of the actual artery.

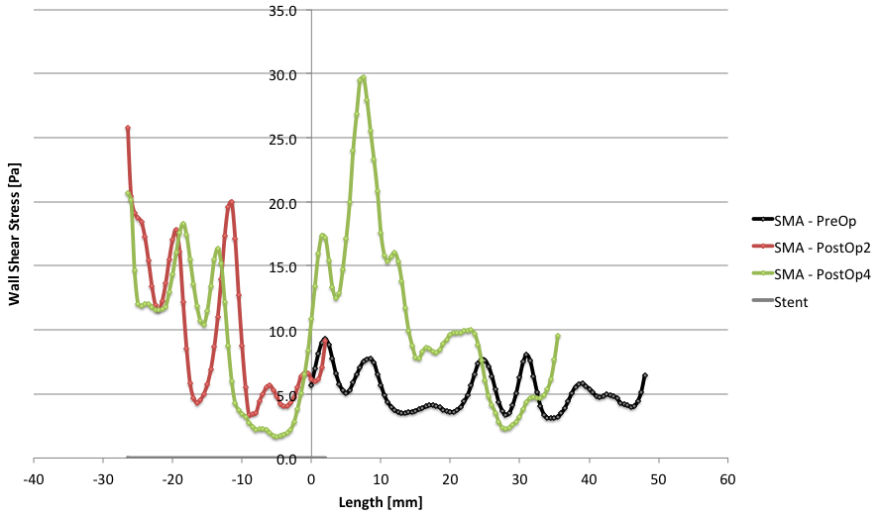

Figure 4-20. Graph of WSS along the superior mesenteric artery of Patient 3.

CSAs on the superior mesenteric artery (Figure 4-21) in PreOp configuration are higher at the beginning of the vessel (around 155 mm^2), this larger zone is clearly visible on the geometry; they decrease along the almost all the artery length reaching 80 mm^2 at the end of the vessel.

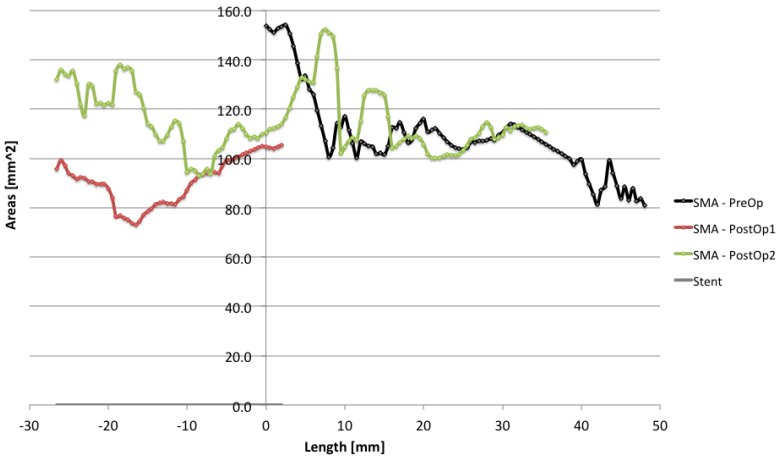

Figure 4-21. Graph of cross sectional areas along the superior mesenteric artery of Patient 3.

One month after surgery, the area of the inner lumen of the stent is around 75- 105 mm^2, with a compression of stent lumen in the intra- aortic lumen. The situation 1 year after- surgery is similar to the PreOp in the actual vessel, but the CSAs of the stent in the aortic lumen are larger if compared to PostOp2.

4.4.3.2 Right Renal Artery

The right renal stent is about 6 cm long and 2/3 of it are inside the inner aortic lumen.

Graphs of total pressure, WSS and CSA of the right renal artery of the third patient are shown in the Appendix C.

PreOp CSA are in a range of 40- 100 mm^2 in the first two centimeters, than the lumen becomes much smaller (15- 20 mm^2). 7 months after surgery the CSA of the stent was a range of 15- 60 mm2; after circa 1 year, the stent doubled its lumen, in order to compress once in the actual vessel (20 mm^2).

4.4.3.3 Left Renal Artery

The left renal artery stent is about 5 cm long and it comes out into the vessel for 3 cm. The vessel occluded after the first CT (PostOp1).

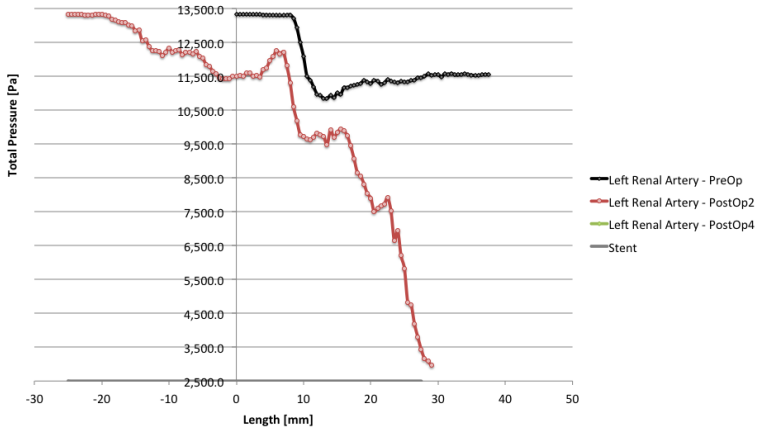

Figure 4-22. Graph of total pressure along the left renal artery of Patient 3.

The difference of total pressure (Figure 4-22) along the left renal artery in the PreOp configuration result around 2000 Pa with a negative difference around 1.5 cm in which a reduction of the lumen is observed. The difference of total pressure increases a lot in the PostOp1 reaching around 10500 Pa, proof of hypertension case likely caused by bad fluid-dynamic. This vessel will occlude before the next CT.

The range of wall shear stress (Figure 4-23) on the left renal artery is between 5 and 80 Pa in the PreOp, and 20-170 for the PostOp situations. The highest WSS are observed at the

beginning of the vessel for both the conformations, almost doubling the value from the PreOp to the conformation one year after surgery.

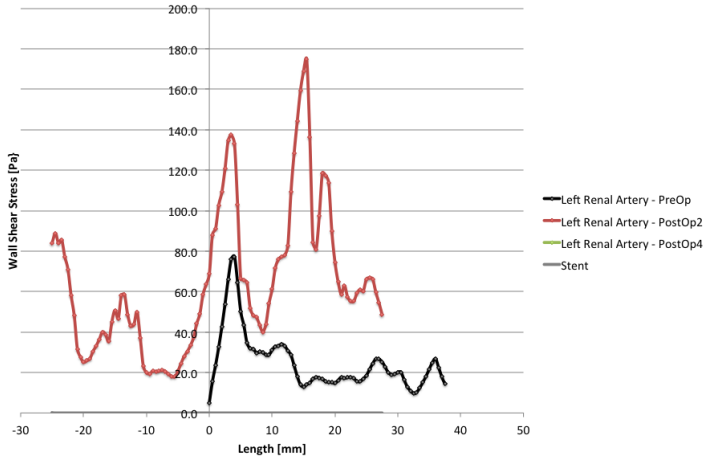

Figure 4-23. Graph of WSS along the left renal artery of Patient 3.

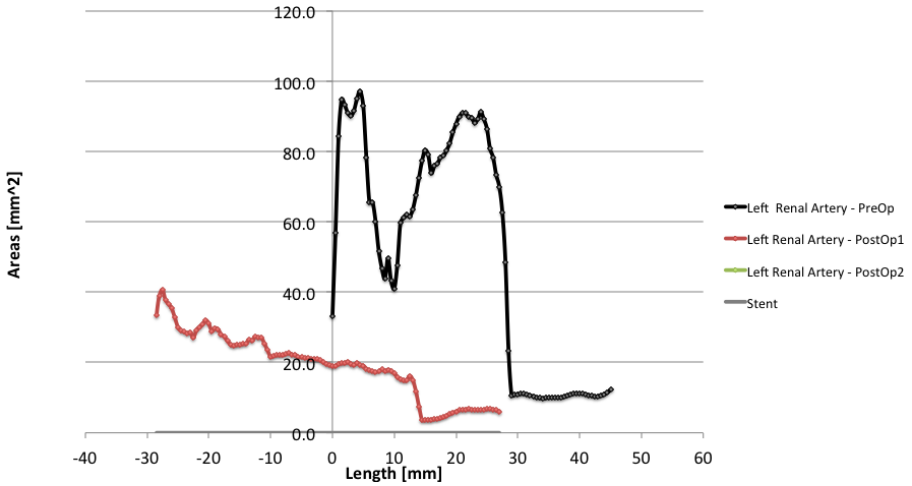

Figure 4-24. Graph of cross sectional areas along the left renal artery of Patient 3.

The CSA of the left renal artery (Figure 4-24) in the PreOp configuration shows an evident stenosis 1 cm after the beginning of the stent and an even stronger reduction of lumen at the end of the vessel (range 10- 100 mm^2). The PostOp2 situation present a stent lumen between 40 and 20 mm^2 and a tidy compression of stent lumen in the actual vessel.

4.4.4 Patient 4

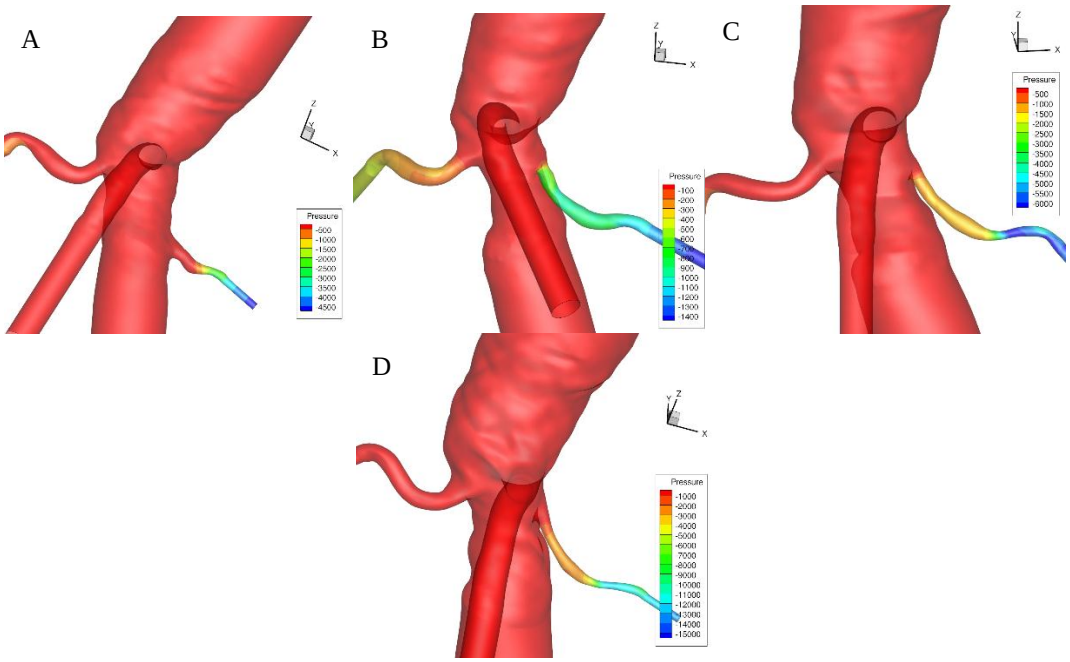

Figure 4-25. Static pressure on the wall on the abdominal tract of Patient 4. A) PreOp; B) PostOp1; C) PostOp2; D) PostOp3.

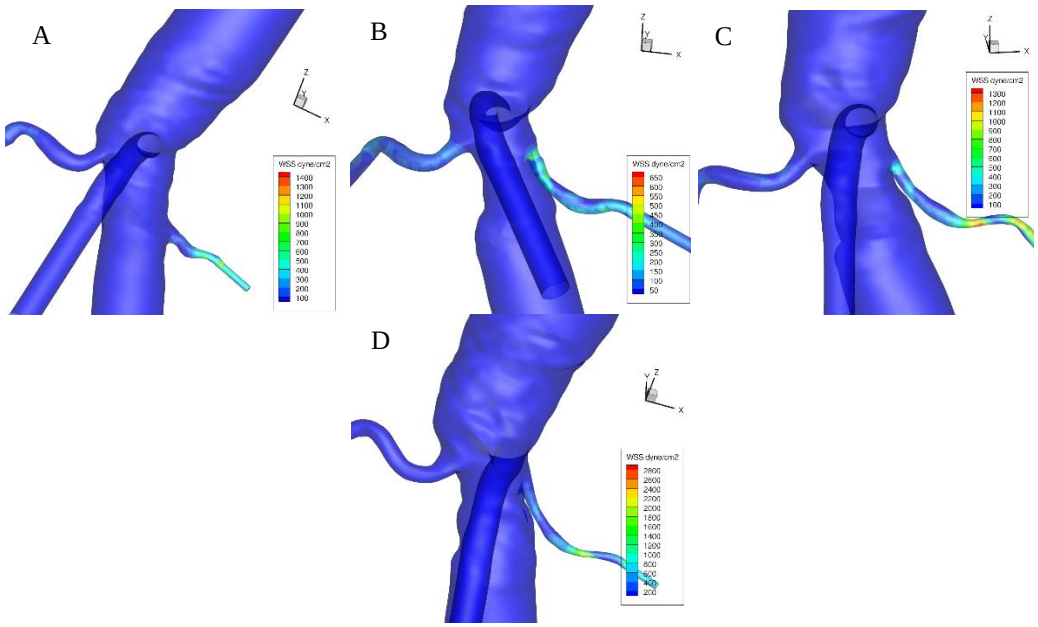

Figure 4-26. Wall shear stress on the abdominal tract of Patient 4. A) PreOp; B) PostOp1; C) PostOp2; D) PostOp3.

Patient 4's static pressure and shear stress distributions on the wall of PreOp, PostOp1, PostOp2, and PostOp3 geometries are shown in Figure 4-25 and Figure 4-26 respectively.

The chimney stent on the left renal artery of the fourth patient was affected by type 1 and 2 endoleaks; this artery was very small in the PreOp situation, soon after surgery the situation improved but in the last CT (6- 8 months after surgery) it showed stenosis case. The other two no-stented vessels did not present any particular issue.

4.4.4.1 Superior Mesenteric Artery

The range of total pressure on the SMA (Figure 4-27) is between -10 and 40 Pa, the situation from the PreOp conformation to the last CT does not change consistently. In particular, between centimeter 5- 6 of the vessel presents a lightly negative zone of difference of total pressures in the PreOp configuration that disappears in the following PostOps but come back around 7 months after surgery.

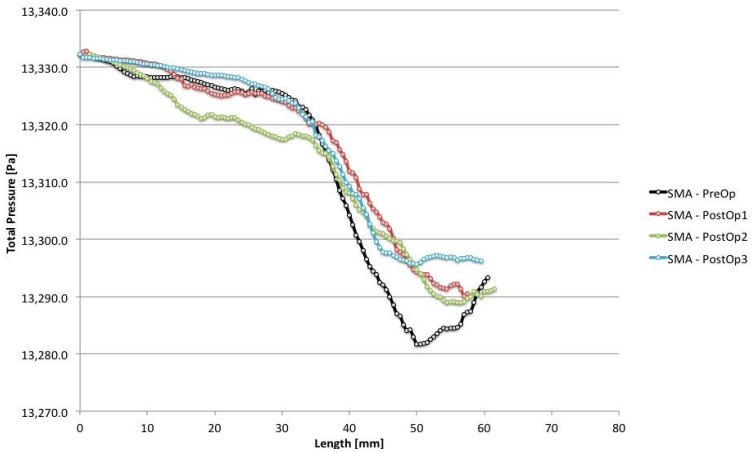

Figure 4-27. Graph of total pressure along the superior mesenteric artery of Patient 4.

The range of difference of static pressure on the SMA is between -5 and 50 Pa, the situation from the PreOp conformation to the last CT does not change consistently. In particular between centimeter 3- 5 of the vessel there is a zone of negative pressures in the PreOp configuration that decreases in the following PostOps but come back after around 7 months after surgery (graph is shown in Appendix D).

The WSS on the superior mesenteric artery are in a range of 0.5- 2.5 Pa among the CTs (Figure 4-28).

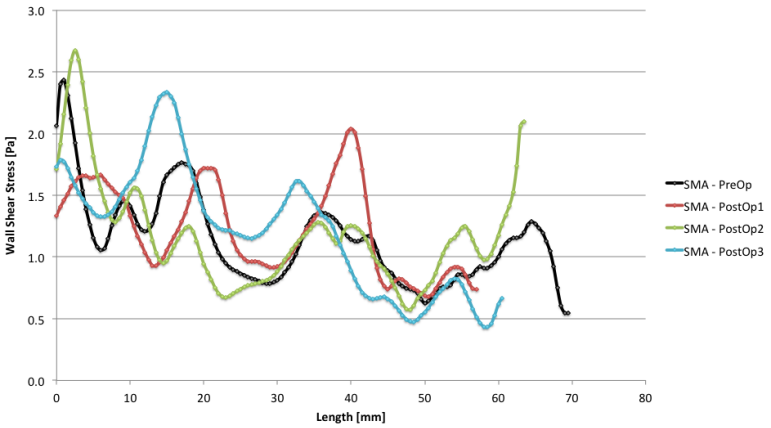

Figure 4-28. Graph of WSS along the superior mesenteric artery of Patient 4.

The CSA on the superior mesenteric artery (Figure 4-29) vary between 50- 115 mm^2 along the vessel. Its shape and conformation remains pretty regular and does not present big changes during the time. There is a light reduction of the lumen from centimeters 1 to 4, which becomes more evident in the last CT.

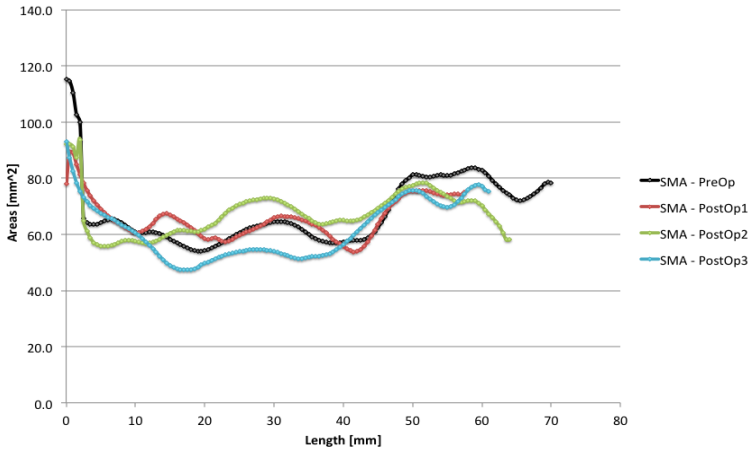

Figure 4-29. Graph of cross sectional area along the superior mesenteric artery of Patient 4.

4.4.4.2 Right Renal Artery

Total pressure differences on the right renal artery are always positive (Figure 4-30).

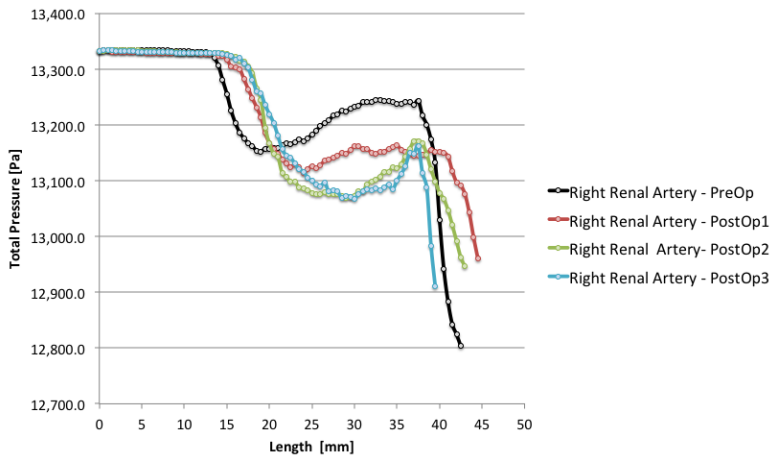

Figure 4-30. Graph of total pressure along the right renal artery of Patient 4.

The trend of the total pressure is pretty similar among CTs; its difference varies from 500 Pa in the PreOp configuration to around 400 Pa in the PostOps.

Static pressure differences on the right renal artery are always positive, the maximum values is located at the beginning of the vessel, around 500 Pa in the PreOp situation and few days after surgery, it lightly increases during the time, reaching 650 Pa 7 months after surgery (graph is shown in Appendix D).

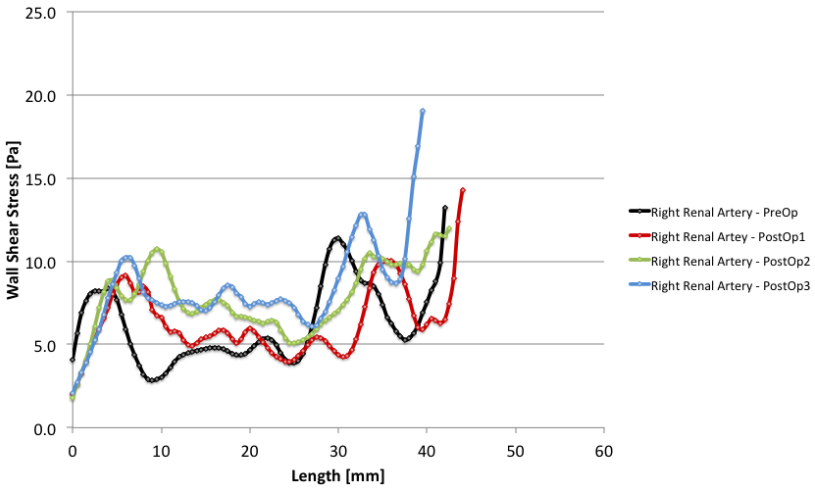

Figure 4-31. Graph of wall shear stress along the right renal artery of Patient 4.

The shear stress on the wall of the right renal artery are in a range of 2- 19 Pa, its trend remains pretty similar among the CTs (Figure 4-31).

The conformation of the right renal artery seems to remain pretty constant the range of CSA goes from 100 mm^2 at the beginning of the vessel for the typical funnel- shape, to a strong decreasing of the vessel lumen from centimeter 1 till the end (Figure 4-32).

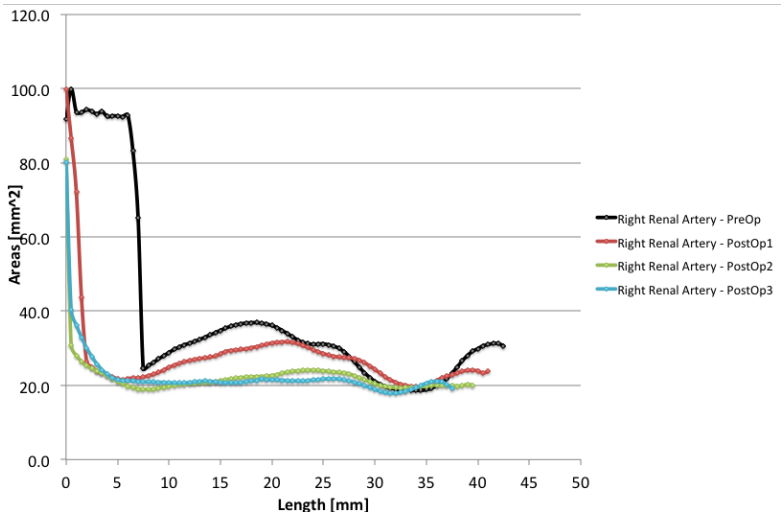

Figure 4-32. Graph of cross sectional area along the right renal artery of Patient 4.

4.4.4.3 Left Renal Artery

The left renal artery stent is about 2 cm long and less than 0.5 enters in the artery.

The situation in term of total pressure on the stented- left renal artery changes consistently among CTs (Figure 4-33).

The difference of total pressure in the pre- surgery conformation is of few Pascals. It strongly increases soon after surgery (around 810 Pa) in correspondence of the entering of the stent into the actual vessel; after 1 month the situation at the end of the stent worsens reaching around 5000 Pa of total pressure drop in the last centimeter of the segmented vessel. After 7 months it is possible to observe around 2000 Pa of difference of total pressure between 1 and 2 cm along the vessel and again a drastic drop in the last centimeter of the artery (3000 Pa).

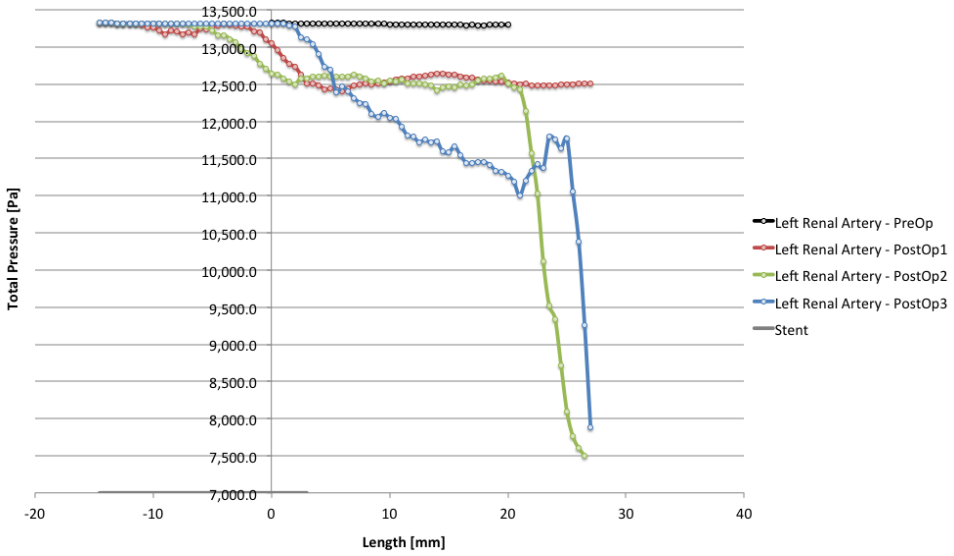

Figure 4-33. Graph of total pressure along the left renal artery of Patient 4.

The situation in term of difference of static pressure on the wall of stented- left renal artery changes consistently. The peak of pressure drop in the pre- surgery conformation is higher than 3000 Pa. It strongly decreases soon after surgery (500 Pa), but already after 1 month the situation worsens reaching 5000 Pa on the stent intra- aortic lumen till the first centimeter after the beginning of the actual vessel and negative values close to the end of the it (1.5- 2 cm). After around 7 months after surgery the ΔP inside the aortic lumen reaches 10 thousand Pa and negative values (-2000 Pa) at the end of the vessel lumen, showing a very critical situation (graph is shown in Appendix D).

The left renal artery's WSS (Figure 4-34) in the PreOp situation are in a range of 10- 90 Pa. They decrease in PostOp1 configuration (5- 30 Pa) long all the segmented tract; but after 1 month they increase again on the same zone (1- 2 cm) of the vessel reaching more than 100 Pa; finally, after 7 months, they reach around 180 Pa.

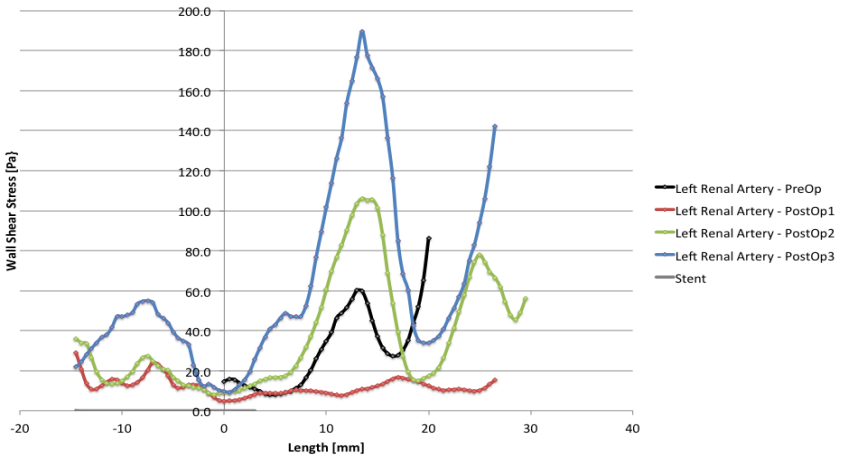

Figure 4-34. Graph of wall shear stress along the left renal artery of patient 4.

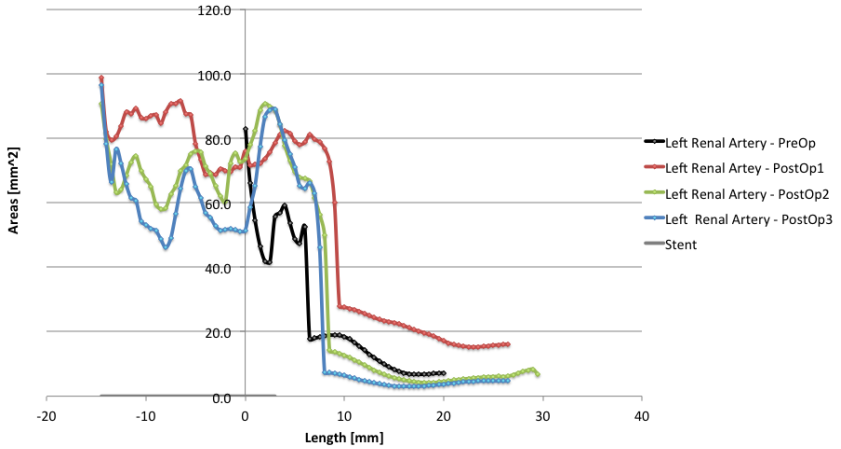

Figure 4-35. Graph of cross sectional area along the left renal artery of Patient 4.

The CSA on the left renal artery (Figure 4-35) are in a range of 40- 80 mm^2 in the first centimeter of the PreOp conformation and then they decrease to 10- 20 mm^2 till the end of the segmentation. The post- surgeries situations follow this trend, showing higher values (50- 90 mm^2) in the intra- aortic lumen and drastically decreasing once entered into the actual vessel.

4.4.5 Patient 5

Patient 5's pressure and shear stress distributions on the wall of PreOp, PostOp2, PostOp3, PostOp5, PostOp6, and PostOp7 geometries are shown in Figure 4-36 and Figure 4-37 respectively.

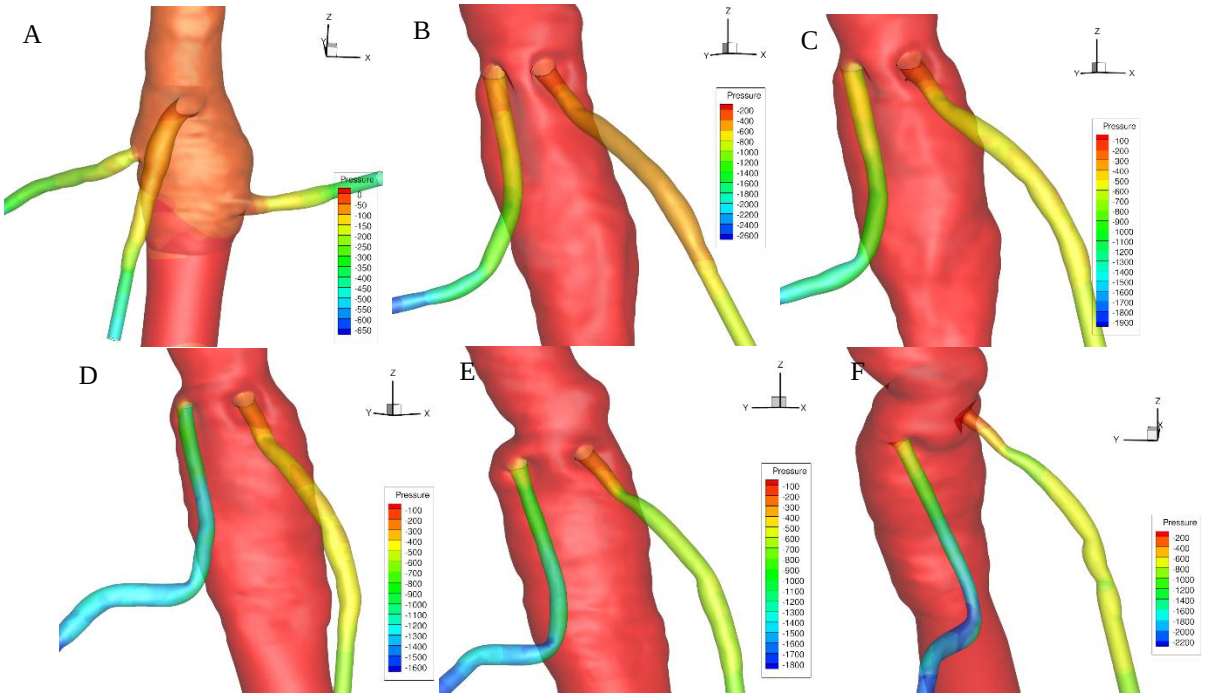

Figure 4-36. Static pressure on the wall of the abdominal tract of Patient 5. A) PreOp; B) PostOp2; C) PostOp3; D) PostOp5; E) PostOp6; F) PostOp7.

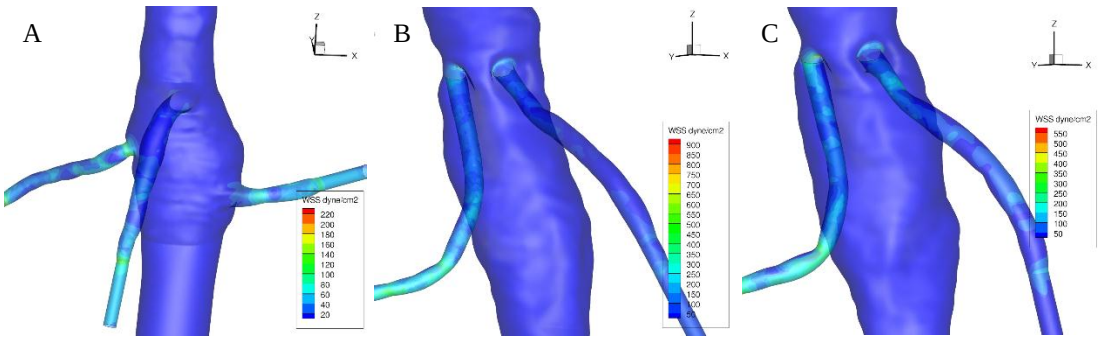

Figure 4-37. Wall shear stress on the abdominal tract of Patient 5. A) PreOp; B) PostOp2; C) PostOp3; D) PostOp5; E) PostOp6; F) PostOp7.

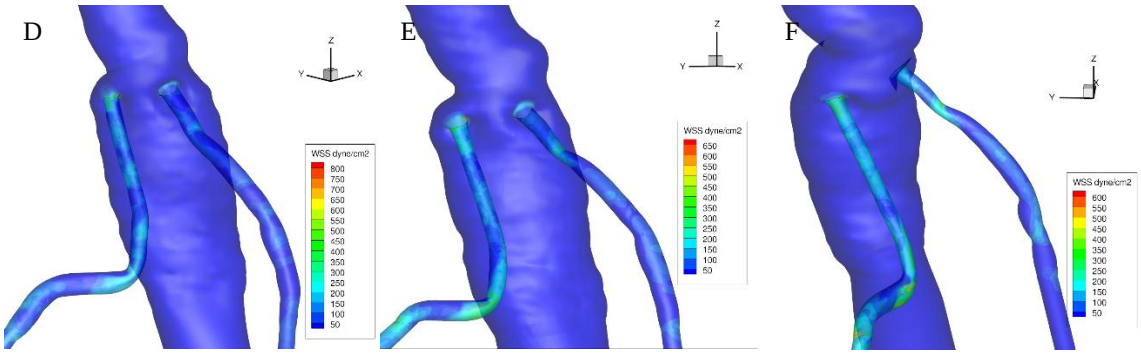

Figure 4-37.Continued.

Patient 5 needed an intentionally occlusion of the left renal artery and two chimney grafts on the SMA and right renal artery. The first CT (PostOp2) showed a pretty good post- surgical situation; the second (PostOp3) presented a compression on the SMA and a developed endoleak around the stent.

Graphs of total pressure, WSS, difference of static pressure and CSA of PreOp situation on the left renal artery are in the Appendix E.

4.4.5.1 Superior Mesenteric Artery

The SMA's stent is about 5.5 cm long and only the first two cm stay in the aortic lumen.

The difference of total pressure (Figure 4-38) in the PreOp conformation is around 50 Pa; it increases in PostOp situations reaching 380 Pa in the PostOp1 (1 moth after- surgery), it stabilizes till 2 years after surgery but then it reaches 1000 Pa after around 4 years after surgical operation. In general the trend shows a negligible difference of pressure in the intra- aortic part of the stent and a critical zone (between 1 and 5 cm of the actual vessel), in which the total pressure drops critically in the PostOps situations.

The peak of difference of static pressure on the SMA in the PreOp conformation is around 300 Pa; it increases in PostOp situations in the intra- aortic lumen zone reaching 450 Pa in the first PostOp (1 moth after- surgery); it decreases until 2 years after surgery but then it reaches 700 Pa after around 4 years after surgical operation. Passing into the actual vessel the values decrease critically, reaching negative pressure drops in the first centimeter of the artery.

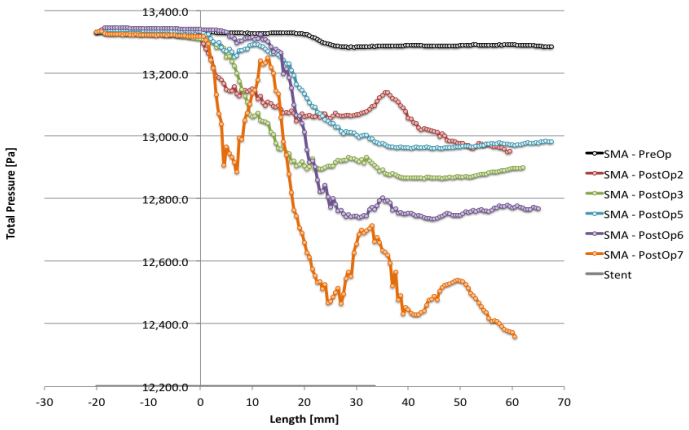

Figure 4-38. Graph of total pressure along the superior mesenteric artery of Patient 5.

WSSs (Figure 4-39) on the actual vessel are in a range of 2- 10 Pa among the CTs, in particular they show higher values at the end of the vessel. In the first two centimeter of the intra-aortic stent, the wall shear stresses are higher at the beginning (especially in PostOp1, 30 Pa), then enter again a range of 5- 15 Pa and in the last two conformations (3- 4 years after surgery) they increase again in correspondence of the transition from the aortic lumen to the artery.

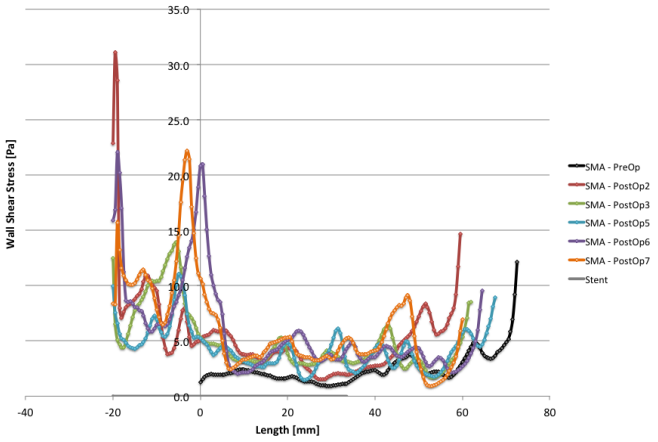

Figure 4-39. Graph of wall shear stress along the superior mesenteric artery of Patient 5.

Cross sectional areas on the SMA (Figure 4-40) are in a range of 20- 75 mm^2 in the PreOp conformation. PostOp situations show CSA between 50- 100 mm^2 in the zone of the graft stent contained in the aortic lumen, and their values brutally decrease after entering into the actual artery to a range of 15- 40 mm^2.

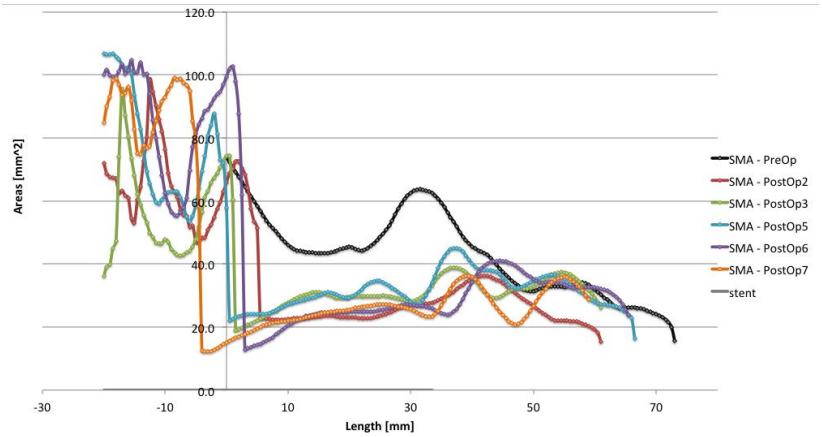

Figure 4-40. Graph of cross sectional area along the superior mesenteric artery of Patient 5.

4.4.5.2 Right Renal Artery

The right renal stent is long more than 5.5 cm and the first 4 cm are contained in the aortic lumen.

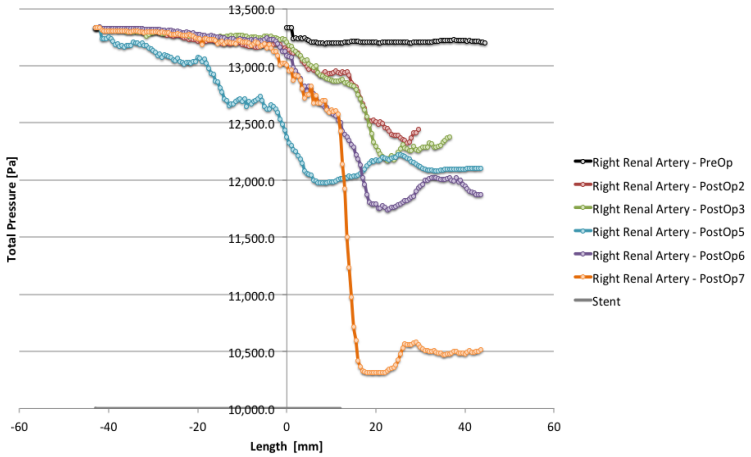

Figure 4-41. Graph of total pressure along the right renal artery of Patient 5.

The difference of total pressure on the right renal artery (Figure 4-41) is less than 100 Pa in the PreOp conformation, in PostOp1 it becomes five times higher, it remains fairly stable until 2 years after surgery (PostOp5), and finally reach 2700 Pa 4 years post- operation. The values of total pressure on the stent graft in the intra- aortic lumen are almost constant and very similar among the PostOp CTs; the critical zone is around 1 and 3 cm of the actual vessel where the CSA reduces drastically.

The peak of static ΔP on the wall of the right renal artery is around 200 Pa in the PreOp conformation at the beginning of the vessel, where in PostOp1 it becomes five times higher, to decrease till 2 years after surgery (around 50 Pa, PostOp5), and finally reach again 200 Pa 4 years post- operation. The values of pressure drop on the stent graft in the intra- aortic lumen are much higher; the peaks reach 1600 Pa in the PostOp1, decrease till 2 years after surgery (400 Pa), and finally increase again reaching 1200 Pa. Negative values of drop pressure are in the last three CT (2- 4 years after surgery) between centimeter 1.5 and 3.

WSSs on the right renal artery (Figure 4-42) maintain stable a range of 5- 20 Pa in the stent wall located in the intra- aortic lumen, with higher values at the beginning (15- 45 Pa). PostOp situations in the actual vessel show a peak of WSS between 1 and 2 cm in a range of 10- 30 Pa and high values at the end of the segmentation too; the general trend during the time is a decreasing of values till 2 years after surgery and a light increase till 4 years after. The PreOp conformation shows lower values of wall shear stresses (2- 12 Pa)

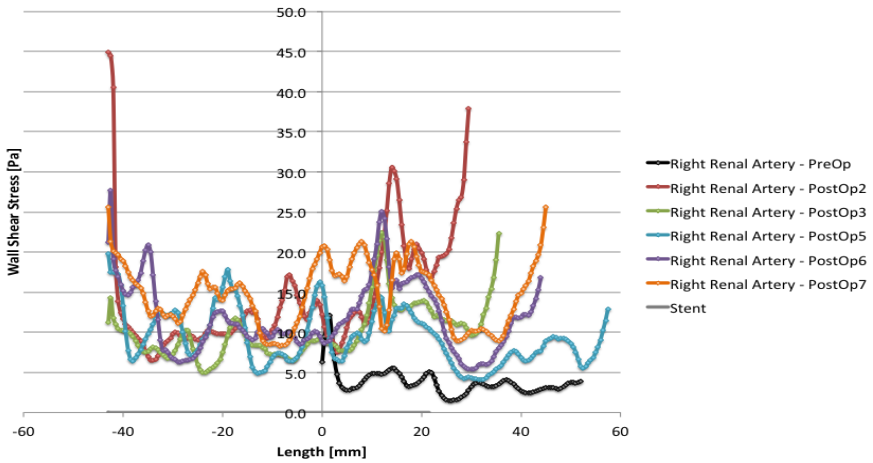

Figure 4-42. Graph of wall shear stress along the right renal artery of Patient 5.

The PostOp cross sectional areas of the right renal stent (Figure 4-43) are in a range of 50- 100 mm^2 in the intra- aortic lumen and they brutally decrease by entering in the actual vessel to 20- 30 mm^2; in general, they follow the trend of the PreOp conformation, which presents an

enlargement of the lumen at the beginning of the vessel for its typical funnel- shape. The stenosis soon after the entering in the artery is clearly visible from the pictures.

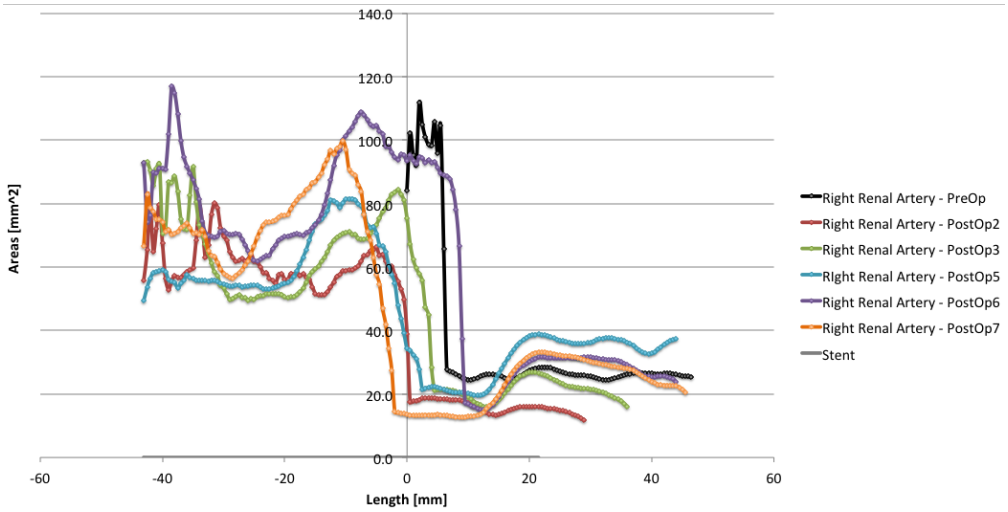

Figure 4-43. Graph of cross sectional area along the right renal artery of Patient 5.

CHAPTER 5
DISCUSSIONS

5.1 Cross Sectional Area

In the PreOp conformations, an enlargement at the beginning of the vessels is usually observed, as physiological conformation (funnel-shape).

From the analyses of the CSA in PostOp conformations on the three smaller vessels it is possible to recognize some critical zones. Sometimes smaller cross sectional areas are at the beginning of the stent, proof of the stent compression in the aortic neck; as soon as the stent comes out into the vessel it can have its own conformation if its size fits perfectly in the artery or if the artery is not stenotic, otherwise it compresses inside the vessel.

The geometry of the abdominal aortic tract changed a lot during the time; but it is possible to recognize the typical range of diameter for aorta inlet, aorta outlet, and each smaller vessel.

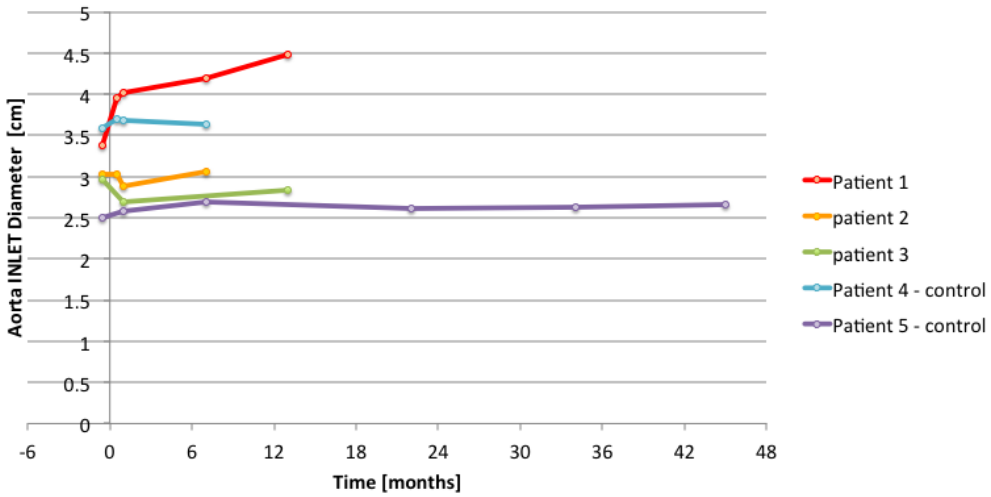

Figure 5-1. Inlet diameters of the extended aortic geometries of the five patients.

The range of diameter of the aorta is about three centimeter above the SMA is 2.5- 4.5 cm (Figure 5-1), reasonable value for diameter at the thoracic level of the aorta. They remain pretty constant except for the first patient who shows 1 cm difference between the PreOp and the PostOp4 configuration.

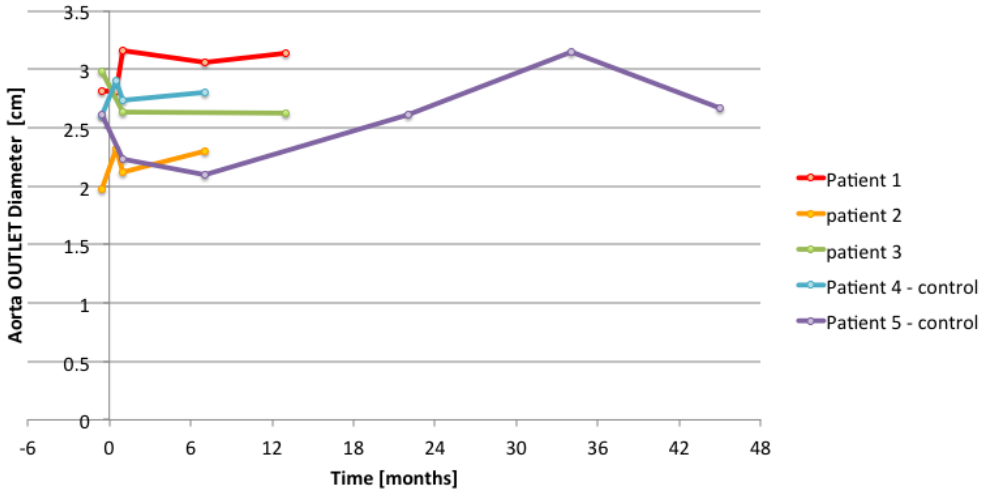

Figure 5-2. Outlet diameters of the extended aortic geometries of the five patients.

Diameter at the aorta outlet results in the range of 2- 3 cm (typical for the abdominal aorta, Figure 5-2). It is important to remember that what is plotted is the actual lumen where the blood flows (without thrombi), and it is not the diameter of the vessel, since it would be much bigger because of the aneurysm. Only the fifth patient aorta outlet underwent big cross sectional areas variation.

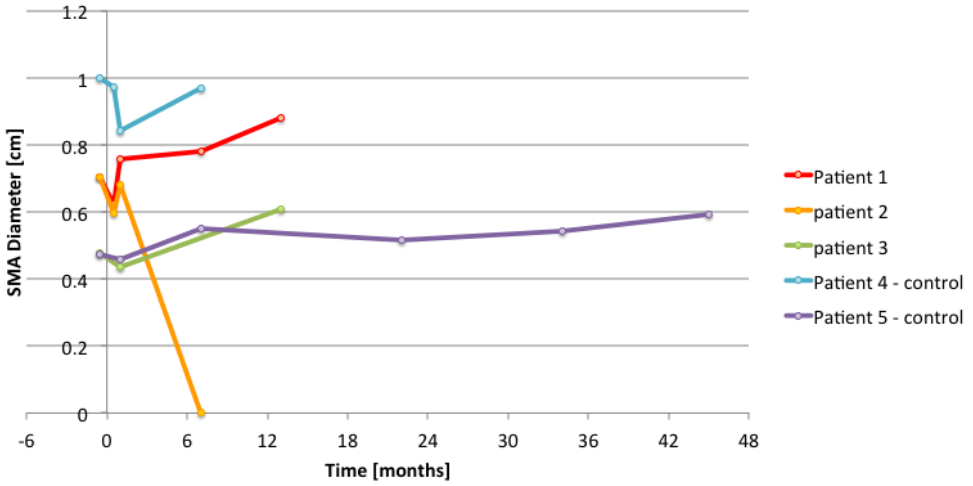

Figure 5-3. Diameters of the superior mesenteric arteries' outlets of the extended aortic geometries of the five patients.

The range of the SMA outlet is around 0.4- 1 cm (Figure 5-3), only one patient's superior mesenteric artery occluded after around 7 months. In general, it lightly decreases soon after surgery and increases again during the time.

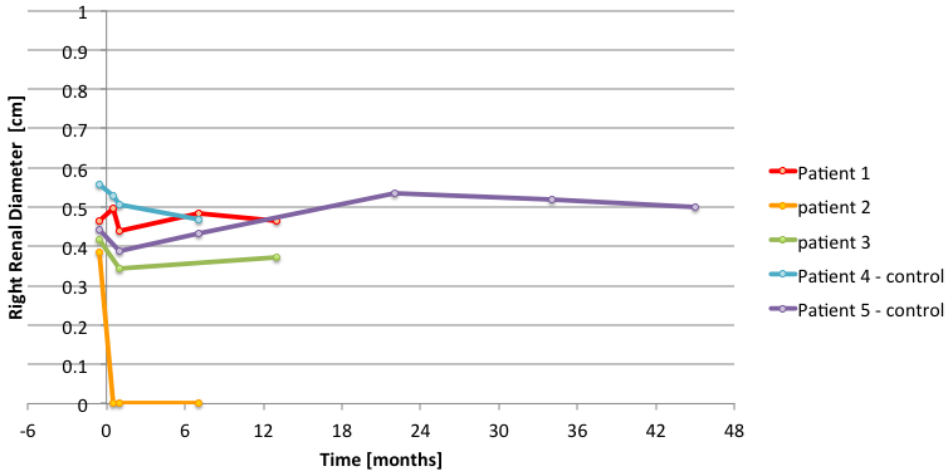

Figure 5-4. Diameters of the right renal arteries' outlets of the extended aortic geometries of the five patients.

The range of no- occluded right renal arteries is 0.35- 0.55 cm (Figure 5-4). Only one right renal artery has been intentionally occluded (patient 2), the other patients showed pretty costant values, except for the fourth patient, which artery's diameter decrease of about 2 mm.

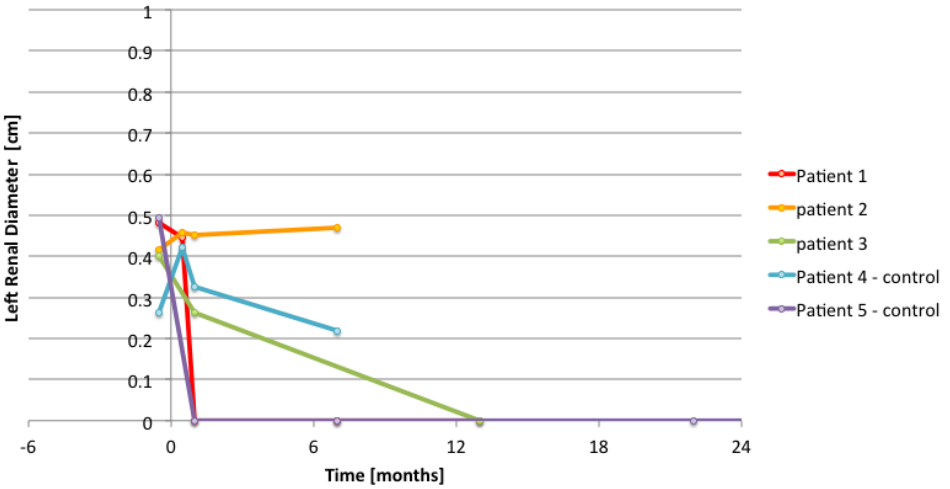

Figure 5-5. Diameters of the left renal arteries' outlets of the extended aortic geometries of the five patients.

The range of no- occluded left renal artery is 0.3- 0.5 cm (Figure 5-5). Left renal arteries spontaneously occluded in two patients (patient 1 and patient 3); patient 5's vessel has been intentionally occluded during surgery, and for patient 3 and patient 4 after a small diameter increasing after surgery, it decreased again to the initial value.

We can try to identify a trigger value for minimum CSAs (arteries that reaches values of CSA smaller than the trigger value may present higher risk of stent failure); 20 mm^2 may seem the best trigger value, but from our study it is not directly associated with graft thrombosis.

It has been used a constant flow rate at the inlet for every patient extracted from Taylor's curves flow rate[27], from which the velocity has been computed dividing by the area of every patient's geometry. A way to normalize this parameter would be to fix the velocity and compute the flow rate for each patient with the values of different areas.

Another way to perform a patient-based evaluation of the outlet percentages could be obtained by considering the patient weights and/or the dimension of the kidneys, since this is related with the amount of blood they are able to filter. A sane kidney is around 6-8 cm long (dimension of a fist) and it filters around 19% of the blood each pulse; if it stops working, its dimension decreases, then usually more blood goes to the other kidney, increasing its dimensions.

Finally, it could be possible to estimate the outflows taking in account the principle of optimal work, which says that the mass flow rate through each outlet artery is proportional to the cube of its diameter.[29]

The flow rate at the inlet of the abdominal aorta (soon after the celiac artery) has been considered 45.19 ml/sec. That means that 40.67 ml of blood arrives into the abdominal aortic tract each beat (in our model one beat lasts 0.9 sec). Considering 1050 kg/m^3 as density of the blood, it is possible to compute the mass flow rate at the abdominal aortic inlet, it is 47.43 g/sec (0.04743 Kg/sec). Thus, the cube of the each vessel's diameter should be proportional to the mass flow rate in the vessel during the time.

Table 5-1. Cube of vessel diameters [mm^3]

	CUBE OF VESSELS DIAMETER [mm^3]							
Patient	PreOp (d-m)	PostOp1 (~d)	PostOp2 (~1 m)	PostOp3 (6-8 m)	PostOp4 (12-14 m)	PostOp5 (~22 m)	PostOp6 (~34 m)	PostOp7 (~45 m)
1						--	--	--
Aorta	22.174	22.137	31.445	28.689	31.019			
SMA	0.351	0.240	0.434	0.475	0.684			
R_renal	0.100	0.123	0.084	0.113	0.101			
L_renal	0.112	0.089	0	0	0			
2					--	--	--	--
Aorta	7.714	12.540	9.581	12.146				
SMA	0.347	0.211	0.317	0				
R_renal	0.058	0	0	0				
L_renal	0.071	0.095	0.091	0.104				
3						--	--	--
Aorta	26.470		18.191		18.080			
SMA	0.108		0.083		0.224			
R_renal	0.072		0.041		0.052			
L_renal	0.065		0.018		0			
4					--	--	--	--
Aorta	17.687	24.472	20.365	21.875				
SMA	0.999	0.921	0.597	0.906				
R_renal	0.173	0.148	0.131	0.103				
L_renal	0.018	0.075	0.035	0.011				
5								
Aorta	17.810		11.042		9.151	17.905	31.121	18.996
SMA	0.106		0.095		0.168	0.138	0.160	0.209
R_renal	0.086		0.058		0.081	0.155	0.141	0.126
L_renal	0.119		0		0	0	0	0

Analyzing the values of the cube of the outlets in Table 5-1, it seems that almost all the amount of blood flow would go to the main aorta; from this first evaluation we could conclude that the principle of optimal work is not suitable for patient affected by aortic aneurysms since the dimensions of their vessels undergo to consistent modifications (enlargement for the aorta and usually stenosis on the smaller branches), and the new pathological vessel dimensions make the theory fail.

5.2 Pressures

The values of total pressure are smaller than those at the end of the segmented vessel in some zones for some of the five patients. In these cases, it possible to observe a particular phenomenon called recirculation, which consist of blood flow going in the opposite direction (from distal to proximal) because of presence of an obstacle, like the wall of the vessel because of its changing of direction.

On the other hand, the static ΔP is negative in some tracts of the PostOp conformations, consequently in these zones the blood flow is driven by inertia, instead of static pressure.

Negative values of difference of static pressure mean higher values at the bottom than in the points of interest; if we consider Bernoulli law (for incompressible flow, like blood, and hypothesizing the vessel as a perfect cylinder, eqn. 5-1), we could say that in these zones there would be higher values of velocity, and so a smaller vessel areas if compared it to the velocities and areas at the end of the vessel (Figure 5-6, A).

$$P_1 + \frac{1}{2}\rho v_1^2 + \rho g h_1 = P_2 + \frac{1}{2}\rho v_2^2 + \rho g h_2 \quad (5\text{-}1)$$

Thus, in the point of interest (point 1 in Bernoulli Law) there will be a stenosis/ compression/ stent kinking or in general reduction of the vessel lumen compared to the distal part.

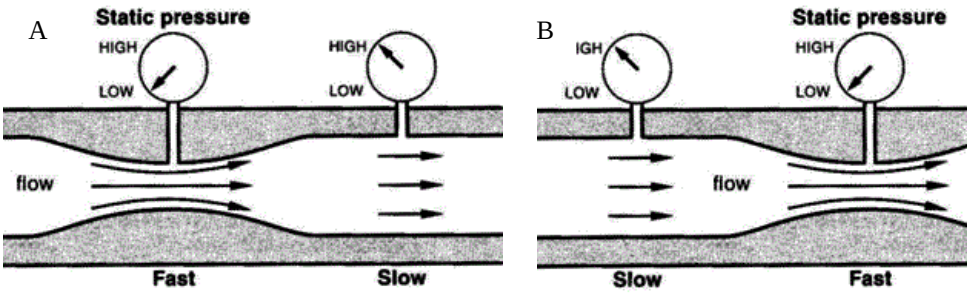

Figure 5-6. Schematics of the Bernoulli law. A) Point of interest (1 in Bernoulli Law) is a stenosis case. B) The stenosis or reduction in lumen area is at point 2 of Bernoulli Law.

The Bernoulli law is the base of very high values of static pressure difference too. In cases of stenosis/ compression/ stent kinking or in general reduction of the vessel lumen at the distal part of the vessel (point 2 in Bernoulli Law), it will experience higher values of static pressure at the point of interest (point 1 in Bernoulli Law); therefore, the more the vessel lumen becomes smaller at the distal part of the vessel and the more both the velocity at the stenosis level and the difference of static pressure between the two points will increase (Figure 5-6, B).

These phenomena can be observed comparing the curves of cross sectional areas and static ΔP through the CTs.

5.2.1 Patient 4

The SMA and right renal artery are un-stented vessels and they show a typical hemodynamic situation on smaller branches for a patient with AAA and comorbidities.

The difference of total pressure on the SMA reaches about -10 Pa on the distal part of the vessel in the PreOp situation and lightly negative values appears in the PostOp2 in the same zone, which means possible recirculation in correspondence of a sudden change of vessel direction. Fairly normal total pressure values on the right renal artery.

The fourth patient had shown negative difference of static pressure on all the configurations of the SMA between centimeter 3 and 5, except for PostOp2. In these cases the Bernoulli phenomena is clearly visible; in these zone it there is a decreasing of the CSAs if

compared to the value of area at the end of the segmented vessel (example of PostOp3, Figure 5-7).

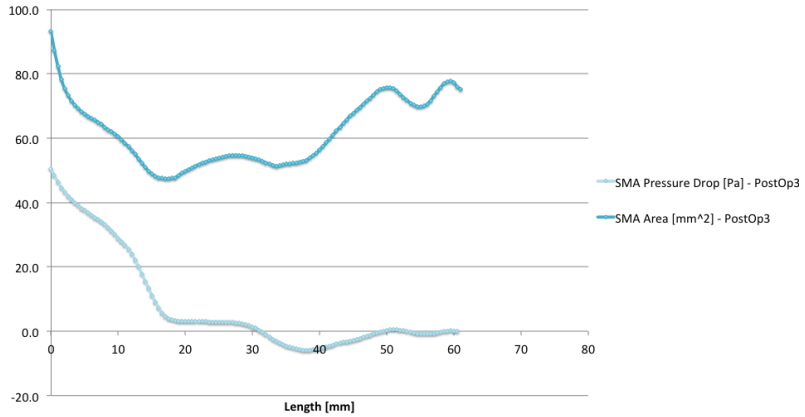

Figure 5-7. Comparison of static pressure drop and CSA on the superior mesenteric artery of PostOp3 conformation of Patient 4.

The right renal has not shown zones of negative difference of static pressure, but it is possible to notice that between 0- 1 cm and 3- 4 cm there are two small reduction of the lumen compared to the end of the vessel, in these zones the trend of the pressure drop changes (Example of PreOp, Figure 5-8).

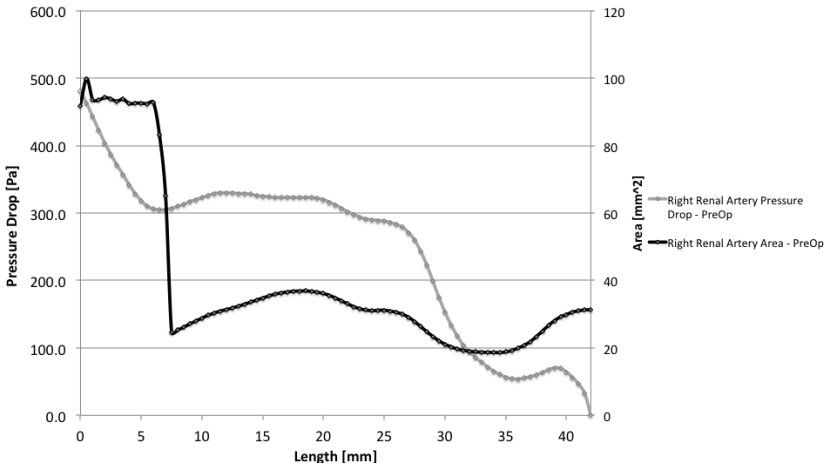

Figure 5-8. Comparison of static pressure drop and CSA on the right renal artery of PreOp conformation of Patient 4.

There are highly negative static ΔP on the PostOp2 and PostOp3 configurations of the left renal artery, between 1.5- 2 mm it corresponds to a lightly smaller CSA around at the beginning of the stenosis if compared to the end of the segmented vessel.

Patient 4 has three different situations on the three arteries. We will consider the static pressure drop peaks on the no- stented SMA and right renal artery as acceptable for patients who suffer of aortic aneurysm and other comorbidities. They differ for one order of magnitude; on the SMA the order of magnitude is 10^1, 10^2 on the right renal artery. The left renal artery shows values around 10^3- 10^4 (Table 5-2).

Table 5-2. Difference of static pressure range [Pa] of the superior mesenteric, right and left renal artery of Patient 4.

STATIC PRESSURE DROP RANGE [Pa]								
Vessels	PreOp (d-m)		PostOp1 (~d)		PostOp2 (~1 m)		PostOp3 (6-8 m)	
	Min	Max	Min	Max	Min	Max	Min	Max
SMA	-3.3	45.6	-2.4	52.5	0	50.3	-5.9	50.39
Right Renal	0	480.9	0	488.6	0	584.4	0	645.8
Left Renal	0	3187.1	0	502.0	-493.3	5041.3	0	10265.9

5.2.2 Patient 2

Patient 2 is the only case of SMA occlusion among the five patients due to a critical kinking of the stent where it enters into the actual vessel. In particular, it has shown negative difference of static pressure on the PreOp configuration of the SMA just before the end of the vessel where there is lumen reduction of the artery, and in the first cm of the artery length in PostOp2. (Figure 5-9).

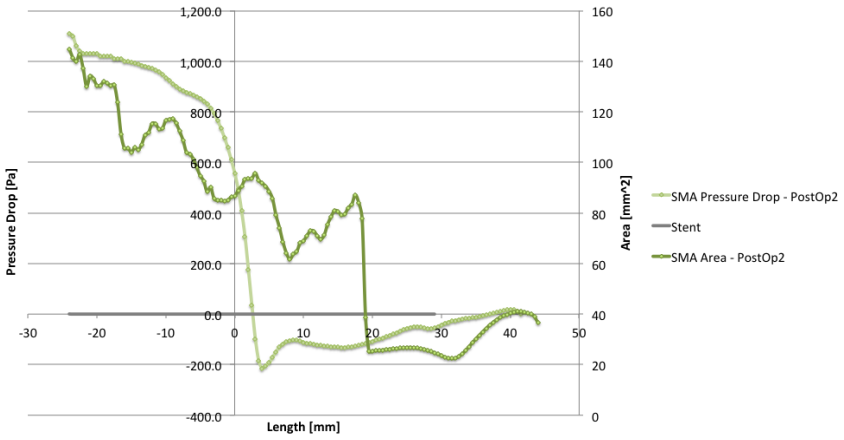

Figure 5-9. Comparison of static pressure drop and CSA on the superior mesenteric artery of PostOp2 conformation of Patient 2.

As it is possible to see in Table 5-3, the range of static pressure drop for the three arteries is really different.

Table 5-3. Difference of static pressure range [Pa] of the superior mesenteric, right and left renal artery of Patient 2.

STATIC PRESSURE DROP RANGE [Pa]								
Vessels	PreOp (d-m)		PostOp1 (~d)		PostOp2 (~1 m)		PostOp3 (6-8 m)	
	Min	Max	Min	Max	Min	Max	Min	Max
SMA	0	171.5	0	273.1	-213.8	1112.7	--	--
Right Renal	0	746.3	--	--	--	--	--	--
Left Renal	0	264.7	0	675.3	-121.5	1528.0	-148.3	1116.6

For the second patient the order of magnitude of the pressure drop on the SMA is about 10^2- 10^3 as on the left renal artery; in both cases peaks of pressure drop are reached in the part of the stent contained in the aortic lumen.

The high values of pressure drop in PostOp2 for both SMA and left renal artery could actually represent cases of hypertension.

It is interesting to observe how high was the value of static pressure drop on the right renal artery in the PreOp situation, from which the reasonable decision to occlude the vessel during the surgery to guarantee better conformation of the other two arteries, and avoid a very likely failure.

5.2.3 Patient 3

The third patient shows an interesting case of high drop of total pressure and negative difference of static pressure in case of deviation of flow, and not necessarily reduction of the vessel lumen. In fact, the CSA on PostOp4 between 0- 2 cm of the SMA is even higher than everywhere else but we can still observe big drop of pressures.

The left renal artery is a clear example of what happens when the difference of total pressure becomes very high around 10000 Pa, because of a stenosis. This vessel will occlude before one year due to a kinking and compression of the stent 1 cm after the beginning of the actual vessel.

As we can see from Table 5-4, the range of static pressure drop for the three arteries is really different.

Table 5-4. Difference of static pressure range [Pa] of the superior mesenteric, right and left renal artery of Patient 3.

STATIC PRESSURE DROP RANGE [Pa]						
Vessels	PreOp (d-m)		PostOp2 (~d)		PostOp4 (~1 m)	
	Min	Max	Min	Max	Min	Max
SMA	-10.4	310.9	-71.5	288	-203.0	881.7
Right Renal	-15.8	1453.2	-353.5	2048.9	0	3282.3
Left Renal	-47.1	2538.2	-1423.3	9770.11	--	--

The Patient 3's peaks of difference of static pressure on the SMA are one order of magnitude smaller than those on the renal arteries (10^2 vs 10^3 almost 10^4 in the PostOp2 of the left renal artery); but they are reached at the beginning of the stent in the intra- aortic lumen.

The high values of static pressure drop on the renal arteries could represent cases of hypertension.

5.2.4 Patient 1

Patient 1 present an example of two very different situations on the renal arteries. The right renal artery showed high values (5000 Pa) of difference of total pressure after one year without occlusion; on the other hand, the total ΔP on the left renal artery was about 600 Pa few days after surgery and, but the vessel occluded soon after.

The right renal presents small negative difference of static pressure values in PostOp1 and PostOp2 between 0.7 and 2 cm of the vessel length, even in this case the areas decrease if compared with the end of the vessel. These phenomena of stenosis are due to kinking of the stent and usually to change of vessels direction.

The left renal artery does not present negative static pressure drop values few days after the surgery.

As we can see from Table 5-5, the range of static pressure drop for the three arteries is really different.

Table 5-5. Difference of static pressure range [Pa] of the superior mesenteric, right and left renal artery of Patient 1.

STATIC PRESSURE DROP RANGE [Pa]										
Vessels	PreOp (d-m)		PostOp1 (~d)		PostOp2 (~1 m)		PostOp3 (6-8 m)		PostOp4 (12-14 m)	
	Min	Max	Min	Max	Min	Max	Min	Max	Min	Max
SMA	0	101.0	-13.4	55.6	-15.5	62.7	-22.8	137.0	-15.0	102.4
Right Renal	0	314.9	-24	365.7	-133	894.0	0	4836.9	0	4876.7
Left Renal	0	66.4	-0.6	405.7	--	--	--	--	--	--

The maximum static pressure drop on the left renal is lower than those on the right artery in the PreOp conformation, it becomes higher on the PostOp1, but still lower than the values that the right renal artery will reach in PostOp2, PostOp3, PostOp4. Therefore, it is not the static ΔP by itself that directly determines the failure of the vessel, since the right renal artery after one year did not fail.

5.2.5 Patient 5

Patient 5 presents an interesting case since his situation has been monitored until 45 months after surgery. In particular, the 50 Pa of difference of total pressure on the PreOp configuration become almost 400 Pa after 1 month, and the situation stabilizes until around 7 months, then after 22 months the difference of total pressure decrease to 350 Pa, but it finally increase again until 45 months reaching 1000 Pa of total pressure drop along the vessel.

On the right renal artery the situation kept on worsening little by little reaching 2800 Pa of difference of total pressure.

PostOp6 and PostOp7 configurations of the SMA of Patient 5 have shown negative static pressure drop at the beginning of the actual vessel; in these zones the Bernoulli phenomena is clearly visible.

Negative static pressure drops on the right renal are between centimeter 1 and 3 on the last three post- operation situations (22, 34, and 45 months after surgery, Figure 5-10), where smaller CSA than the end of the segmented vessel appear.

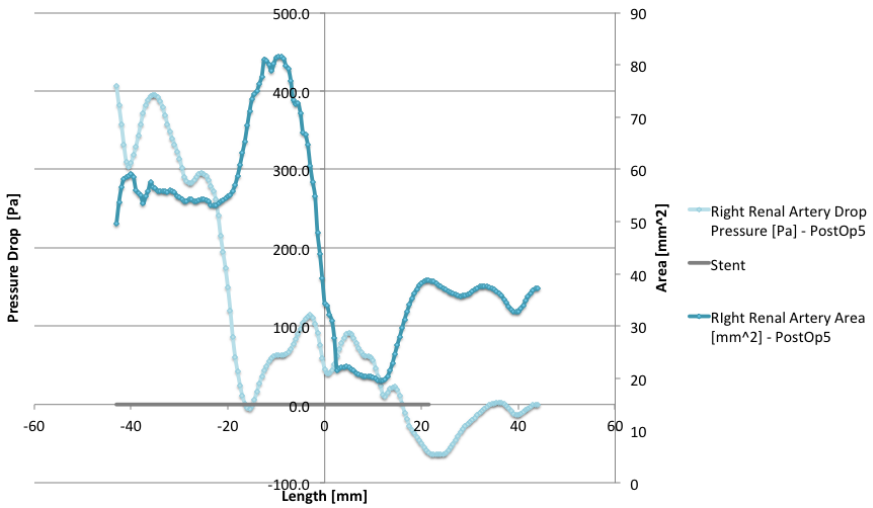

Figure 5-10. Comparison of static pressure drop and CSA on the right renal artery of PostOp5 conformation of Patient 5

No negative static pressure drops appear on the PreOp of the left renal artery.

Patient 5 has peaks of static ΔP of 10^2 order of magnitude on the SMA and those on the right renal artery are one order of magnitude bigger (10^3, Table 5-6).

Table 5-6. Difference of static pressure range [Pa] of the superior mesenteric, right and left renal artery of Patient 5.

STATIC PRESSURE DROP RANGE [Pa]												
Vessels	PreOp (d-m)		PostOp2 (~1 m)		PostOp3 (6-8 m)		PostOp5 (~22 m)		PostOp6 (~34 m)		PostOp7 (~45 m)	
	Min	Max	Min	Max	Min	Max	Min	Max	Min	Max	Min	Max
SMA	0	299.3	0	460.6	0	424.4	0	326.3	-105.8	496.0	-88.53	735.95
Right Renal	0	229.4	0	1743.7	0	976.9	-64.3	406.1	-33.4	1013.8	-23.0	1311.0
Left Renal	0	254.8	--		--		--		--		--	

5.2.6 Consideration on Pressure among the Five Subjects

We will consider the values obtained on the two sane vessels of the fourth patient as reference for subjects affected by AAA, and other comorbidities, but with 'healthy' smaller vessels.

In general, negative differences of static pressure are observed close to zones of stenosis/ compression/ kinking of the stent, such as the beginning of the vessel (when the vessel is stenotic), close to the end of the stent or the vessel or any other change of direction of the vessel

to reach the organs. Thus, the general reason of this phenomena is a brutal morphological change of the vessels direction/ lumen area.

Moreover, it seems that the values of static pressure drop on the two renal arteries in the part of the stent contained in the aortic lumen can become much higher if compared with those on the SMA.

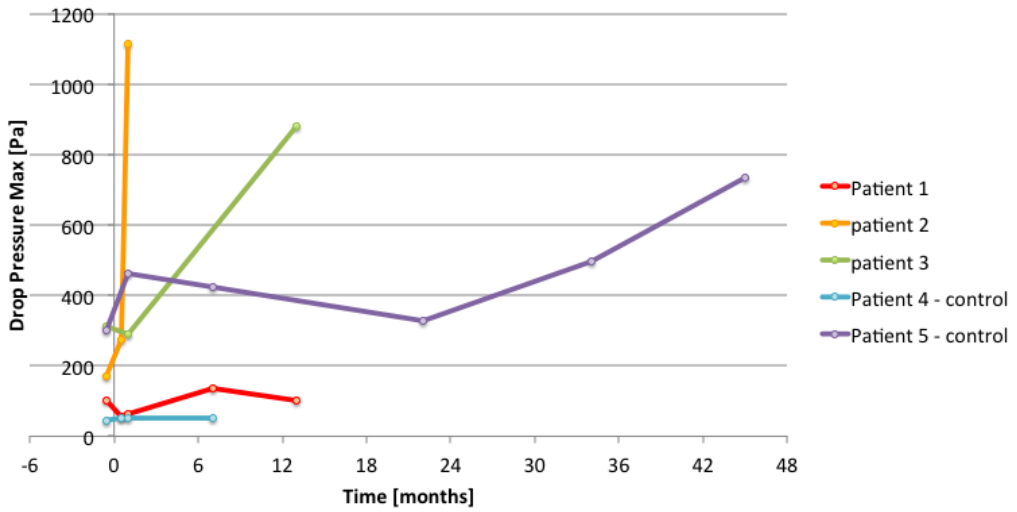

Figure 5-11. Maximum values of static pressure difference on the SMA for each patient during the time.

For Bernoulli principle, the acute stenosis on the superior mesenteric artery of patient 2 (1 month after surgery) and patient 5 (34 and 45 months post- operation) causes the high values of maximum static pressure drop (Figure 5-11).

As previously observed, the drop of static pressure depends from the length of the analyzed vessel too; in fact, this is one other reason for the very high values computed on Patient 5 (PostOp6 and PostOp7) and Patient 3 (PostOp4), since the segmented vessel is 9 and 6.3 cm long respectively.

Plausible values of static ΔP on a un-stented SMA would lower than 100 Pa for a segment 6 cm long (Patient 4), and acceptable values around 150 Pa for a stented vessel 5 cm long.

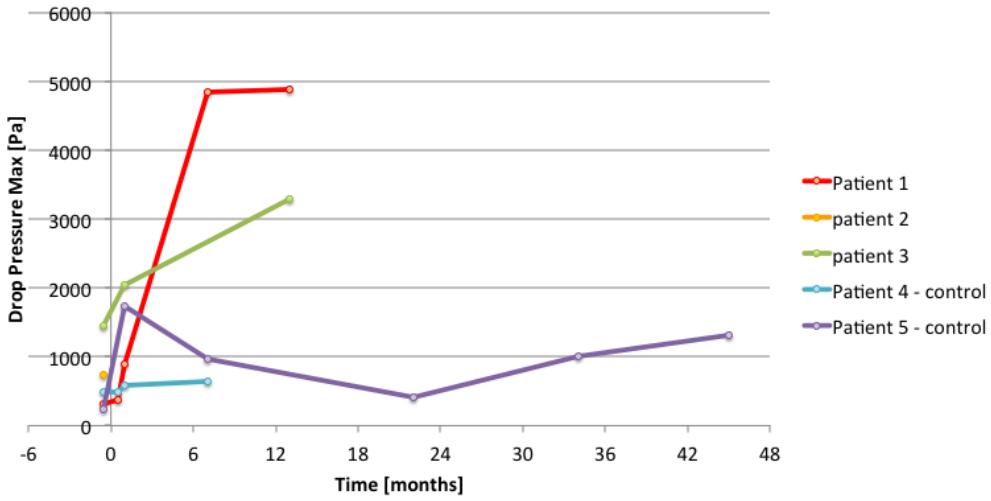

Figure 5-12. Maximum values of static pressure difference on the right renal artery for each patient during the time.

High values of static pressure drop on the right renal artery of the Patient 1 are due to the stenosis (kinking of the stent) detected on PostOp2, but worsened on the next to CTs. The fairly high values on the right renal artery of Patient 3 and Patient 5 are caused by the long length of the segmented tract (8.5- 9 cm). Acceptable values on this artery detected up to 700 Pa (Figure 5-12).

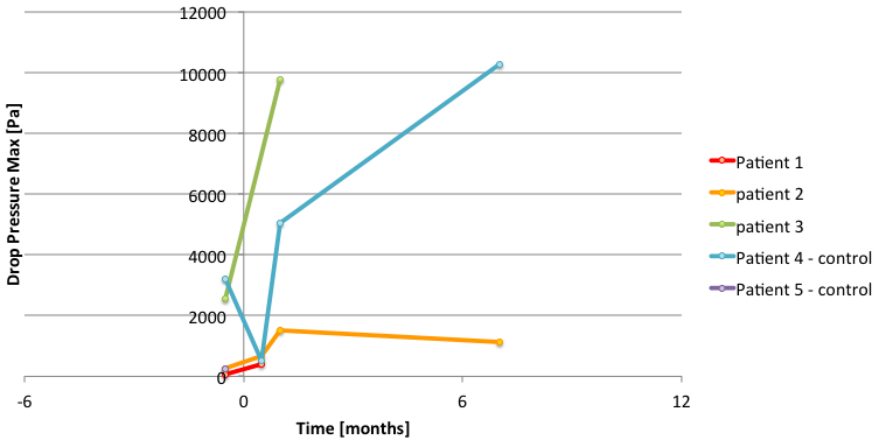

Figure 5-13. Maximum values of static pressure difference on the left renal artery for each patient during the time.

On the left renal artery, Patient 3 and patient 4 experienced high values of static pressure drop, both of them showed a segmented vessel tract of about 6.5- 7 cm. The main reason of these is a critical stenosis, which brought to stent failure on patient 3's PostOp4 (Figure 5-13).

In conclusion, maximum values of pressure drops have been detected between few hundreds and 1000 Pa on the SMA, and always higher than 800 on the two renal arteries. Non-stented SMA showed around 100 Pa static pressure drop value; and low than 700 Pa for the right renal artery. An explanation of this difference between the vessels could be the diverse natural conformation of the vessels. Renal arteries are naturally perpendicular to the aorta, thus they undergo to completely shape- modification after surgery, when they are forced to follow the chimney shape; on the other hand, the superior mesenteric artery has a natural caudal conformation, which is easily adaptable to the new vessel shape.

If we try to identify a trigger value for total pressure differences, 2000 Pa may seem the best value, but from our study it is not directly associated with graft thrombosis.

5.3 Wall Shear Stress

Where the lumen of the vessel decrease, the velocity increases and consequently higher wall shear stresses are usually observed; therefore, it is important to notice where the highest values of WSS appears.

Also in this case, the most stressed zones are the beginning of the stent and the insertion into the vessel (zero on the x- axes). A visible and significant reduction of cross sectional areas usually correspond to these zones, this could be caused by a compression (in case of stent graft in the aorta lumen), or a kinging of the stent for any reason (for example change of vessel direction). This observation is valid for every vessel, even for the SMA where the values of wall shear stresses usually do not change in term of order of magnitude.

Moreover, some studies[12] reported that values of WSS between -0.4 and 0.4 Pa are dangerous for atherosclerosis formation; on the other hand, WSS bigger than 7 Pa would cause thrombosis. In our study, values of WSS minor than 0.4 Pa are not present on any artery, but almost all stented vessels have shown wall shear stresses higher than 7 Pa.

5.3.1 Patient 4

The two un-stented vessel of Patient 2 presented values of WSS that fit fairly enough in the range estimated for normal artery (1-7 Pa). The right renal artery has peak values which exceeds 7 Pa. Values of WSS are higher than 7 Pa on the stented left renal artery, in correspondence of the stenosis and the peak of WSS reaches almost 200 Pa in PostOp3 configuration (Table 5-7). The WSS on the superior mesenteric artery are one order of magnitude smaller if compared to the values on the renal arteries.

Table 5-7. Average with standard deviation and maximum value of wall shear stress [Pa] of the superior mesenteric, right and left renal artery of Patient 4.

WALL SHEAR STRESS [Pa]								
Vessels	PreOp (d-m)		PostOp1 (~d)		PostOp2 (~1 m)		PostOp3 (6-8 m)	
	M+SD	Max	M+SD	Max	M+SD	Max	M+SD	Max
SMA	1.1 ± 0.4	2.4	1.2 ± 0.4	2.0	1.2 ± 0.4	2.7	1.2 ± 0.5	2.3
Right Renal	6.2 ± 2.4	13.2	6.3 ± 2.1	14.3	7.8 ± 2.1	12.0	8.3 ± 2.7	19.1
Left Renal	30.1 ± 19.7	86.1	11.9 ± 4.4	24.0	37.1 ± 28.3	106.2	62.7 ± 47.0	189.5

5.3.2 Patient 2

The wall shear stresses on the SMA during the PreOp are in a range of 1-6 Pa. The WSS in the PostOp situations reaches a maximum value of 40.5 Pa in the last CTs. The peaks of WSS correspond to the transition from the aortic lumen into the actual vessel where the critical stenosis is located, causing its occlusion soon after (Graph in Appendix B).

In the after surgery conformations of the left renal artery, the highest values of WSS are located before the beginning of the actual vessel. High wall shear stresses are reached at the end of the vessel in the PreOp configuration. Even if the segmentation till the end of the renal artery has not been possible, it is possible to observe that the range of WSS on the left renal artery on the PostOp situations is between 5 and 30 Pa, a fairly similar range if compared with 3- 25 Pa in the PreOp (Graph in Appendix B).

The range of WSS for the three arteries is very different. The SMA presents averages of wall shear stresses smaller than 10 Pa, even if shows four times higher peaks. On the left renal artery it is possible to observe more than doubled average of WSS (Table 5-8).

Table 5-8. Average with standard deviation and maximum value of wall shear stress [Pa] of the superior mesenteric, right and left renal artery of the Patient 2.

WALL SHEAR STESS [Pa]								
Vessels	PreOp (d-m)		PostOp1 (~d)		PostOp2 (~1 m)		PostOp3 (6-8 m)	
	M+SD	Max	M+SD	Max	M+SD	Max	M+SD	Max
SMA	2.6 ± 0.9	5.5	4.0 ± 2.3	13.0	8.7 ± 6.9	40.5	--	
Right Renal	10.8 ± 4.1	25.2	--		--		--	
Left Renal	7.9 ± 4.8	25.1	10.7 ± 3.2	18.2	18.16 ± 4.2	31.7	15.7 ± 5.1	28.2

5.2.3 Patient 3

The SMA presents fairly normal values of wall shear stresses (maximum 30 Pa). On the other hand, the right and left renal arteries show values much higher than 7 Pa on the PostOp2 conformation where there is compression of the vessel, which will cause occlusion of the left renal artery (Table 5-9).

Table 5-9. Average with standard deviation and maximum value of wall shear stress [Pa] of the superior mesenteric, right and left renal artery of Patient 3.

WALL SHEAR STRESS [Pa]						
Vessels	PreOp (d-m)		PostOp2 (~1 m)		PostOp4 (12-14 m)	
	M+SD	Max	M+SD	Max	M+SD	Max
SMA	5.2 ± 1.6	9.3	10.0 ± 5.8	25.7	10.3 ± 6.5	29.7
Right Renal	14.0 ± 3.9	29.0	31.8 ± 21.2	126.4	27.1 ± 13.0	80.1
Left Renal	24.5 ± 14.3	74.4	64.1 ± 36.0	174.8	--	

The average of WSSs on the renal arteries reaches values 3- 6 times higher than the SMA. Nonetheless, in PostOp3 on the SMA they reach a fairly high value (30 Pa), in the area where there is no compression or kinking, but there is a deviation of the vessel due to the presence of the right renal artery.

5.2.4 Patient 1

Both on the right and left renal artery there is risk of thrombosis in the stenotic zone, where WSSs reach values much higher than 7 Pa (Table 5-10).

Table 5-10. Average with standard deviation and maximum value of wall shear stress [Pa] of the superior mesenteric, right and left renal artery of Patient 1.

WALL SHEAR STRESS [Pa]										
Vessels	PreOp (d-m)		PostOp1 (~d)		PostOp2 (~1 m)		PostOp3 (6-8 m)		PostOp4 (12-14 m)	
	M+SD	Max	M+SD	Max	M+SD	Max	M+SD	Max	M+SD	Max
SMA	2.2 ± 0.6	3.3	3.1 ± 1.2	5.9	2.6 ± 0.7	5.7	4.0 ± 2.3	16.6	3.9 ± 2.5	17.9
Right Renal	7.7 ± 2.8	13.7	7.8 ± 4.0	16.1	15.4 ± 6.3	31.8	33.0 ± 20.0	96.9	29.1 ± 19.8	93.0
Left Renal	10.1 ± 2.6	15.1	23.2 ± 11.0	56.4	--		--		--	

The average of WSS on the right renal artery result more than the double of the SMA's values; the values on the left renal in the PreOp and PostOp1 conformations are comparable to those of the right artery, which means that if the vessel did not occlude we could have observed similar or higher values to the right renal. Nonetheless, it is not the WSS by itself that directly determines the failure of the vessel, since on the right renal artery we will observe higher values, but the vessel and the stent did not fail after one year.

5.2.5 Patient 5

Both SMA and right renal artery have very low WSS almost everywhere along the segmented vessel, but still higher than 0.4 Pa, with peaks in some zones which do not exceed 50 Pa. The mean values of wall shear stress on the right renal artery are more than two times higher than the values on the SMA (Table 5-11, 5-12).

Table 5-11. Average with standard deviation of wall shear stress [Pa] of the superior mesenteric, right and left renal artery of Patient 5.

WALL SHEAR STRESS AVERAGE ± ST DEV [Pa]						
Vessels	PreOp (d-m)	PostOp2 (~1 m)	PostOp3 (6-8 m)	PostOp5 (22 m)	PostOp6 (34 m)	PostOp7 (45 m)
SMA	2.5 ± 1.5	5.4 ± 4.4	5.0 ± 2.8	4.3 ± 1.9	5.9 ± 4.2	6.3 ± 4.2
Right Renal	4.0 ± 2.1	14.6 ± 7.4	10.2 ± 3.5	8.9 ± 3.2	11.8 ± 4.4	14.7 ± 4.0
Left Renal	4.1 ± 1.4	--	--	--	--	--

Table 5-12. Maximum value of wall shear stress [Pa] of the superior mesenteric, right and left renal artery of Patient 5.

WALL SHEAR STRESS MAXIMUM [Pa]						
Vessels	PreOp (d-m)	PostOp2 (~1 m)	PostOp3 (6-8 m)	PostOp5 (22 m)	PostOp6 (34 m)	PostOp7 (45 m)
SMA	12.1	28.6	13.9	11.1	22.0	22.2
Right Renal	16.1	44.9	22.5	19.82	27.7	25.7
Left Renal	8.4	--	--	--	--	--

5.3.6 Consideration on Wall Shear Stress among the Five Subjects

In conclusion, for each patient the order of magnitude of WSS on the renal arteries is usually much higher if compared to the WSS on the superior mesenteric artery. The following graphs will show the maximum values of WSS for each patient during the time; it is then possible to observe the different ranges on the three vessels (SMA in Figure 5-14, right renal artery in Figure 5-15, left renal artery in Figure 5-16).

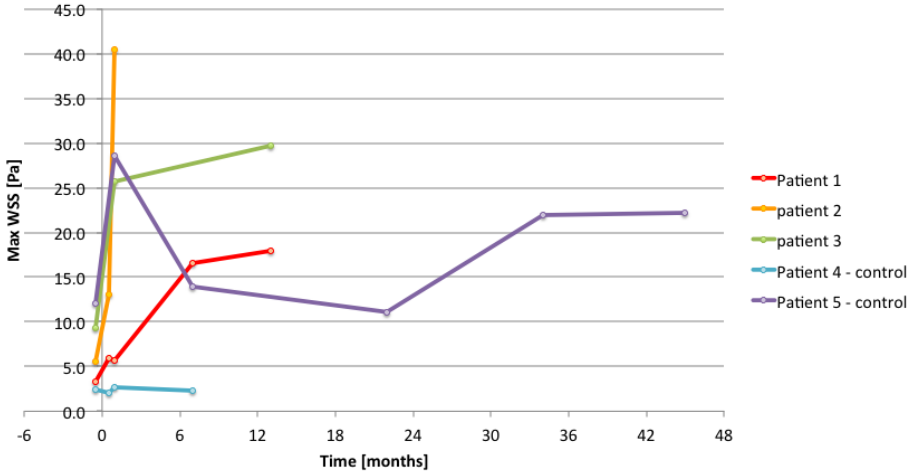

Figure 5-14. Maximum values of wall shear stress on the SMA of the five patients during the monitored time.

The maximum of WSS on the stented superior mesenteric artery is in a range of 2- 40 Pa for all the patient; no-stented vessel showed lower WSS (2.5 Pa).

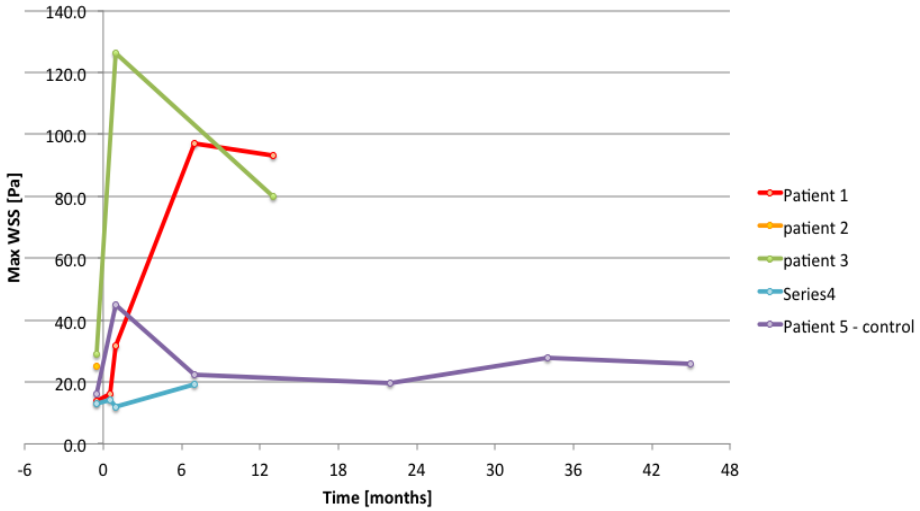

Figure 5-15. Maximum values of wall shear stress on the right renal artery of the five patients during the monitored time.

Maximum values of wall shear stresses on the right renal artery are in a range of 13- 127 Pa. Right renal artery of patient 1 and patient 3 have shown the highest values (96- 127 Pa), the reason of it is that they had acute stenosis (patient 1) and compression by the SMA (patient 3).

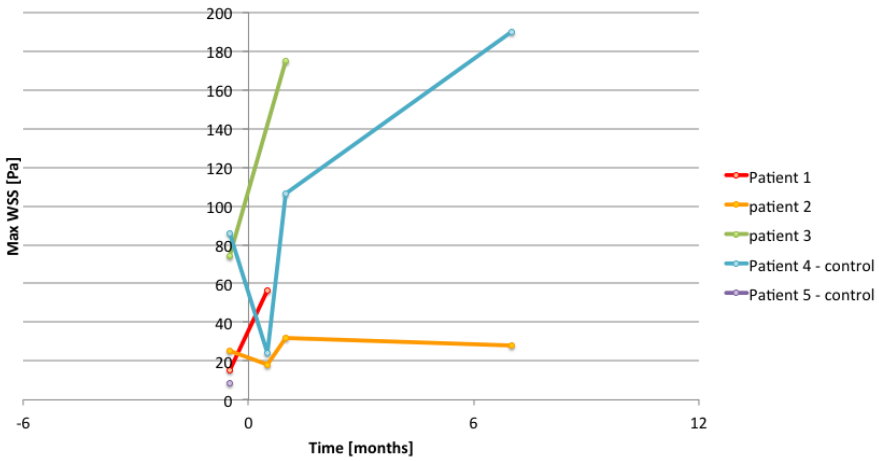

Figure 5-16. Maximum values of wall shear stress on the left renal artery of the five patients during the monitored time.

The highest maximum value of WSS are on the Patient 1, Patient 2 and Patient 4 left renal last conformations (50- 190 Pa) due to compression and stenosis of the vessels. The observed range of values is between 10 and 190 Pa.

In conclusion, the range of WSS average results to be between 2- 11 Pa on the stented SMA and 5-33 Pa on the stented right renal artery and between 5 Pa and 65 Pa on the stented left renal artery; on the other hand, the maximum values of WSS are much higher on the three vessels. The peak of WSS on SMA, right and left renal artery are respectively in ranges of 2- 40 Pa, 13- 127 Pa, and 10- 190 Pa, which are fairly high values according to Malek et al. (1999) [12]. In their study, they concluded that values bigger than 7 Pa would represent risk of thrombosis in the vessel lumen, therefore both the right and left renal artery of the five patient would risk thrombosis.

An explanation of this phenomena could be found once again in the conformation of these vessels. Since the natural shape of the renal arteries is perpendicular to the aortic vessel, it undergoes to modification after surgery when they are forced to acquire the chimney shape/ profile. This means that the vessel will need to abruptly change direction along the path in order to reach the organ; which consequently brings a sudden change in the blood flow direction. When the blood flowing into a vessel collides with the wall artery, high WSS on that area of the wall will appear. Moreover, the presence of the stent would give a more rigid structure to the vessel, which could limit its changes of direction, causing kinking and lumen reduction. The situation for the SMA is quite different thanks to its natural caudal conformation, since the vessel undergoes smoother changes of direction. In conclusion, any brutal change in the vessel direction/ lumen area make the hemodynamic situation of the vessel change, causing higher WSS.

The values of WSS on the non- stented vessels results to be between 2 and 20 Pa (2- 2.8 Pa on the SMA and 13- 20 Pa on the renal artery), fairly reasonable values if considered

maximum values and compared with the study reported by Malek et al. (1999) [12], in which a physiological artery presented values between 1- 7 Pa.

Despite striking anatomic and hemodynamic changes from pre-op, only 3 of 13 branch grafts occluded within the follow-up period. An analysis of WSS values associated with graft thrombosis demonstrates that a change in the maximum shear stress greater than 35 Pa (350 dynes/cm2) is correlated with branch graft occlusion.

5.4 Different Flow Rate at the Inlet

Results referred to the ± 25% of the 'normal' blood flow have shown that the values of WSS on the three arteries in case of +25% blood flow are in average around 1.32-1.50 times higher than the values obtained in the 'normal' flow rate case; same range resulted by comparing values of WSS in the normal flow rate case to -25% case. In term of Pressure drop, this range is in average between 1.24 and 1.66 for both cases.

In case the computed velocity in the aorta results too low, due to a big aortic CSA, we should consider the results of WSSs and pressure drops obtained with + 25% of flow rate (about 1.33 times the shown hemodynamic values); in case of small aortic area at the inlet, we should consider the values obtained with the -25% of the 'normal' blood flow (about 0.75 times the shown hemodynamic values).

CHAPTER 6
CONCLUSIONS

6.1 Overall Conclusions

Risk zones have been detected where lumen reduction is experienced, because of stenosis, lumen compression, kinking of the stent.

In conclusion, negative difference of static pressure and higher WSS are observed close to these risk zones, usually located at the beginning of the proper vessel (when the vessel shows stenosis cases or most likely due to deviation of flow), close to the end of the stent or the vessel and at any other point in which the vessel direction brutally change. This phenomena is explained thanks Bernoulli law; it happens because the stent, which has at the beginning a vertical direction (parallel to the aortic vessel), needs to curve into an almost perpendicular direction in order to enter into the vessel causing a hemodynamic perturbation.

In particular, the maximum values of difference of static pressure and the WSS on the two renal arteries resulted much higher if compared with those on the SMA. Maximum values of static pressure drop have been observed in a range of 100- 1100 Pa for the superior mesenteric artery and higher than 800 Pa on the renal arteries (even if, in both cases, the length of the segmented tracts influenced these results). Values of non- stented SMA are around 100 Pa; lower than 700 Pa for the non-stented right renal artery.

On the other hand, maximum values of WSS on the SMA are between 2- 40 Pa, and on the renal arteries the range is from 13 Pa to 127 Pa for the right renal and 10- 190 Pa for the left renal. WSS values of non- stented vessels resulted between 2- 20 Pa (2-3 Pa for the SMA and 13-20 for the renal artery), a bit higher if compared with results obtained in previous studies.[12] The explanation of this difference between renal and superior mesenteric arteries is the natural conformation of the vessels; the SMA has a natural caudal shape that remains almost unvaried

after surgery. The renal artery naturally develops in a direction almost perpendicular to the aortic vessel; then after surgery they are forced to conform to the stent position, which needs to be parallel to the aorta at least for the first 2-3 cm, to guarantee stability of the stent. After these first centimeters the stent graft will enter into the artery generating brutal change of direction with all its consequences.

Finally, the critical parameter that seem to correlate to stent graft thrombosis is the maximum value of wall shear stress; the identified trigger value is 35 Pa, for values higher than this there is high risk of graft failure due to thrombus.

6.2 Future Work

Many aspects of this phenomena could be deepened.

A study velocity path lines and the time-average Reynolds (Re_m) and the Womersley (α) numbers for the pre- and post- operative models in the SMA, right and left renal arteries in order to understand the state of flow (laminar/transient) in these smaller vessels could be performed.

In general, we can say at the inlet it is within

$$Re_{peak} = \frac{v\, D\, \rho}{\mu} = 537.6\text{- } 963.63 << 2000 \rightarrow \text{laminar flow}$$

with v_{peak} = 0.04-0.129 m/s, D = 0.0249- 0.0448 m, ρ = 1050 kg/m^3, and μ = 0.0035 Pa s.

Then the flow is always laminar at the inlet. But what happens when the area gets much smaller and the peak velocity increases?

Moreover, an experimental setup performing a 3D patient-based model of the aortic aneurysm PreOp and PostOp (with endovascular repair) could be realized in order to compare the computational results with the experimental ones.

A third interesting option will be to analyze Fenestrated Endograft Technique cases by a computational point of view and compare these hemodynamic results with those obtained for the

CG Technique in order to understand hemodynamical differences and comprehend their fluid-dynamical characteristics. And maybe think about a new technique that mixes the advantages of both.

APPENDIX A
PATIENT 1 - MORPHOLOGICAL AND HEMODYNAMICAL RECORDS

Morphological situation of patient 1 on PreOp and PostOp1 (the superior mesenteric artery is on the other side of the aorta).

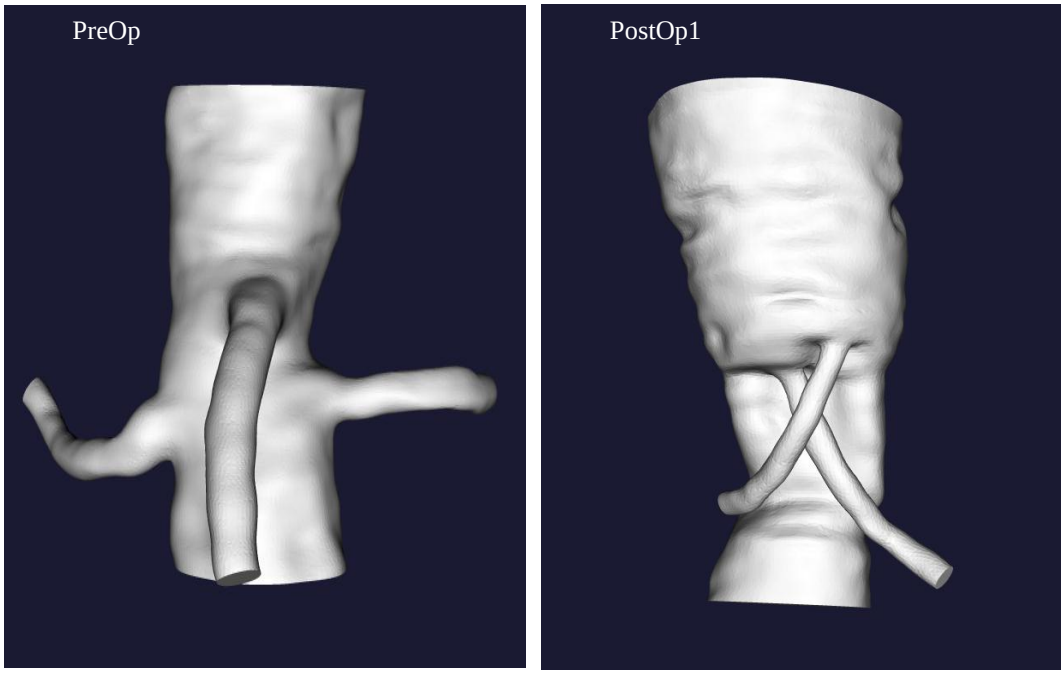

SUPERIOR MESENTERIC ARTERY

Difference of static pressure

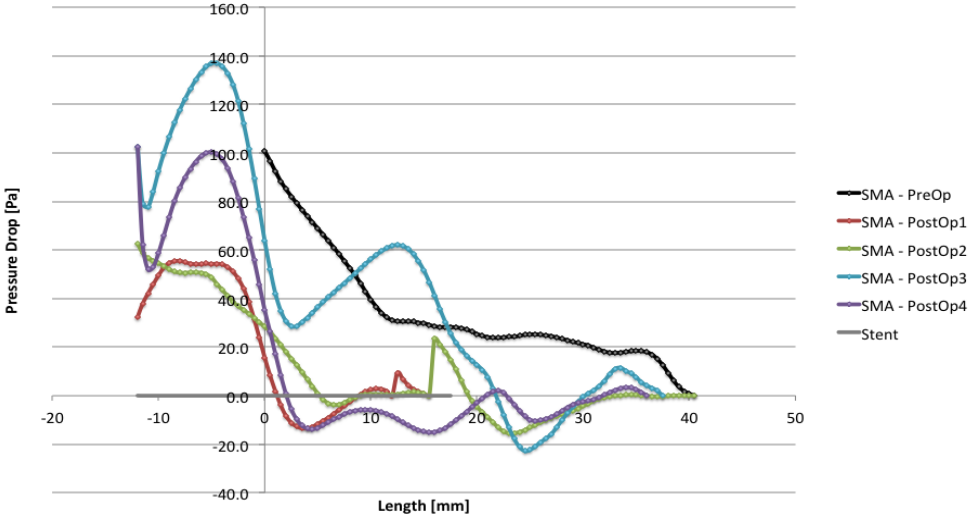

Gradient of total pressure

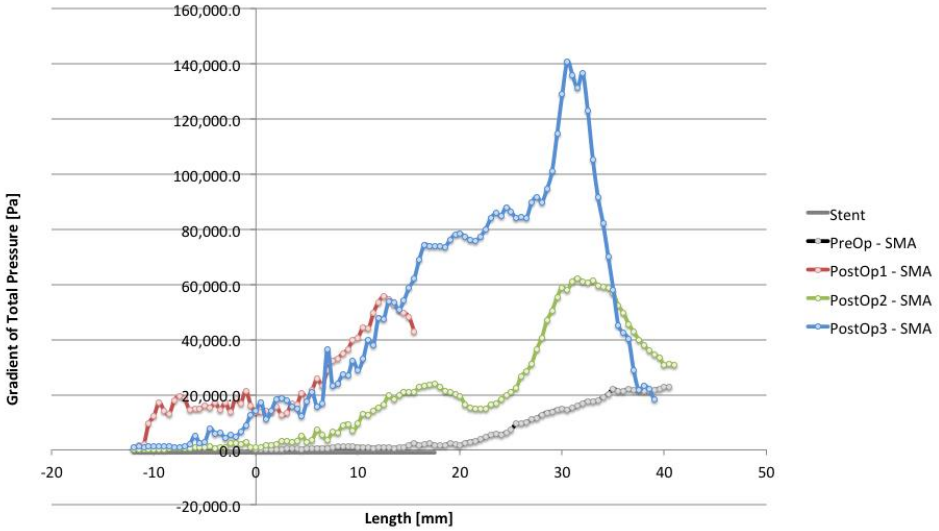

RIGHT RENAL ARTERY

Difference of static pressure

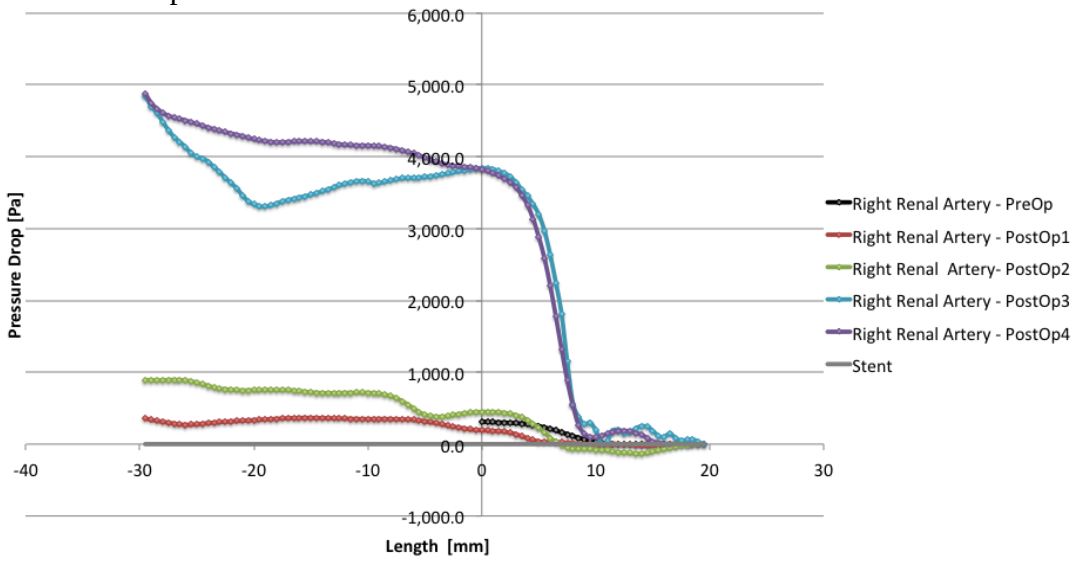

Gradient of total pressure

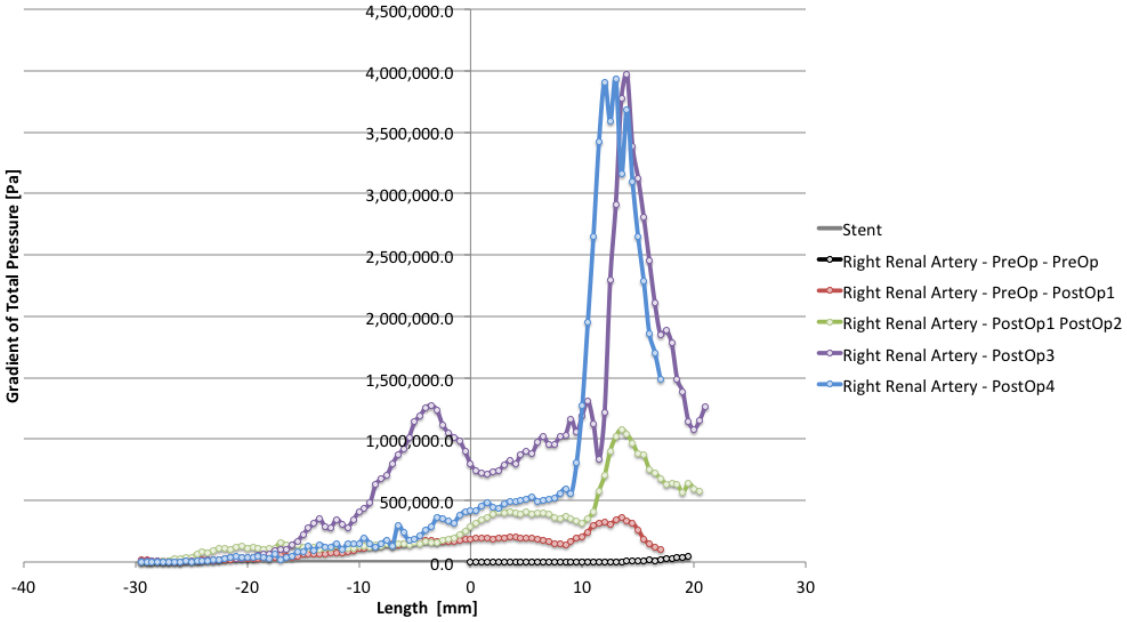

LEFT RENAL ARTERY

Difference of static pressure

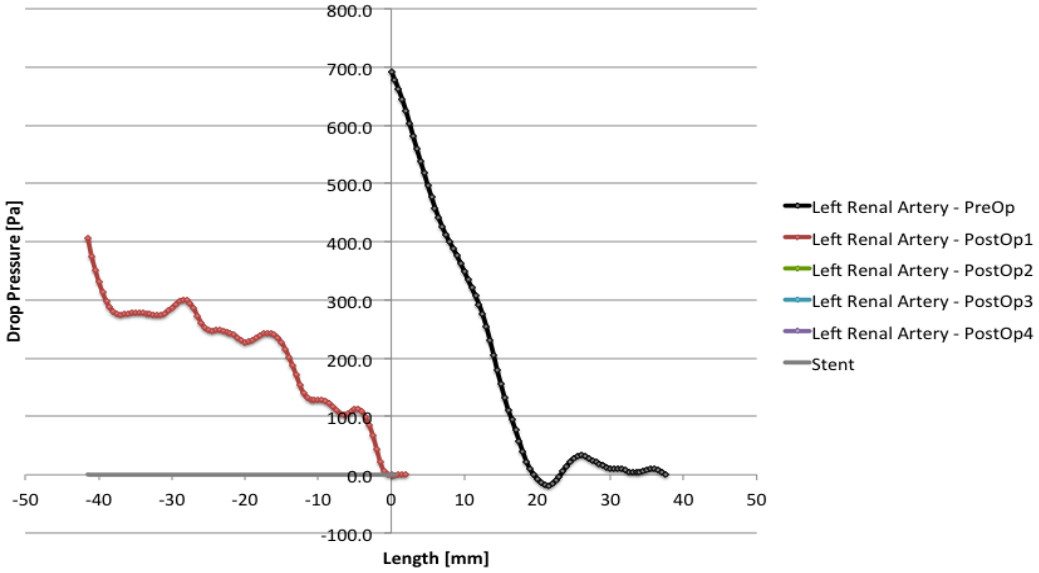

Gradient of total pressure

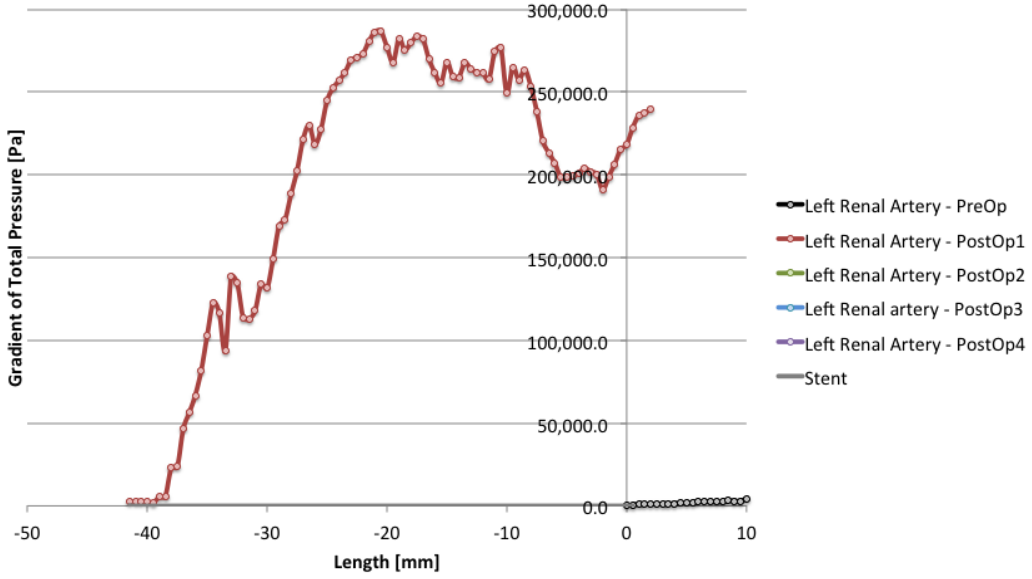

APPENDIX B
PATIENT 2 - MORPHOLOGICAL AND HEMODYNAMICAL RECORDS

Morphological situation of patient 2 on PreOp and PostOp1 (the right renal artery has been intentionally occluded).

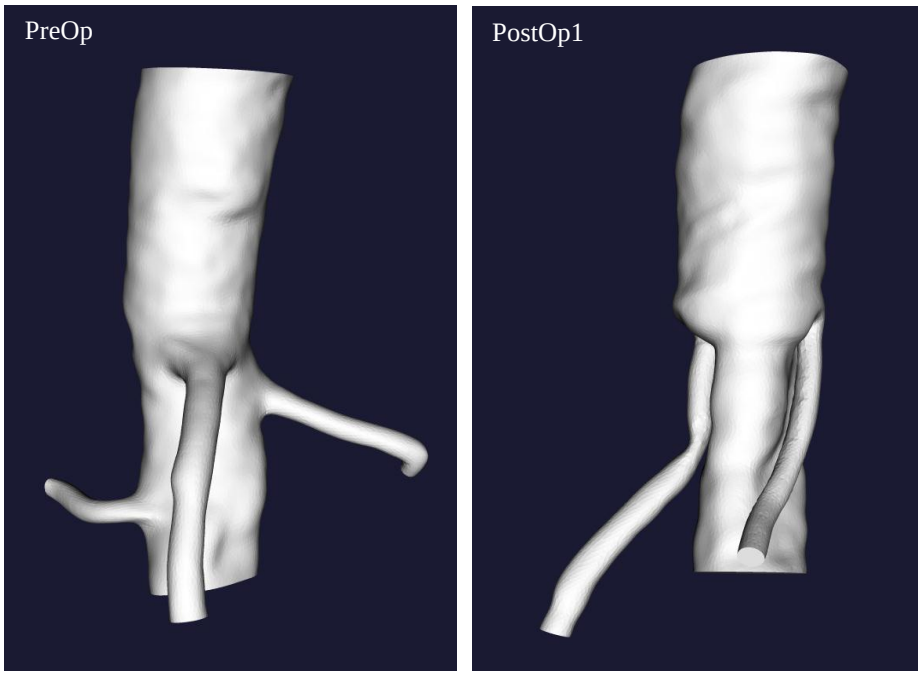

SUPERIOR MESENTERIC ARTERY

Difference of static pressure

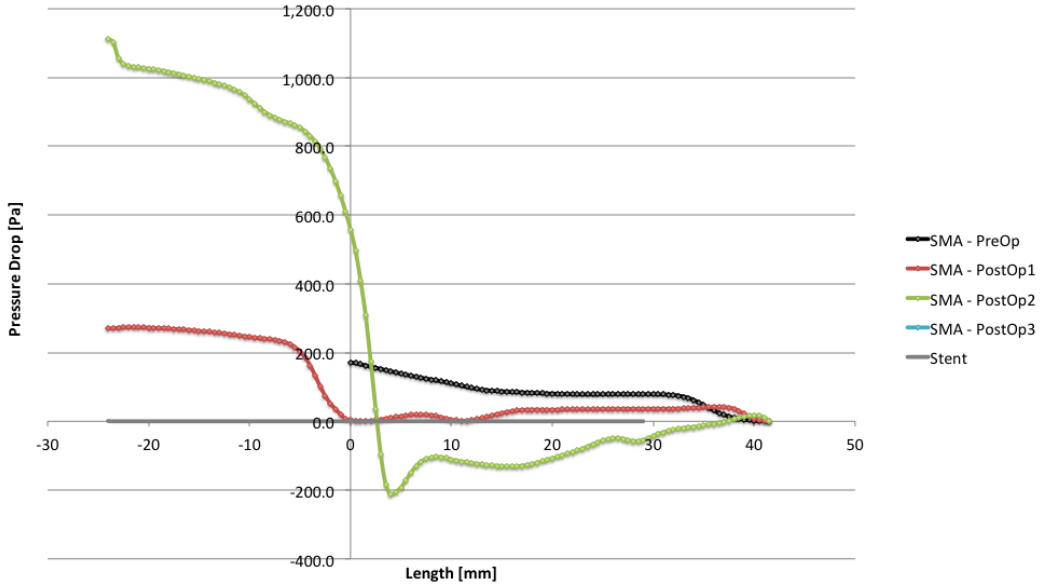

Gradient of total pressure

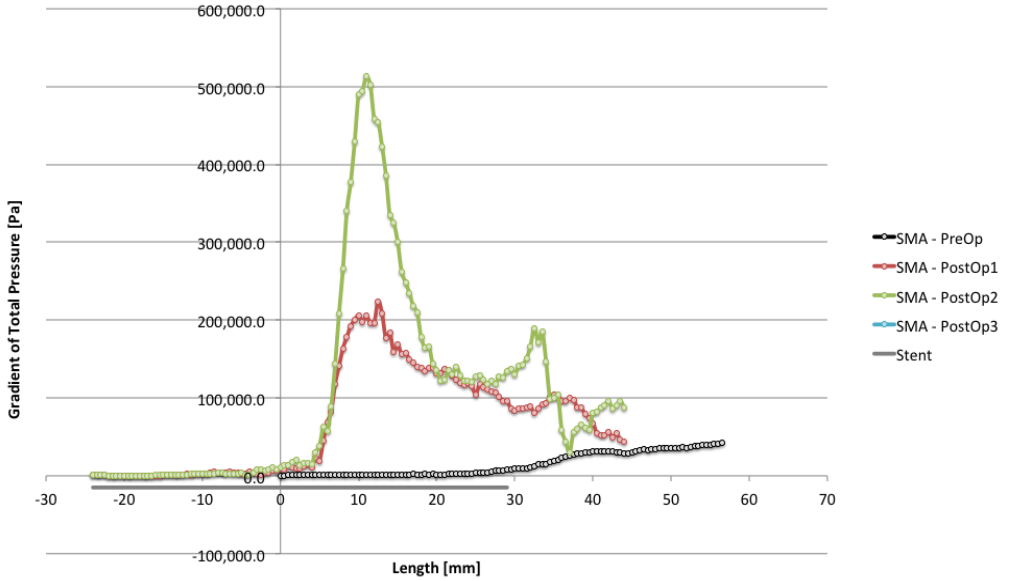

Intentionally occluded vessel: RIGHT RENAL ARTERY

CSA

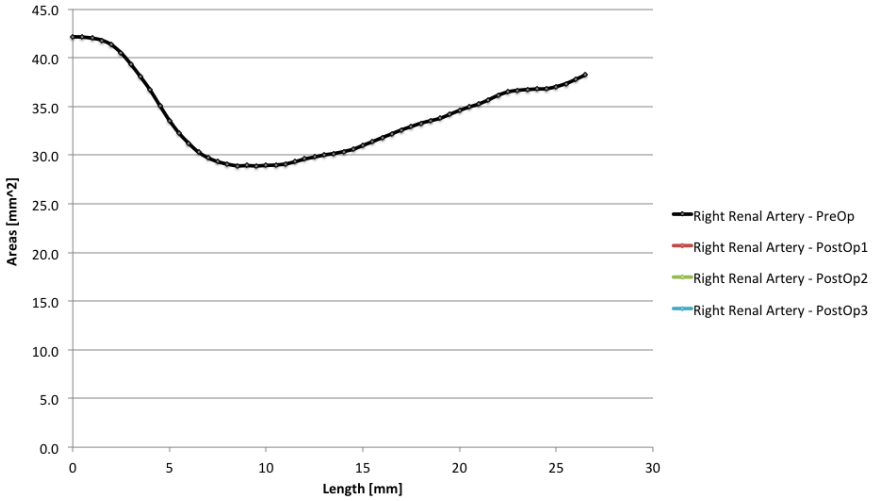

Total pressure

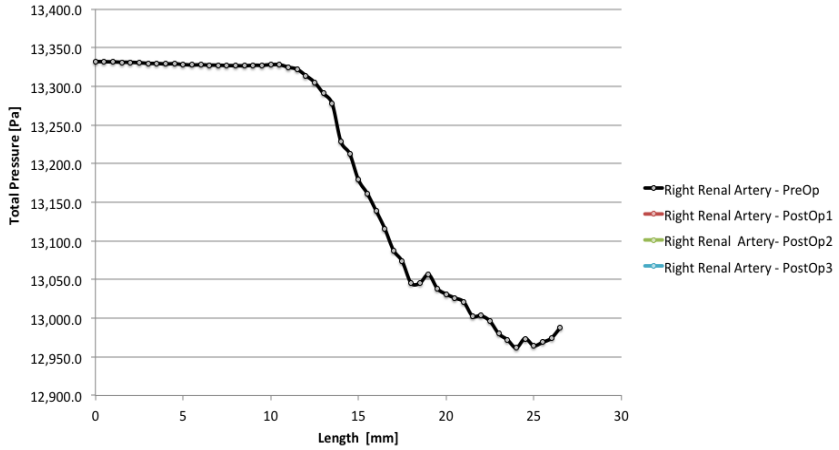

WSS

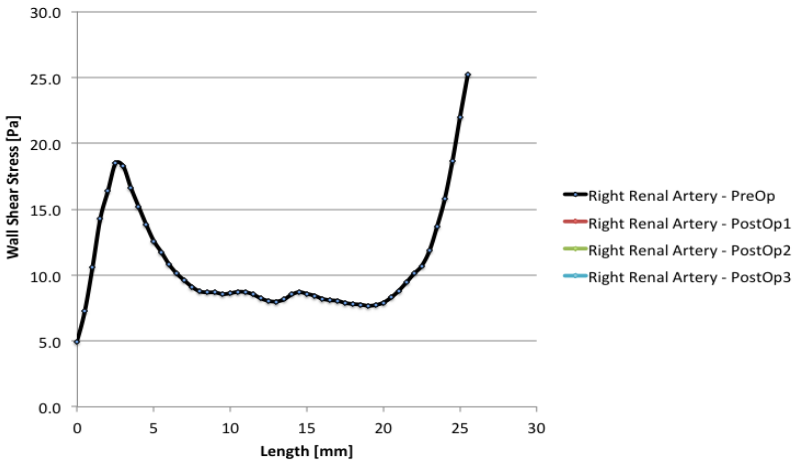

Difference of static pressure

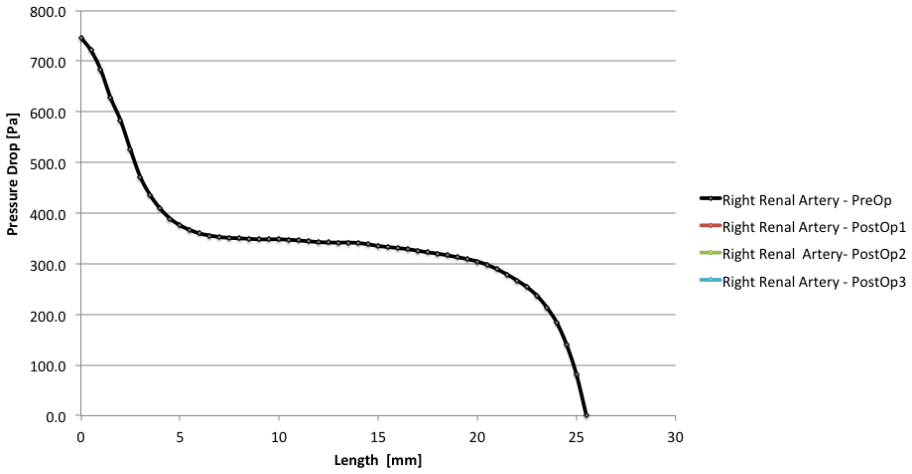

Gradient of total pressure

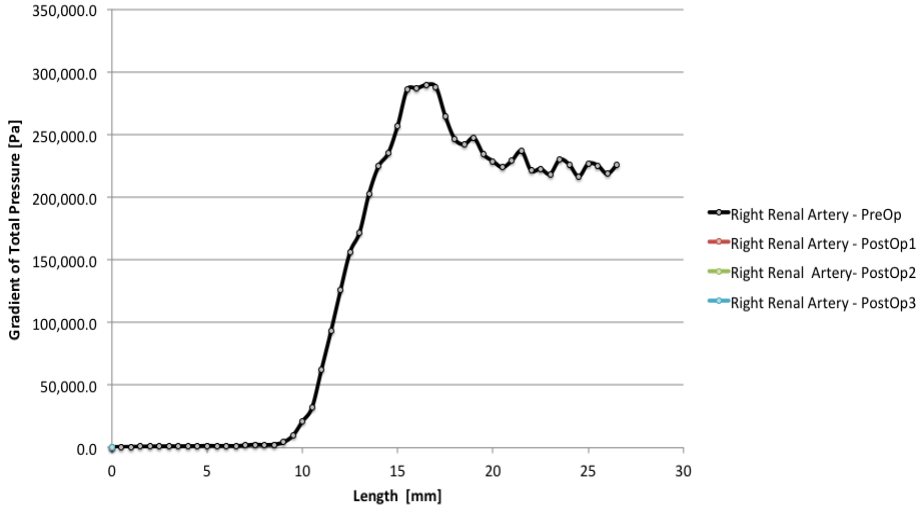

LEFT RENAL ARTERY

CSA

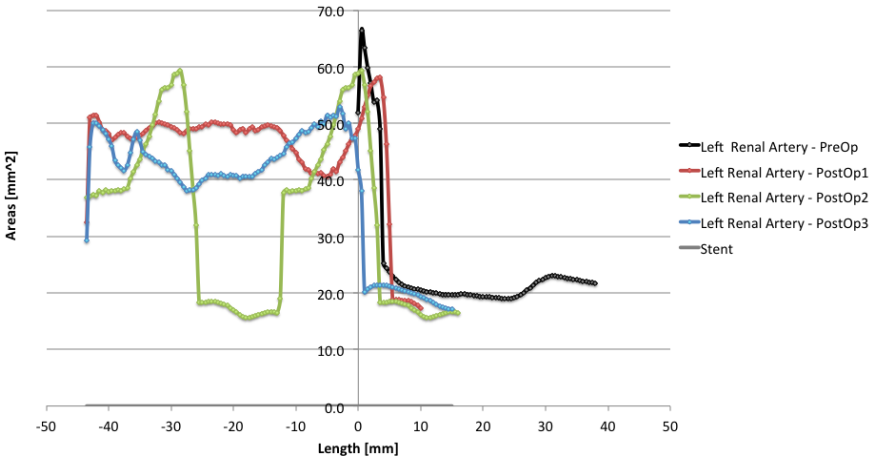

Total pressure

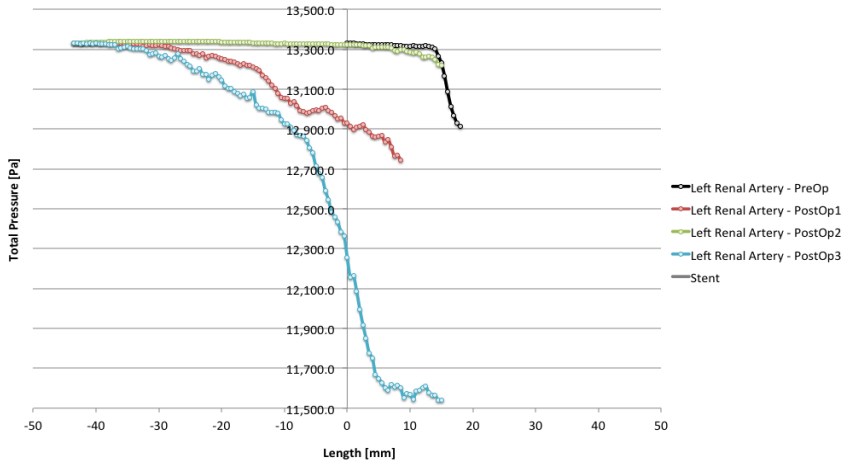

WSS

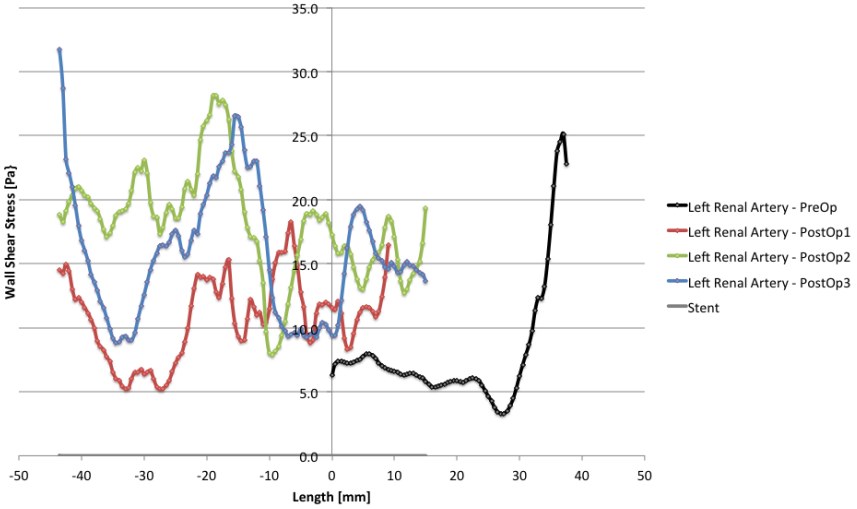

Difference of static pressure

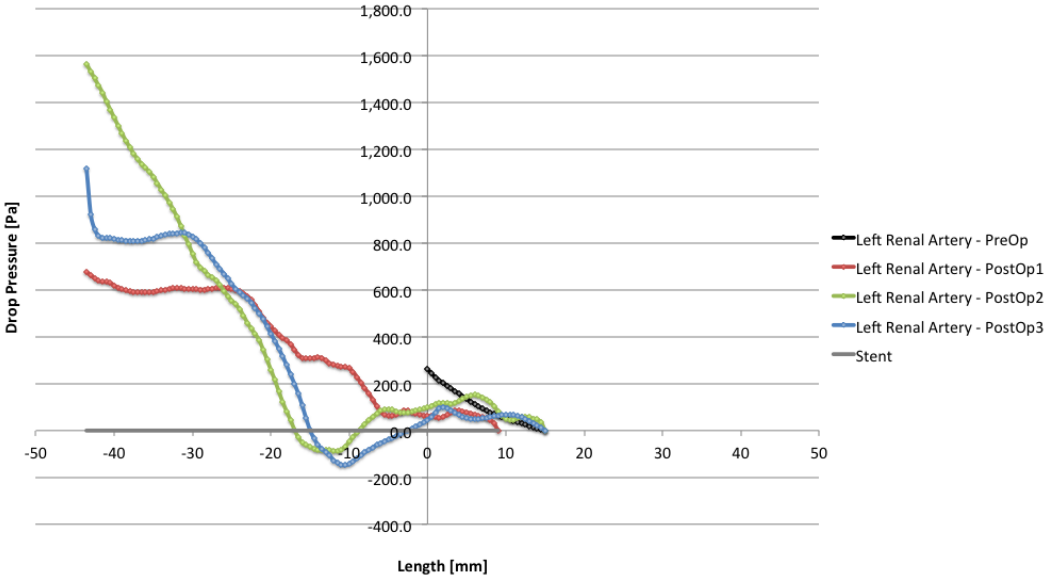

Gradient of total pressure

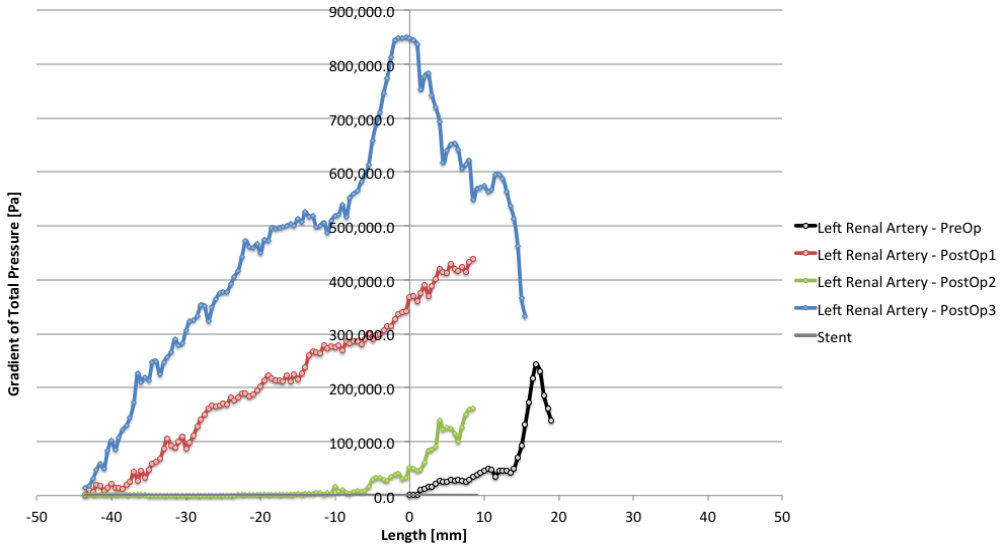

APPENDIX C
PATIENT 3 - MORPHOLOGICAL AND HEMODYNAMICAL RECORDS

Morphological situation of patient 3 on PreOp and PostOp1.

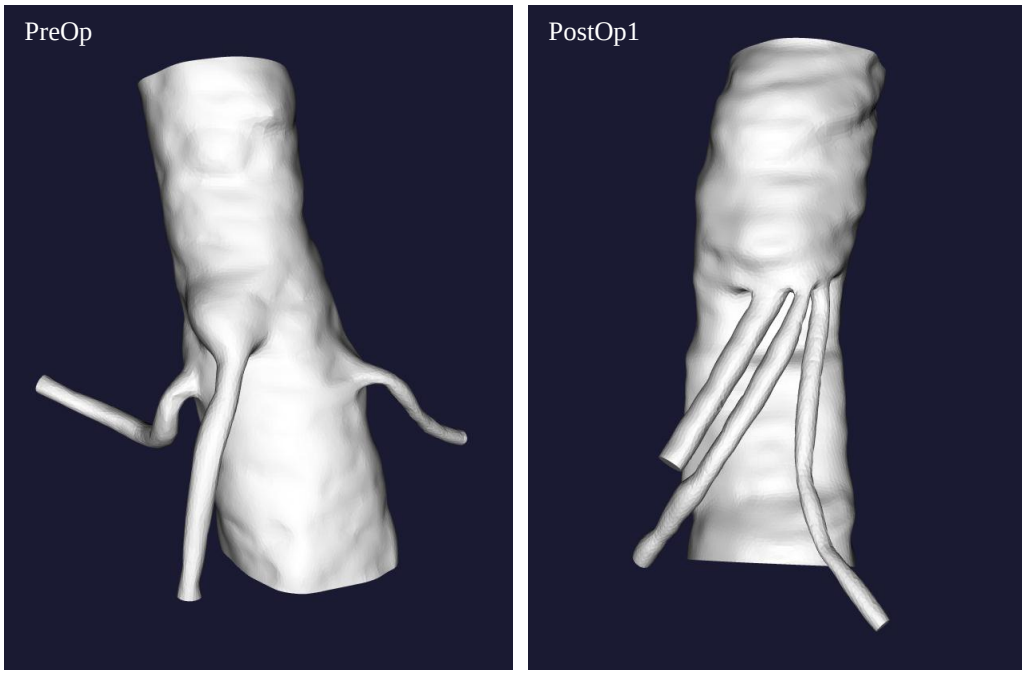

SUPERIOR MESENTERIC ARTERY

Difference of static pressure

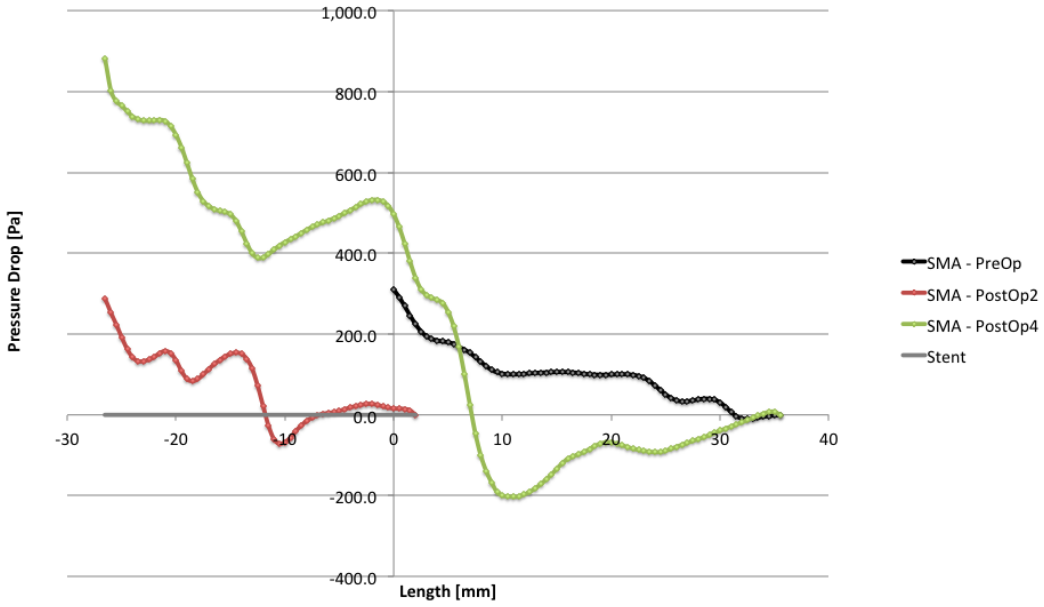

Gradient of total pressure

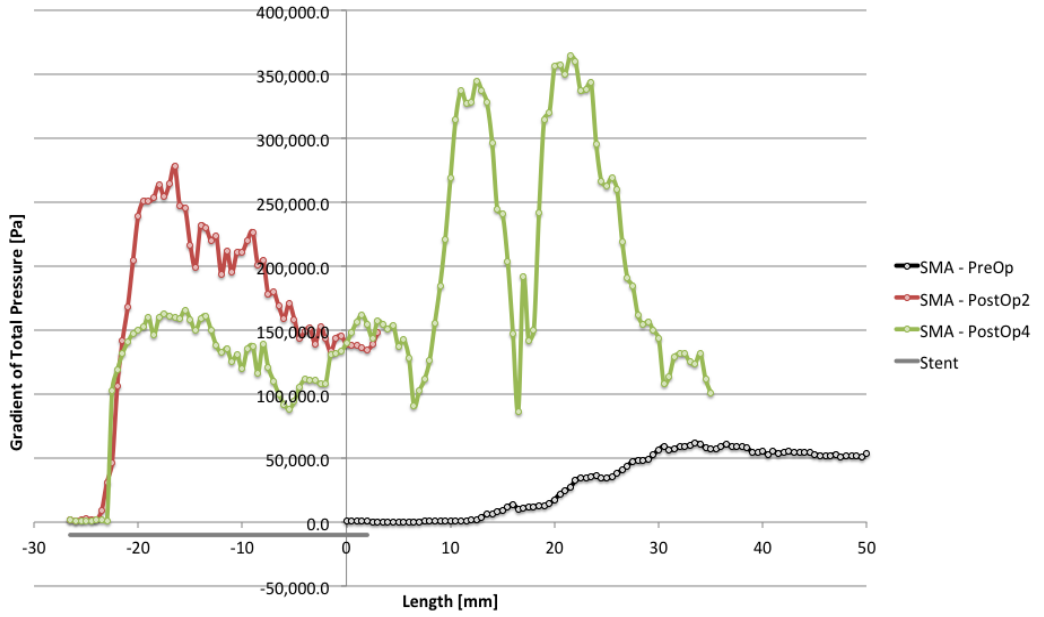

RIGHT RENAL ARTERY

CSA

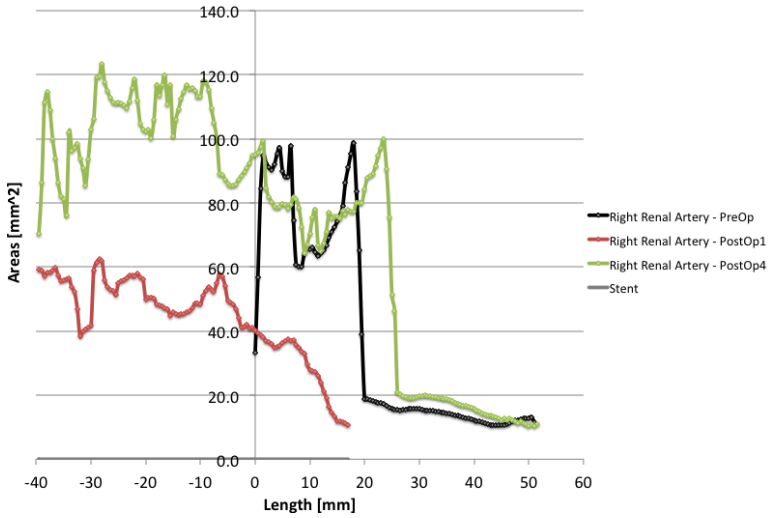

Total pressure

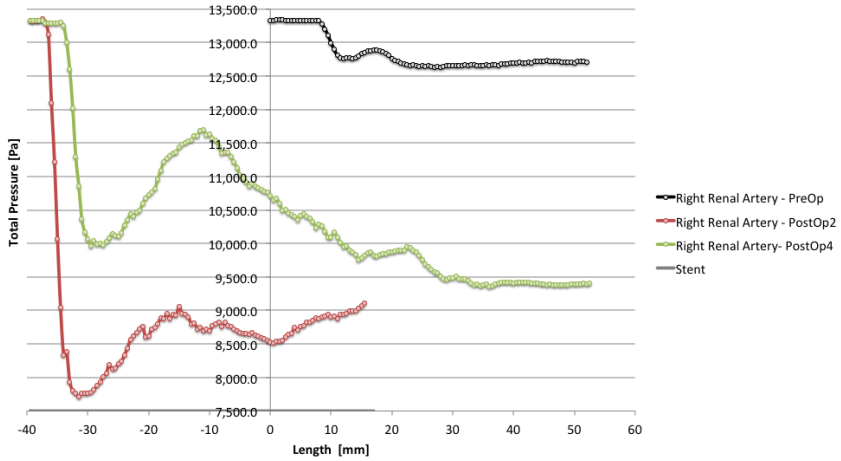

WSS

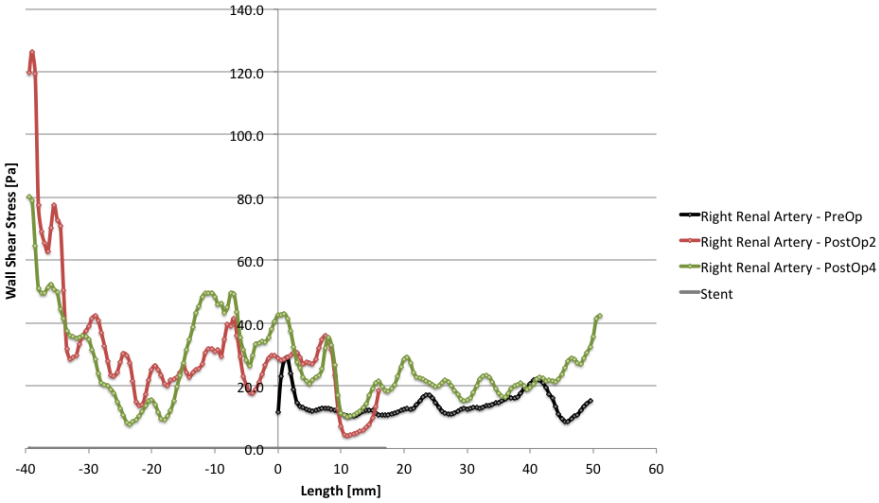

Difference of static pressure

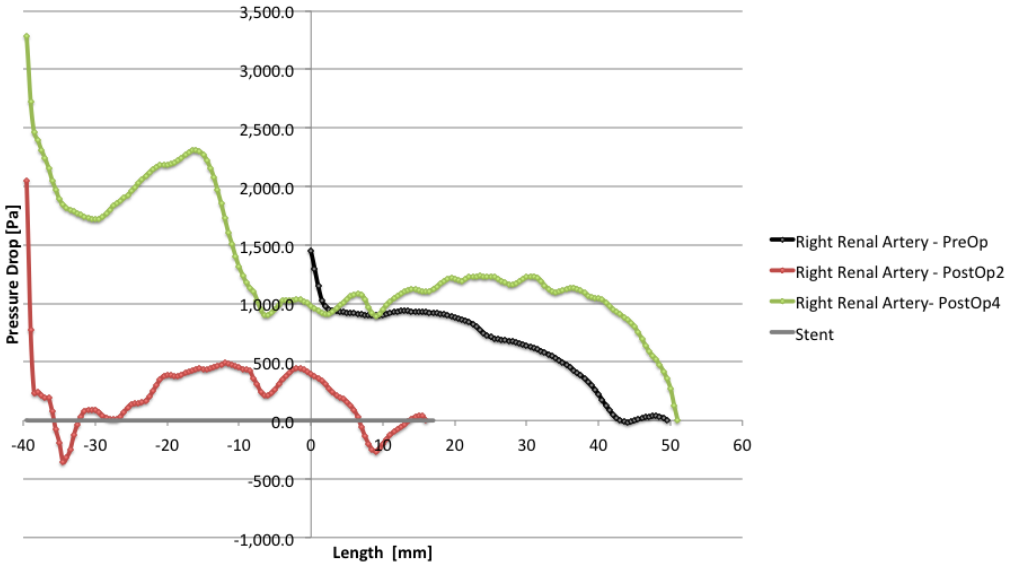

Gradient of total pressure

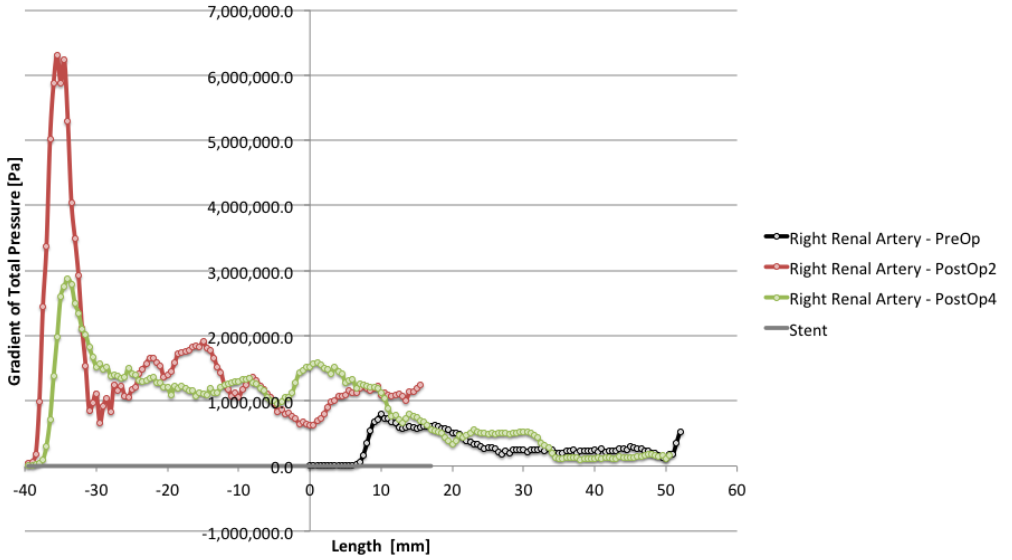

LEFT RENAL ARTERY

Difference of static pressure

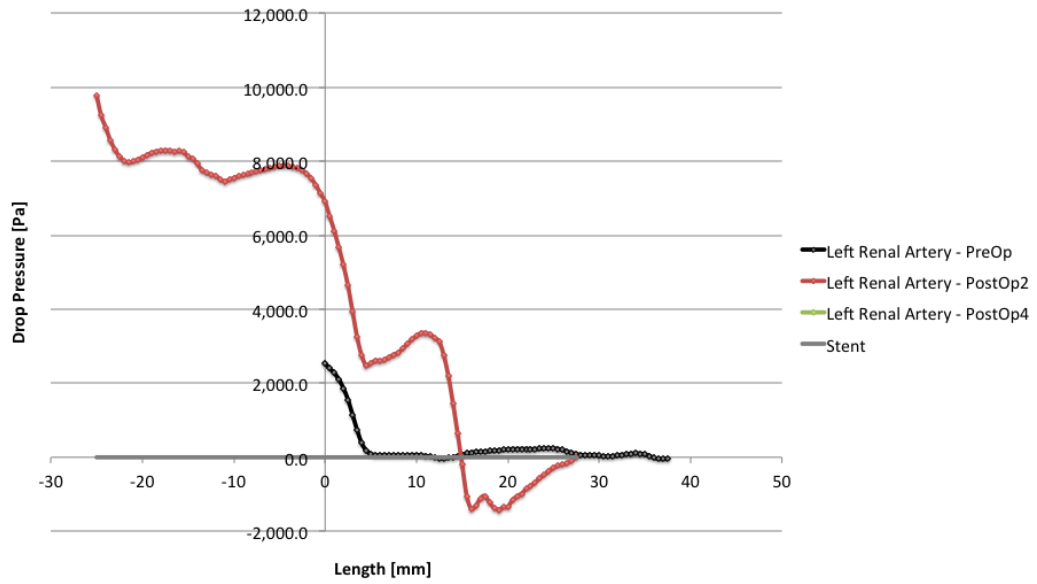

Gradient of total pressure

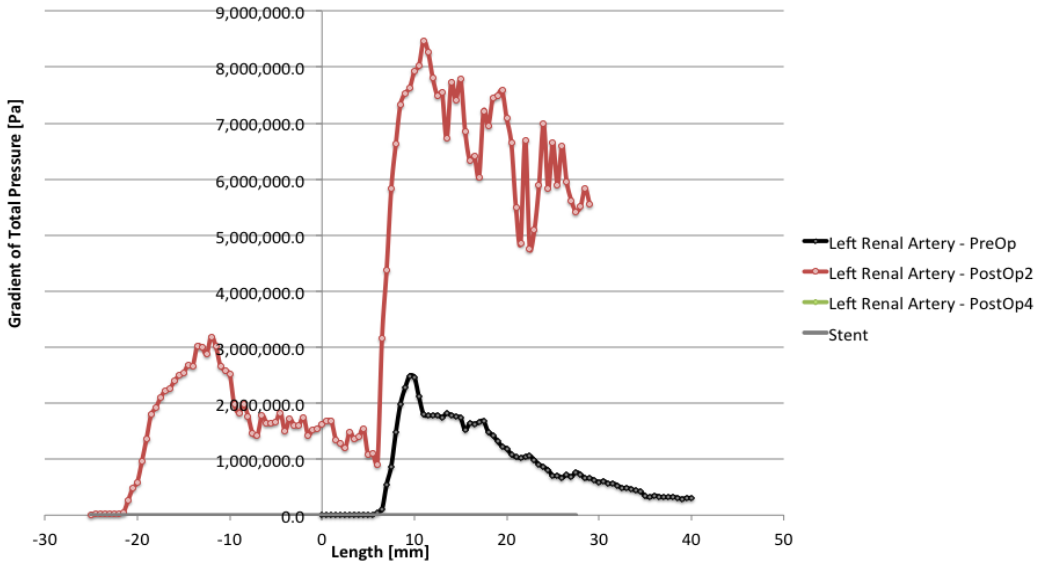

- 25% AORTA INLET RESULTS

SUPERIOR MESENTERIC ARTERY

Total Pressure

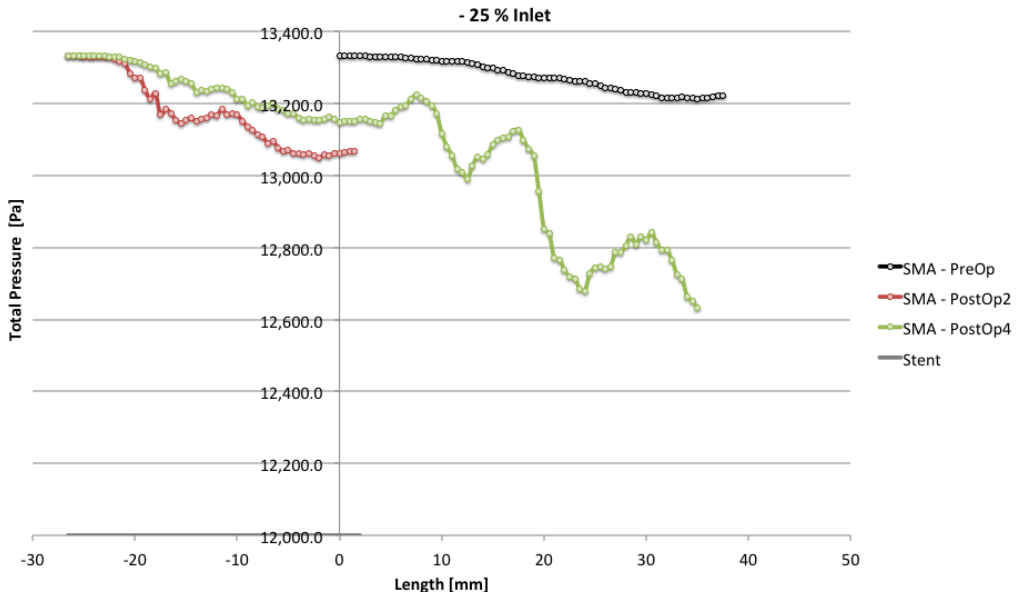

WSS

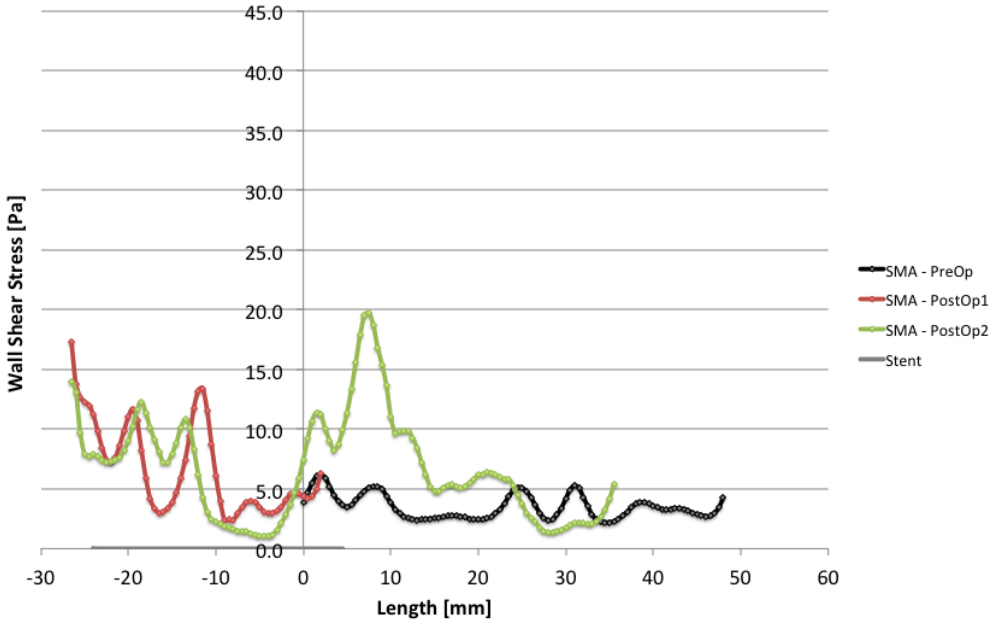

Difference of static pressure

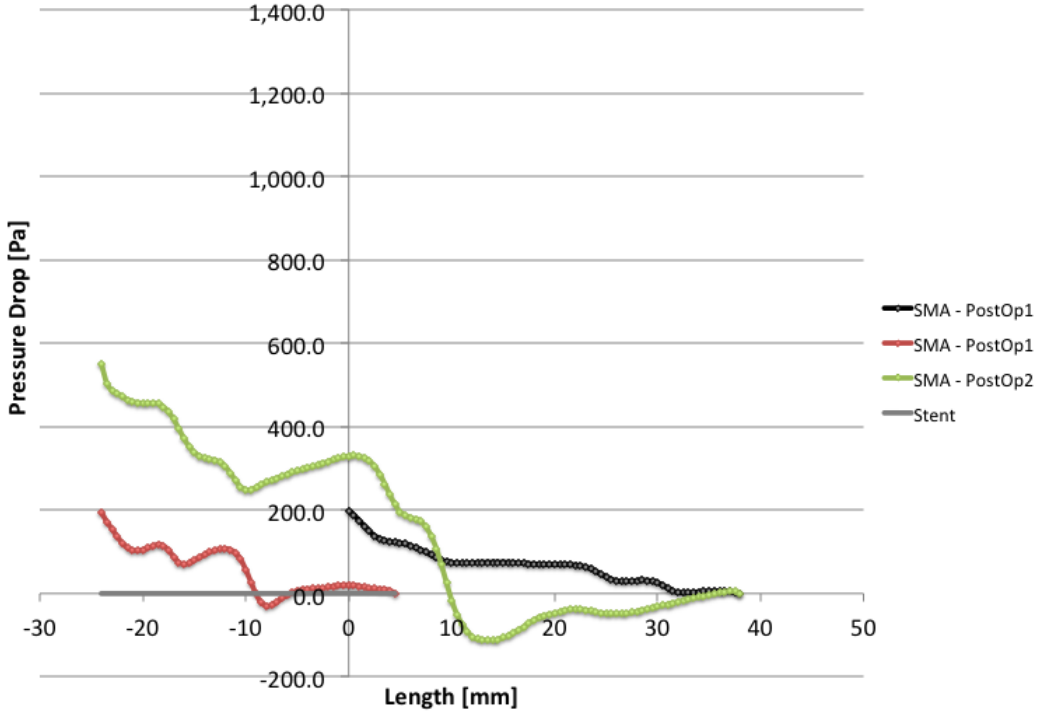

Gradient of total pressure

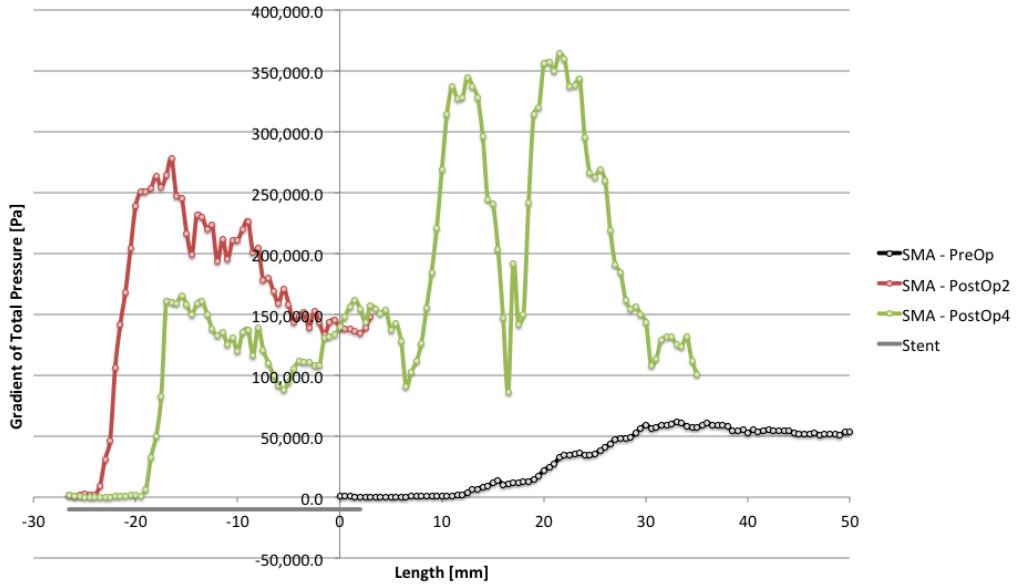

+ 25 % AORTA INLET RESULTS

SUPERIOR MESENTERIC ARTERY

Total Pressure

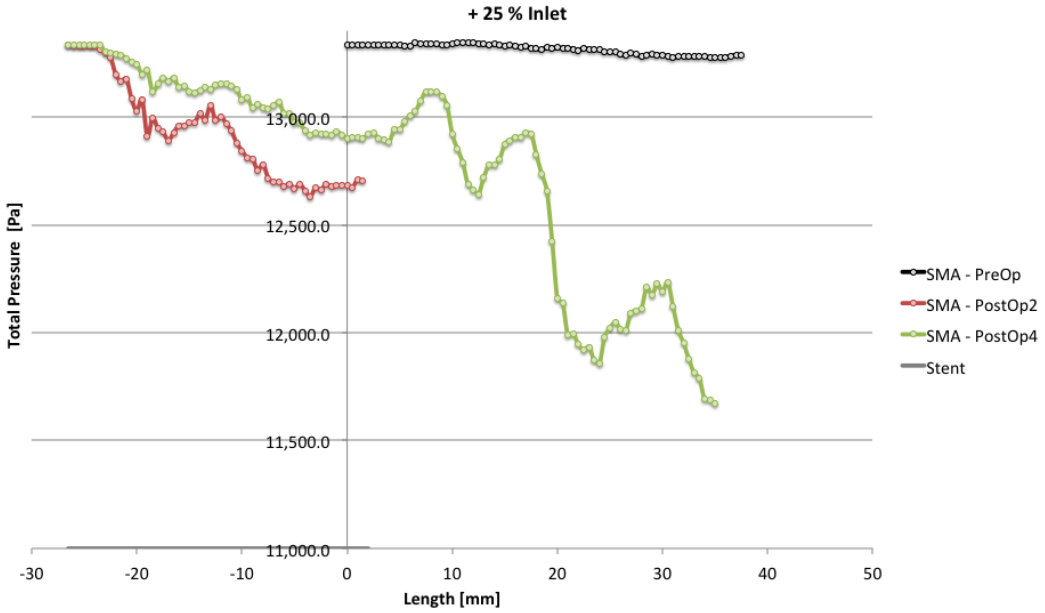

WSS

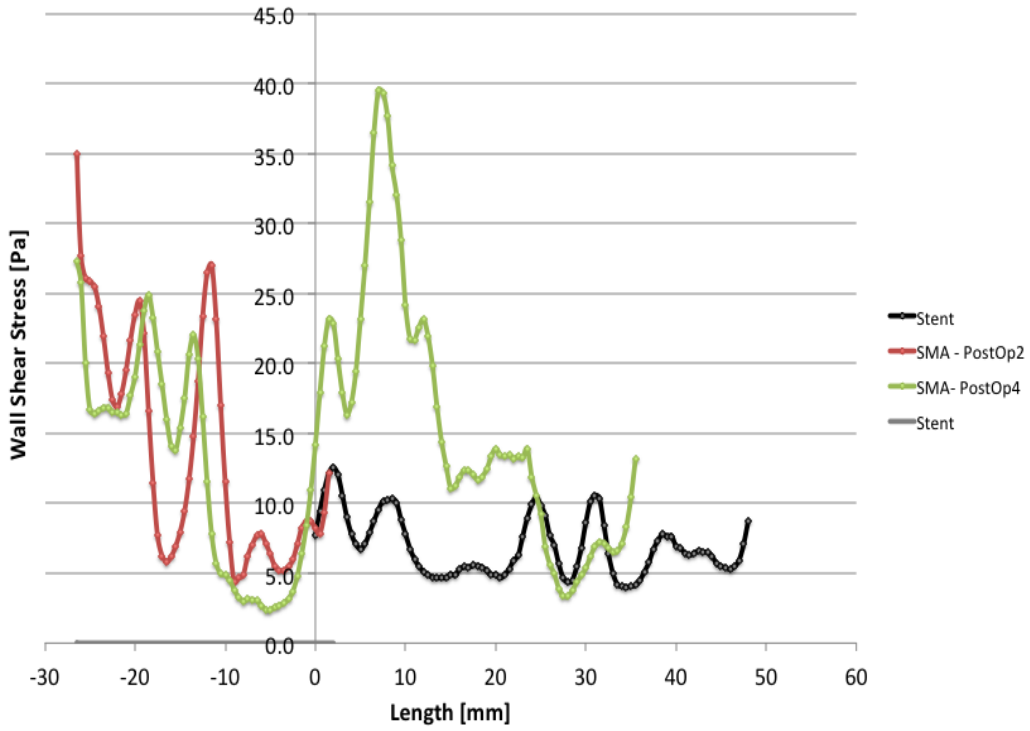

Difference of static pressure

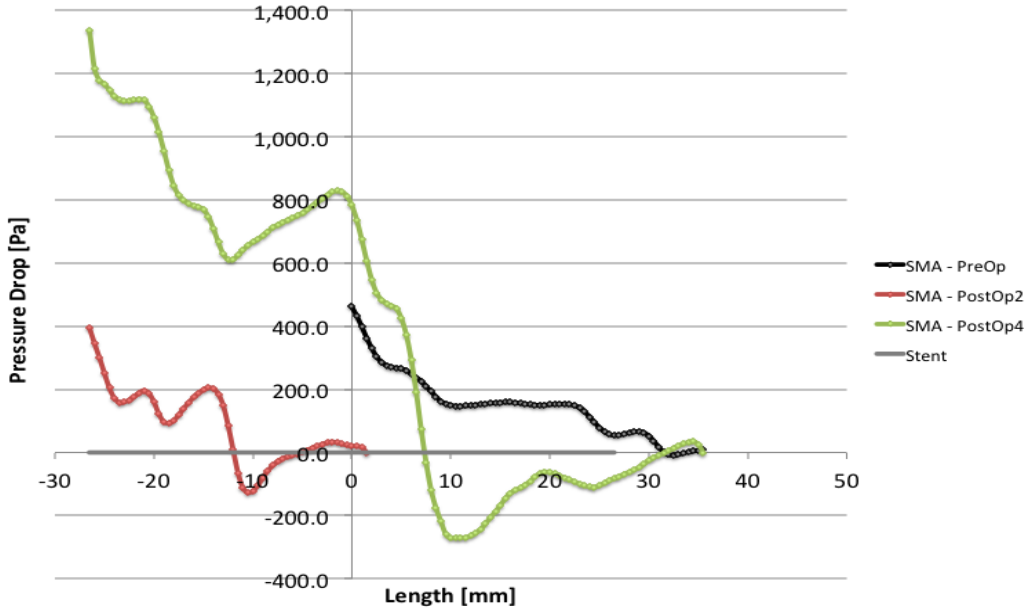

Gradient of pressure

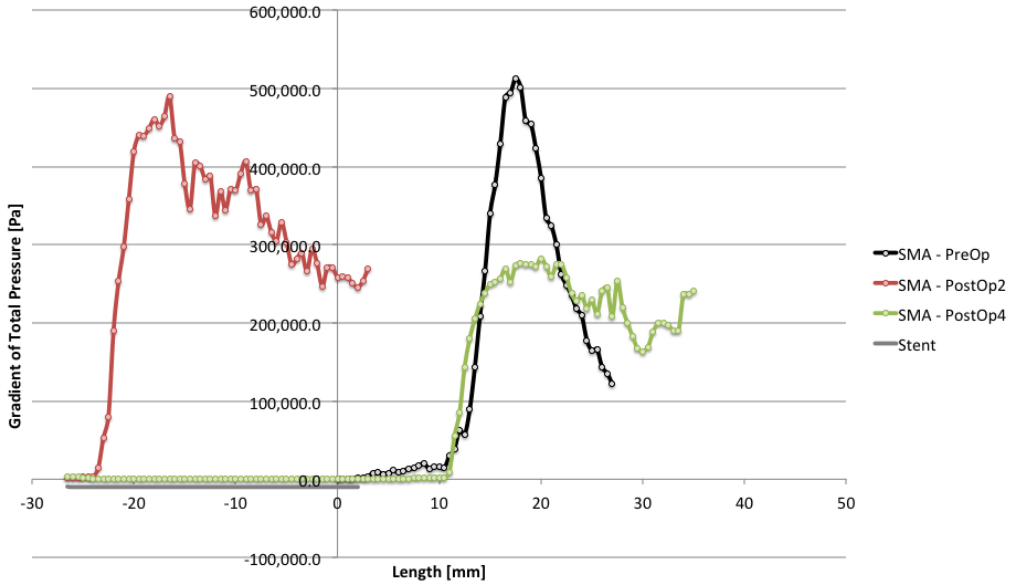

APPENDIX D
PATIENT 4 - MORPHOLOGICAL AND HEMODYNAMICAL RECORDS

Morphological situation of patient 4 on PreOp and PostOp1.

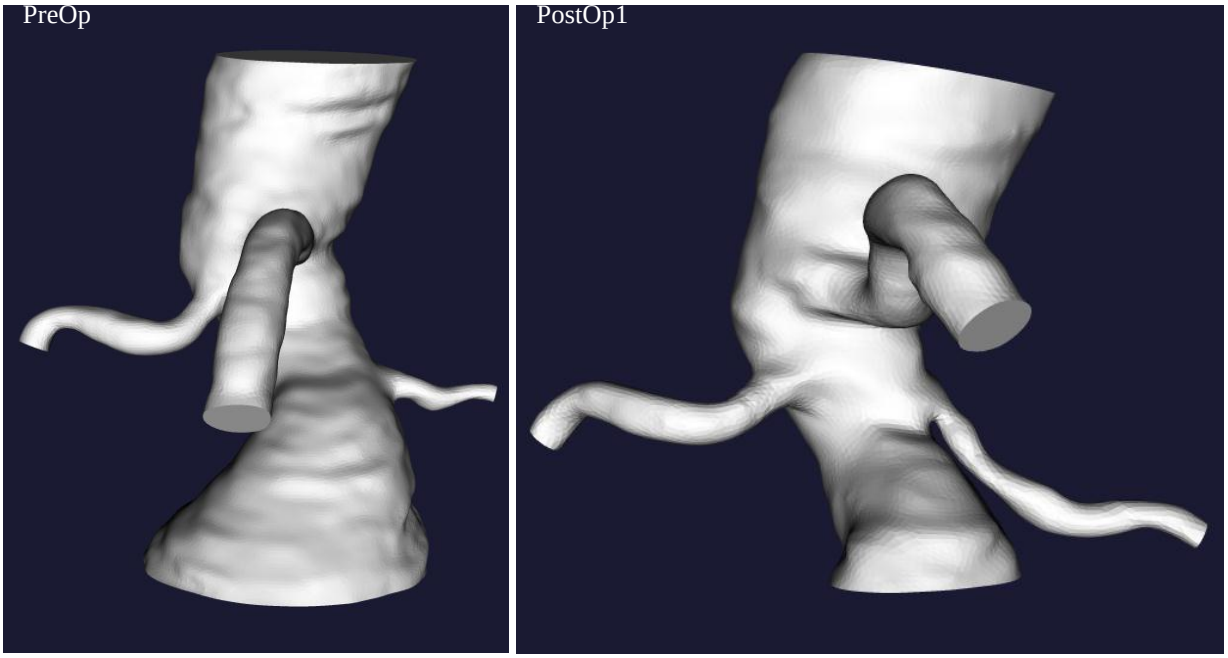

SUPERIOR MESENTERIC ARTERY

Difference of static pressure

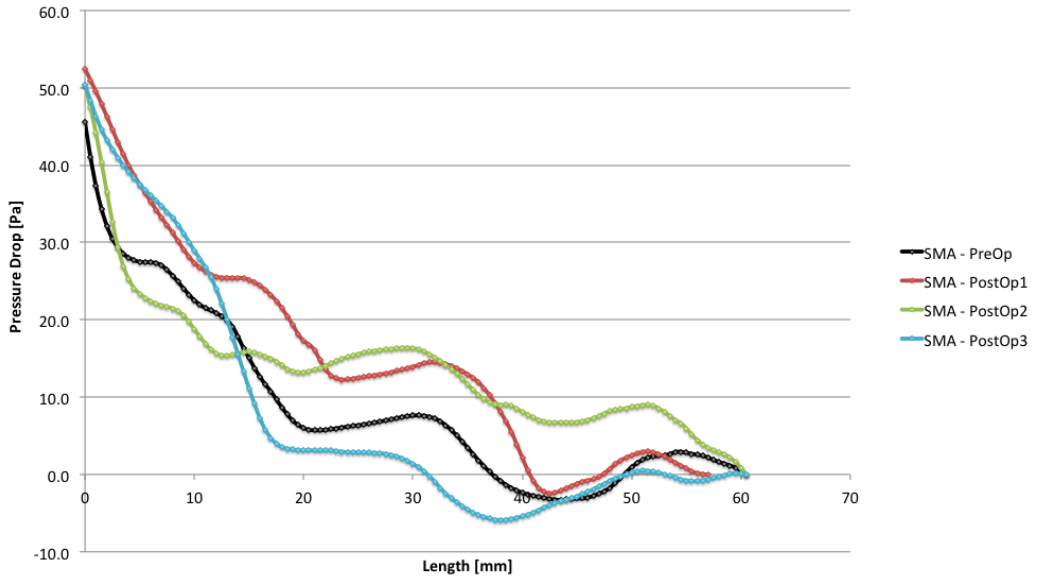

Gradient of total pressure

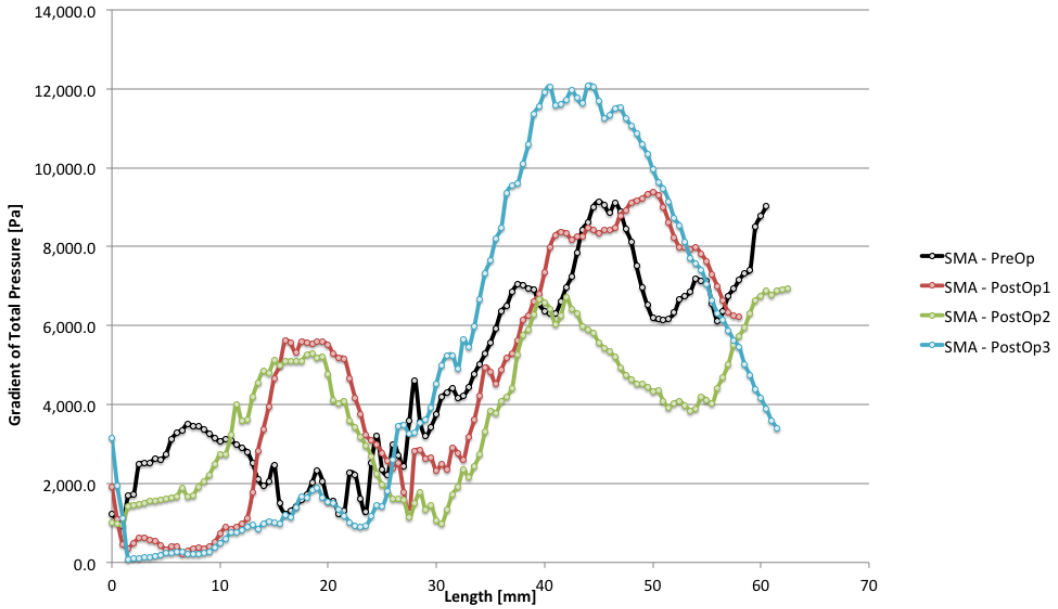

RIGHT RENAL ARTERY

Difference of static pressure

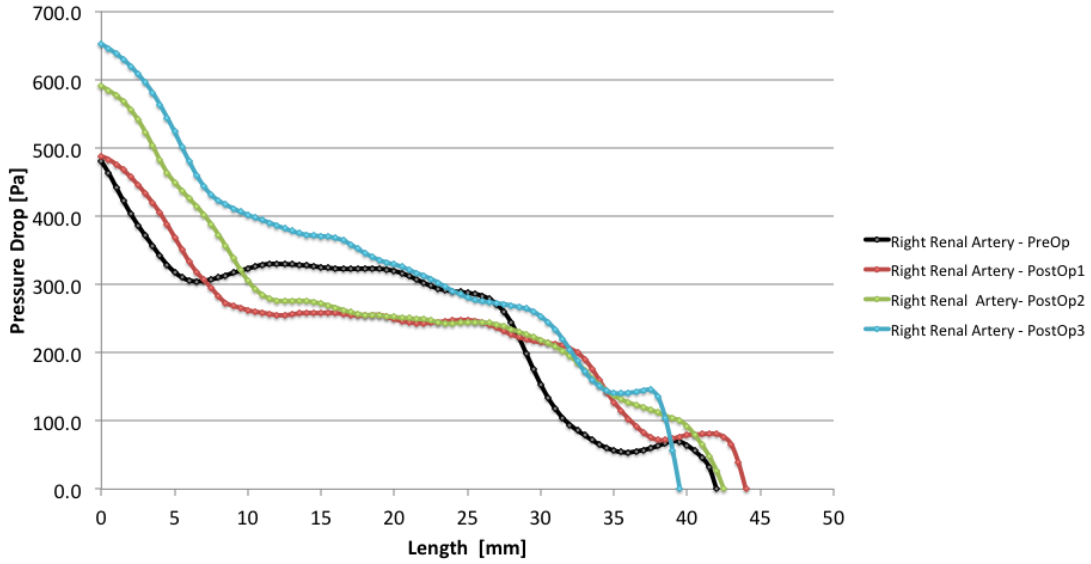

Gradient of total pressure

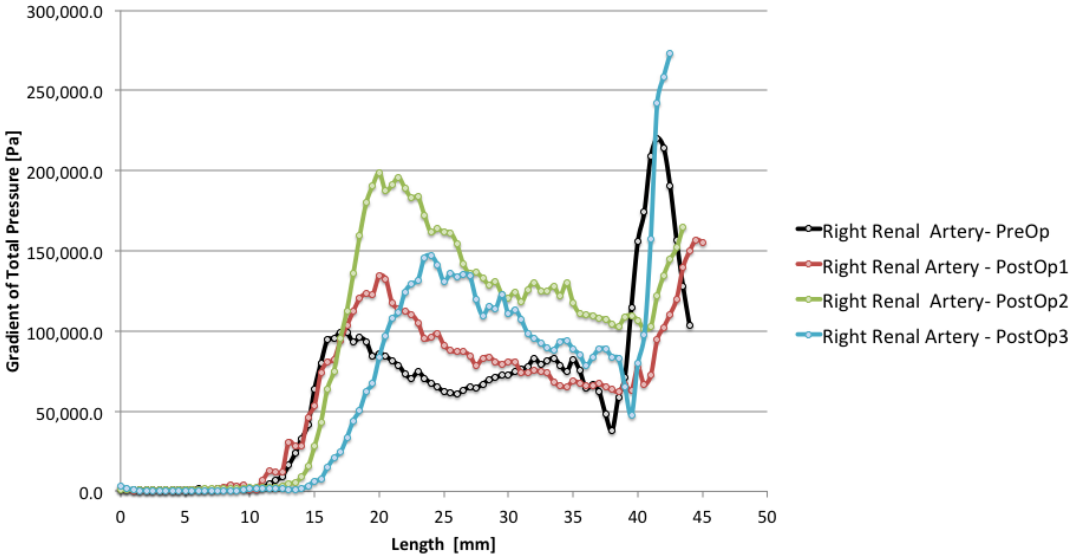

LEFT RENAL ARTERY

Difference of static pressure

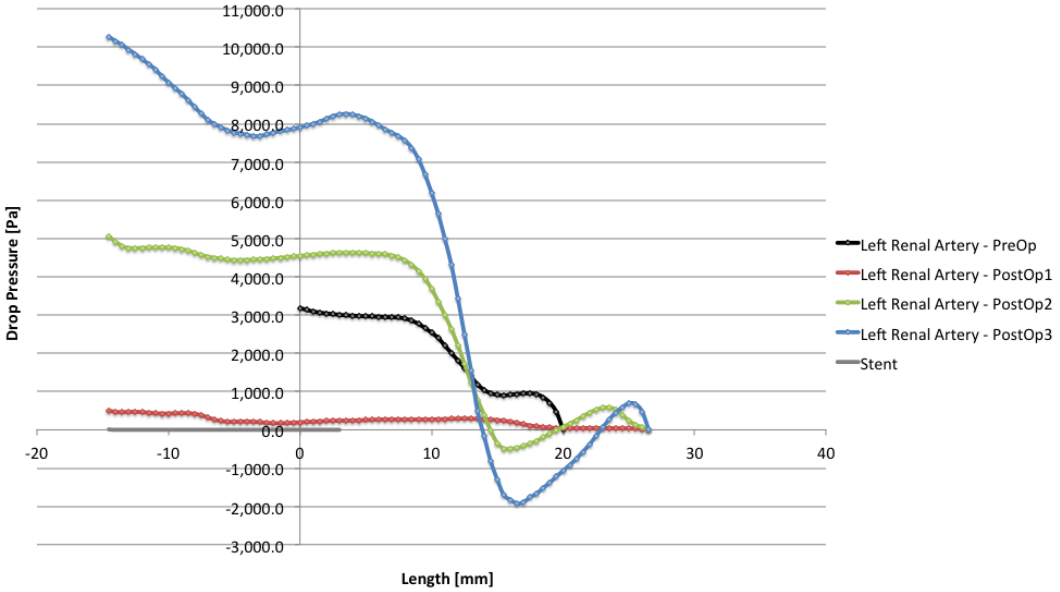

Gradient of pressure

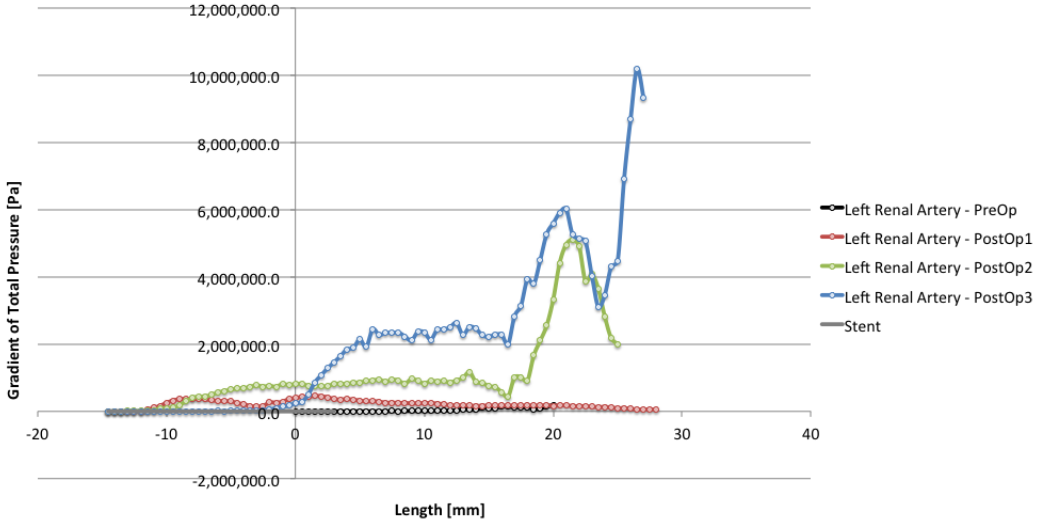

APPENDIX E
PATIENT 5 - MORPHOLOGICAL AND HEMODYNAMICAL RECORDS

Morphological situation of patient 5 on PreOp and PostOp1 (left renal artery has been intentionally occluded).

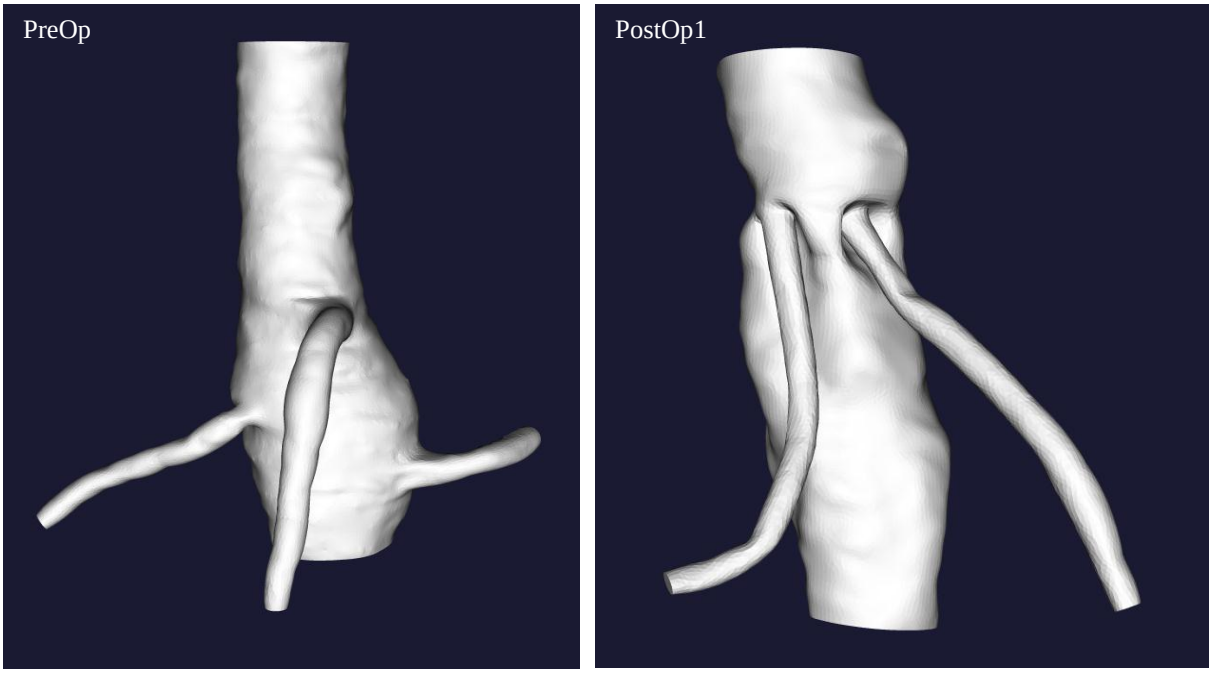

SUPERIOR MESENTERIC ARTERY

Difference of static pressure

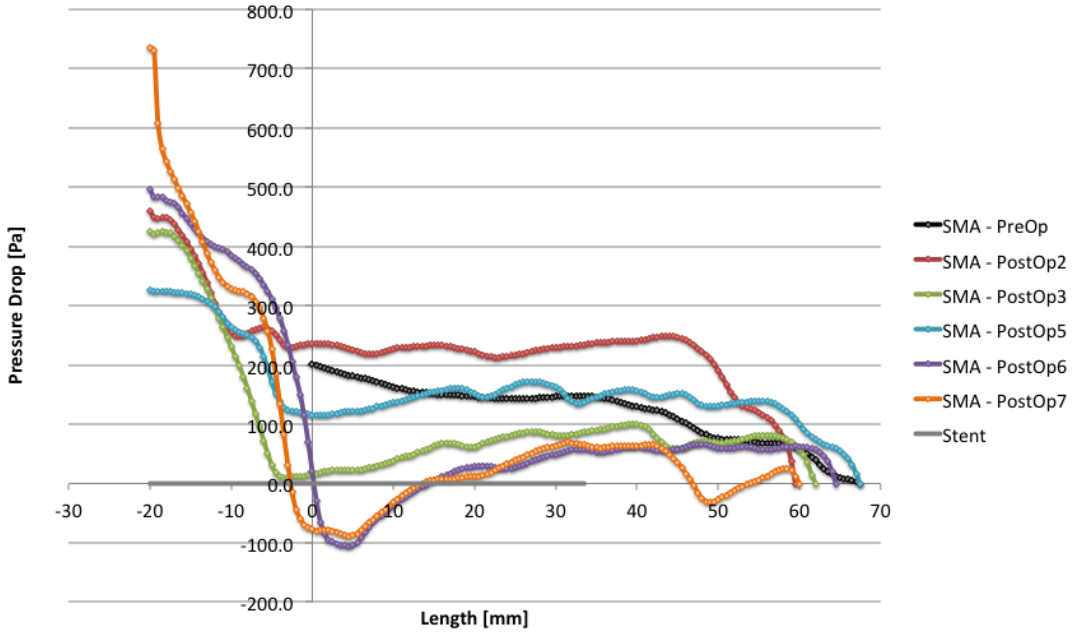

Gradient of total pressure

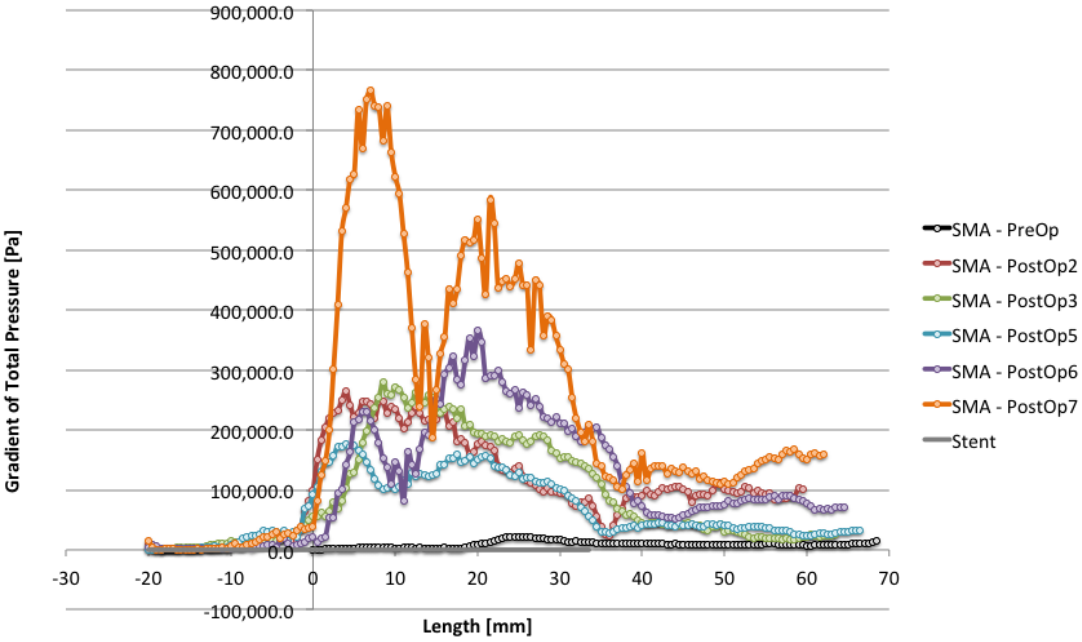

RIGHT RENAL ARTERY

Difference of static pressure

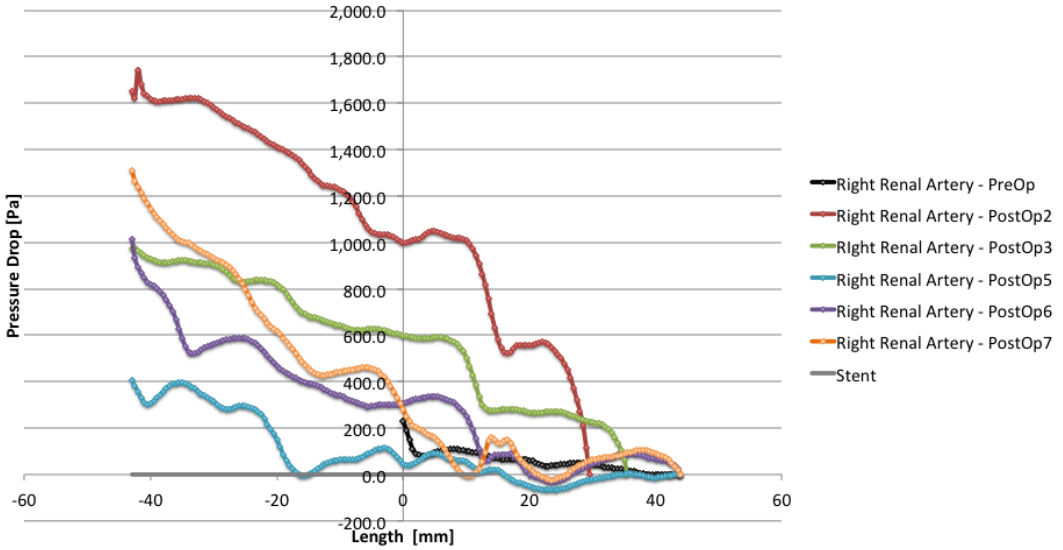

Gradient of total pressure

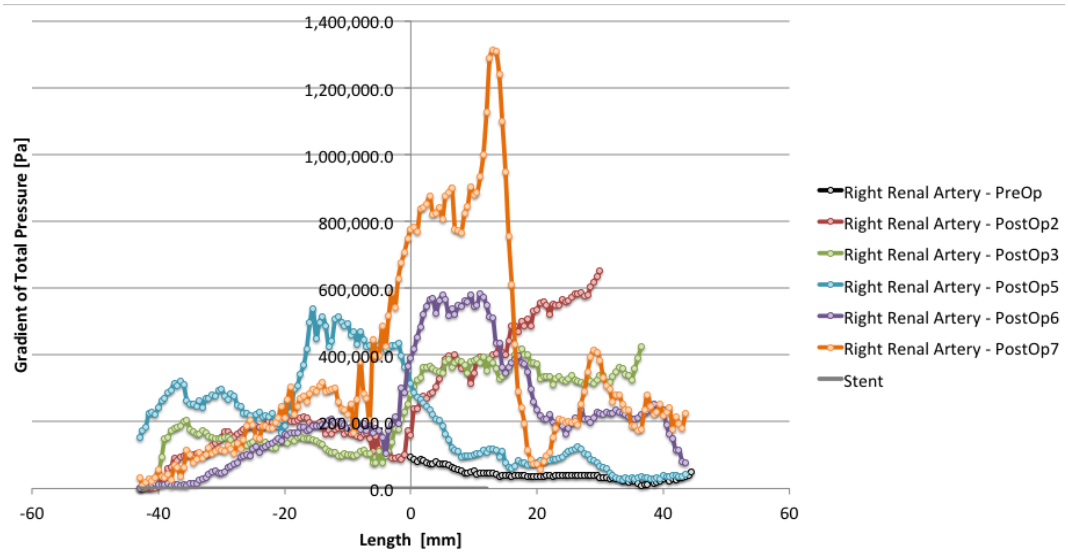

Intentionally occluded vessel: LEFT RENAL ARTERY

CSA

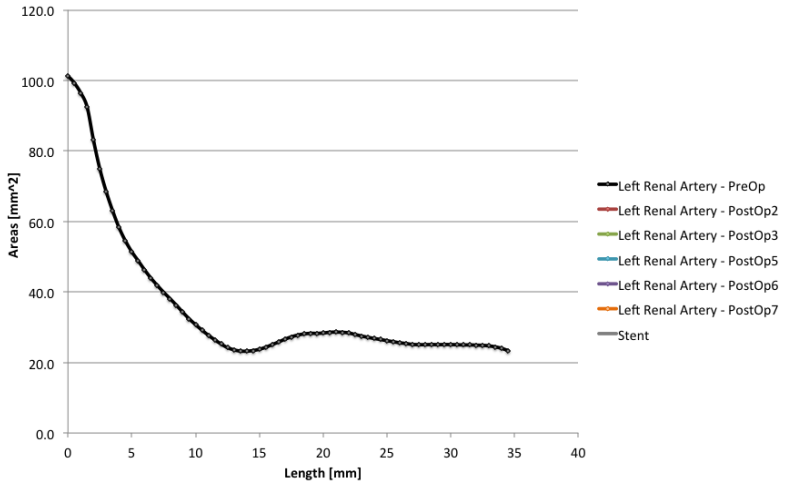

Total Pressure

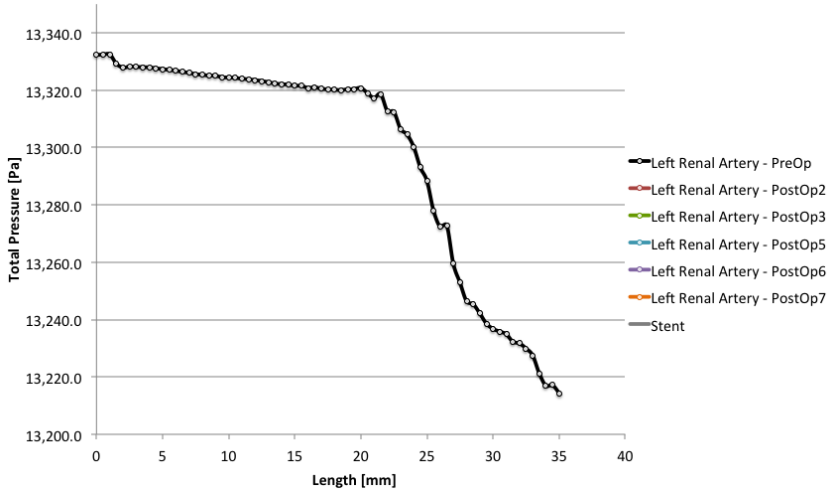

WSS

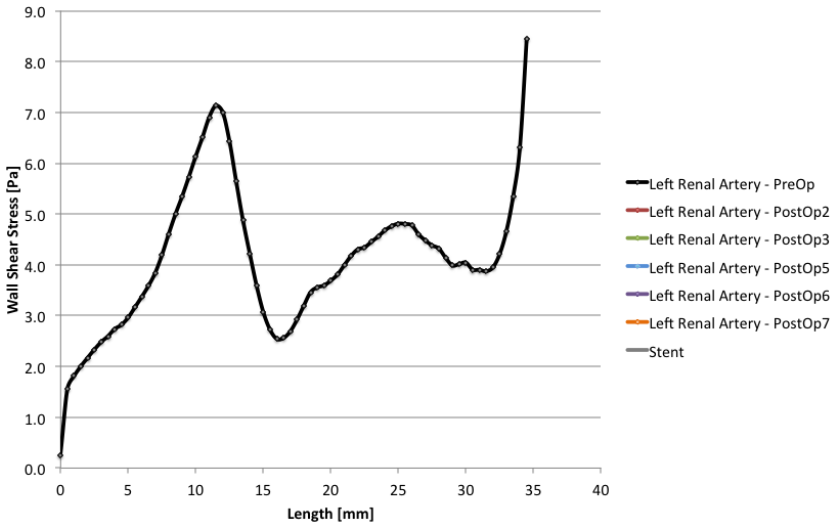

Difference of static pressure

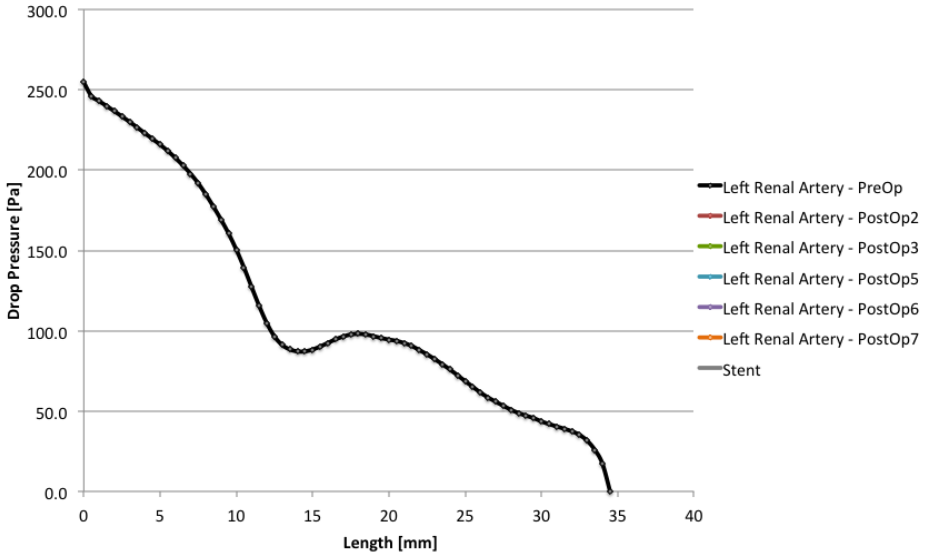

Gradient of total pressure

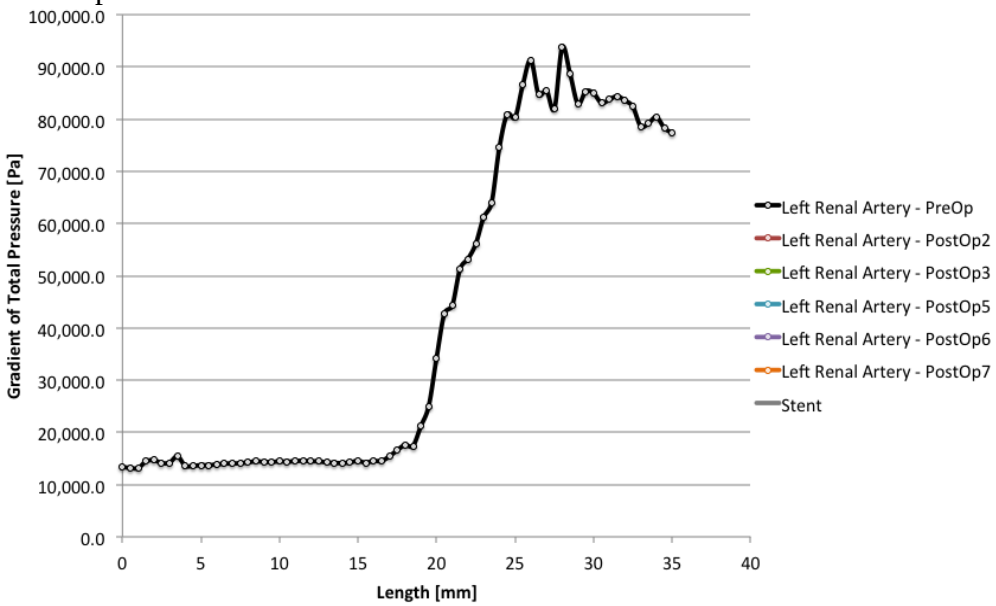

LISTS OF REFERENCES

1. Waterman, P. J. CFD: Shaping the Medical World. *Deskt. Eng.* at <http://www.deskeng.com/de/cfd-shaping-the-medical-world/>

2. Löhner, R., Cebral, J., Soto, O., Yim, P. & Burgess, J. E. Applications of patient-specific CFD in medicine and life sciences. *Int. J. Numer. Methods Fluids* **43,** 637–650 (2003).

3. Ahn, S. S. *et al.* Reporting standards for infrarenal endovascular abdominal aortic aneurysm repair. *J. Vasc. Surg.* **25,** 405–410 (1997).

4. Kuivaniemi, H., Platsoucas, C. D. & Tilson, M. D. Aortic Aneurysms: an Immune Disease with a Strong Genetic Component. *Circulation* **117,** 242–252 (2008).

5. Celi, S. & Berti, S. *InTech Biomechanics and fe modelling of aneurysm review and advances in computational models.pdf free ebook download*. (InTech, 2012). at <http://ebookbrowsee.net/intech-biomechanics-and-fe-modelling-of-aneurysm-review-and-advances-in-computational-models-pdf-d538553768>

6. Nordon, I. M., Hinchliffe, R. J., Loftus, I. M. & Thompson, M. M. Pathophysiology and epidemiology of abdominal aortic aneurysms. *Nat. Rev. Cardiol.* **8,** 92–102 (2011).

7. Humphrey, J. D. & Taylor, C. A. Intracranial and abdominal aortic aneurysms: similarities, differences, and need for a new class of computational models. *Annu. Rev. Biomed. Eng.* **10,** 221–246 (2008).

8. National Vital Statistics Report. at </nchs/products/nvsr.htm>

9. Dalman, R. L., Tedesco, M. M., Myers, J. & Taylor, C. A. AAA Disease. *Ann. N. Y. Acad. Sci.* **1085,** 92–109 (2006).

10. Dingemans, K. P., Teeling, Peter, Lagendijk, Jaap H. & Becker, A. E. Extracellular matrix of the human aortic media: An ultrastructural histochemical and immunohistochemical study of the adult aortic media. *Anat. Rec.* **258,** 1–14 (2000).

11. Suh, G.-Y. *et al.* Hemodynamic changes quantified in abdominal aortic aneurysms with increasing exercise intensity using mr exercise imaging and image-based computational fluid dynamics. *Ann. Biomed. Eng.* **39,** 2186–2202 (2011).

12. Malek AM, Alper SL & Izumo S. HEmodynamic shear stress and its role in atherosclerosis. *JAMA* **282,** 2035–2042 (1999).

13. Lumsden, A. B., Lin, P. H., Chen, C. & Parodi, J. *Advanced Endovascular Therapy of Aortic Disease*. (John Wiley & Sons, 2008).

14. Choke, E. *et al.* A review of biological factors implicated in abdominal aortic aneurysm rupture. *Eur. J. Vasc. Endovasc. Surg. Off. J. Eur. Soc. Vasc. Surg.* **30,** 227–244 (2005).

15. Eagle, K. A., Oh, J. K., Ramanath, V. S. & Sundt, T. M., III. Acute aortic syndromes and thoracic aortic aneurysm. *Mayo Clin. Proc.* **84,** 465+ (2009).

16. Ohrlander, T. *et al.* The chimney graft: a technique for preserving or rescuing aortic branch vessels in stent-graft sealing zones. *J. Endovasc. Ther. Off. J. Int. Soc. Endovasc. Spec.* **15,** 427–432 (2008).

17. T. Gregory Walker & John F. Cardella. Clinical Practice Guidelines for Endovascular Abdominal Aortic Aneurysm Repair: Written by the Standards of Practice Committee for the Society of Interventional Radiology and Endorsed by the Cardiovascular and Interventional Radiological Society of Europe and the Canadian Interventional Radiology Association. *2010* **21,** 1632–165 (2010).

18. Coscas, R., Kobeiter, H., Desgranges, P. & Becquemin, J.-P. Technical aspects, current indications, and results of chimney grafts for juxtarenal aortic aneurysms. *J. Vasc. Surg.* **53,** 1520–1527 (2011).

19. Umscheid, T., Tessarek, J., Austermann, M. & Torsello, G. Retrograde Stenting of a Recurrent Degenerative Aneurysm of the Superior Mesenteric Artery. *J. Endovasc. Ther.* **15,** 244–245 (2008).

20. Maldonado, T. S. & Gagne, P. J. Controversies in the Management of Type 11 'Branch' Endoleaks Following Endovascular Abdominal Aortic Aneurysm Repair. *Vasc. Endovascular Surg.* **37,** 1–12 (2003).

21. Morris, L., Delassus, P., Walsh, M. & McGloughlin, T. A mathematical model to predict the in vivo pulsatile drag forces acting on bifurcated stent grafts used in endovascular treatment of abdominal aortic aneurysms (AAA). *J. Biomech.* **37,** 1087–1095 (2004).

22. Li, Z. & Kleinstreuer, C. Blood flow and structure interactions in a stented abdominal aortic aneurysm model. *Med. Eng. Phys.* **27,** 369–382 (2005).

23. Li, Z. & Kleinstreuer, C. Analysis of biomechanical factors affecting stent-graft migration in an abdominal aortic aneurysm model. *J. Biomech.* **39,** 2264–2273 (2006).

24. Li, Z. & Kleinstreuer, C. A comparison between different asymmetric abdominal aortic aneurysm morphologies employing computational fluid–structure interaction analysis. *Eur. J. Mech. - BFluids* **26,** 615–631 (2007).

25. Segalova, P. A., Xiong, G., Venkateswara Rao, K. T., Zarins, C. K. & Taylor, C. A. Evaluating Design of Abdominal Aortic Aneurysm Endografts in a Patient-Specific Model Using Computational Fluid Dynamics. *J. Med. Devices* **5,** 041005–041005 (2011).

26. Guller, J., Samman, M., Deyer, T. W., Lookstein, R. & Nowakowski, S. Repair of a splenic artery aneurysm using a novel balloon-expandable covered stent. *Vasc. Med.* **11,** 111–113 (2006).

27. Taylor, C. A., Hughes, T. J. R. & Zarins, C. K. Finite element modeling of blood flow in arteries. *Comput. Methods Appl. Mech. Eng.* **158,** 155–196 (1998).

28. Antiga Luca. Patient-Specific Modeling of Geometry and Blood Flow in Large Arteries. (1999). at <http://lantiga.github.io/media/AntigaPhDThesis.pdf>

29. Oka, S. & Nakai, M. Optimality principle in vascular bifurcation. *Biorheology* **24,** 737–751 (1987).

BIOGRAPHICAL SKETCH

Rosamaria Tricarico was born 1989 in Conversano (BA, Italy). She earned a bachelor degree in biomedical engineering from Politecnico of Milan (IT) in 2011. She started a master's in biomedical engineering at Politecnico of Milan and she joined the Atlantis Dual Degree Program in 2013 in order to gain a Master of Science from the University of Florida in Gainesville (FL).